Profiling the Control of Hepatic Glucose and Lipid Metabolism for Evaluating Novel Strategies of Insulin Delivery

Ana Francisca Leal Silva Soares

Universidade de Coimbra
2011

PROFILING THE CONTROL OF HEPATIC GLUCOSE AND LIPID METABOLISM FOR EVALUATING NOVEL STRATEGIES OF INSULIN DELIVERY

Ana Francisca Leal Silva Soares

Dissertação apresentada à Faculdade de Ciências e Tecnologia da Universidade de Coimbra para prestação de provas de Doutoramento em Bioquímica, na especialidade de Biofísica Celular.

Março 2011

Orientação/Supervision

Rui de Albuquerque Carvalho & John Griffith Jones
Faculdade de Ciências e Tecnologia
Universidade de Coimbra

Francisco José Veiga
Faculdade de Farmácia
Universidade de Coimbra

O trabalho experimental descrito nesta tese foi realizado nas seguintes instituições:

Universidade de Coimbra (Coimbra, Portugal),
Departamento de Ciências da Vida da Faculdade de Ciências e Tecnologia,
Laboratório de Tecnologia Farmacêutica da Faculdade de Farmácia,
Centro de Neurociências e Biologia Celular;

Université Joseph Fourier (Grenoble, França),
Département de Pharmacochimie Moléculaire;

Universitat de Barcelona (Barcelona, Espanha),
Departament de Bioquímica i Biologia Molecular, Facultat de Farmàcia.

Ana Francisca Soares usufruiu de uma Bolsa Individual de Doutoramento da Fundação para a Ciência e Tecnologia com a referência SFRH/BD/29624/2006.

O espectrómetro de RMN 600 MHz usado nestas experiências faz parte da Rede Nacional de RMN e foi adquirido no quadro do Programa Nacional para Re-equipamento Científico, contrato REDE/1517/RMN/2005 com financiamento do POCI 2010 (FEDER) e da Fundação para a Ciência e Tecnologia.

AGRADECIMENTOS

ACKNOWLEDGEMENTS/REMERCIEMENTS/AGRADECIMIENTOS

Durante o período de investigação que conduziu a esta Tese, muitas foram as pessoas que, das mais variadas formas, me inspiraram, apoiaram, ensinaram ou colaboraram directamente em muitos dos trabalhos. Gostaria de dirigir os meus especiais e sinceros agradecimentos a algumas delas.

Ao Professor Doutor Rui Carvalho, agradeço a disponibilidade com que sempre acompanhou este meu percurso, os conhecimentos que me transmitiu e a confiança que em mim depositou. Quero também manifestar a minha admiração pelo rigor que empenha no trabalho científico que produz, que tenho para mim como exemplo de qualidade.

To Doctor John Jones I would like to express my gratitude for his scientific guidance and constant support throughout these years. His inspiring enthusiasm and optimism encourage me to move forward in the road of science.

Ao Professor Doutor Francisco Veiga, agradeço antes de mais ter-me proporcionado a oportunidade de iniciar este percurso científico. Agradeço ainda o incentivo e apoio na procura de colaborações que permitiram o meu enriquecimento tanto no âmbito científico como pessoal.

Je remercie au Professeur Denis Wouessidjewe pour me recevoir chez l'Équipe Nanoparticules et Vectorisation à l'Université Joseph Fourier à Grenoble et pour m'avoir donné l'accès a tout les ressources nécessaires pour la réalisation des études de formulation décrits dans cette Thèse. Je veux aussi remercier les connaissances transmises par Anabelle Gèze et Luc Choisnard, la coopération de Christophe Ribuot, et la cordialité et sympathie de tout le monde au Département de Pharmacochimie Moléculaire.

A la Doctora Isabel Vázquez, quiero agradecer la pronta disponibilidad para recibirme en el grupo de Nutrición, Crecimiento y Metabolismo Intermediario en Peces en la Universidad de Barcelona. Le agradezco la oportunidad magnifica de aprender las técnicas de biología

molecular que añadieron una importante contribución a estos estudios. También querría agradecer al Doctor Isidoro Méton y a Diego Gonzalez por compartir sus conocimientos conmigo. Además soy grata por el cariño con que todos me acogieron en particular y quiero dejar una palabra de reconocimiento y amistad también al Ivan Viegas, Mari Carmen Salgado y Marina Giralt. Ao Ivan quero ainda agradecer a sua generosidade e apoio.

Agradeço à Professora Doutora Madalena Caldeira o carinho e cordialidade com que sempre me recebeu e as suas palavras de incentivo.

Gostaria ainda de deixar algumas palavras àqueles que foram meus colegas e companheiros na Universidade de Coimbra nalgum momento durante estes cinco anos. À Patrícia Nunes agradeço a generosidade, disponibilidade e preciosa ajuda no laboratório e também o contagiante entusiasmo com que sempre me incentiva. Ao João Duarte quero expressar o meu reconhecimento pelo entusiasmo, rigor e sentido crítico com que encara a ciência e que sempre me inspiram. Ao João e à Patrícia quero ainda agradecer o tempo que dedicaram à revisão desta Tese. À Catarina Reis quero manifestar o meu apreço pelo seu constante apoio e preocupação. À Fátima Martins, ao Marco Alves e à sempre disponível Ana Maria Silva agradeço a ajuda nos trabalhos laboratoriais, o companheirismo e boa disposição. Quero também expressar o meu apreço pela boa companhia e espirito de inter-ajuda à Cristina Barosa, Teresa Delgado, Daniela Pinheiro, Joana Barra, Filipa Simões e Rita Gonçalves. Ainda, gostaria de agradecer a boa disposição na partilha de agradáveis momentos à Doutora Ivana Jarak, à Cristina Lemos e ao Ludgero Tavares, bem como ao Doutor Ângelo Tomé e ao Dr. Manuel Matos.

Aos meus amigos e amigas, em especial à Teresa, Joana e Rita agradeço a constante presença e a força que vem das alegrias que partilhamos. À minha família agradeço os domingos e a energia que eles me dão.

À minha mãe e ao meu pai sou grata pelo permanente e incondicional apoio e por terem cuidado de me dar as melhores condições ao seu alcance. Graças aos seus esforços pude (e posso) escolher.

Energy is eternal delight
William Blake

TABLE OF CONTENTS

SYMBOLS, ABBREVIATIONS AND EXPRESSIONS

AAC	Area above the curve
ACC	Acetyl coenzyme A carboxylase
Acetyl-CoA	Acetyl coenzyme A
Ad libitum	Latin expression meaning "at one's pleasure"
ADP	Adenosine diphsosphate
AE	Association efficacy
AMP	Adenosine monophsosphate
ANOVA	Analysis of variance
apoB	Apolipoprotein B
ATP	Adenosine triphoshphate
AUC	Area under the curve
BW	Body water
^{13}C	Carbon 13
C1D	Doublet component of carbon 1 resonance
C1Q	Quartet component of carbon 1 resonance
C1S	Singlet component of carbon 1 resonance
cAMP	Cyclic adenosine monophsosphate
CD	Cyclodextrin
cDNA	Complementary deoxyribonucleic acid
ChREBP	Carbohydrate response element binding protein
CL	Citrate lyase
CPT1	Carnitine palmitoyltransferase 1
δ	Chemical shift
D	Doublet
Dh	Hydrodynamic diameter
DHAP	Dihydroxyacetonephosphate
DM	Diabetes *mellitus*
DMSO	Dimethyl sulfoxide
DNA	Deoxyribonucleic acid
DNL	*De novo* lipogenesis
e.g.	*exempli gratia*, Latin expression meaning "for the sake of example"

EGP	Endogenous glucose production
et al.	*et alii*, Latin expression meaning "and others"
EWAT	Epididymal white adipose tissue
$F2,6P_2$	Fructose-2,6-bispohsphate
F6P	Fructose-6-phosphate
FAS	Fatty acid synthase multienzyme complex
FBP	Fructose-1,6-bisphosphate
FBPase	Fructose-1,6-bisphosphatase
FoxO1	Forkhead box O1
G1P	Glucose-1-phosphate
G3P	Glycerol-3-phosphate
G6P	Glucose-6-phosphate
G6Pase	Glucose-6-phosphatase
Gal1P	Galactose-1-phosphate
[1-^{13}C]galactose	Galactose enriched with ^{13}C in carbon 1
γ-CDC_{10}	Gamma-cyclodextrin esters with 10 carbon alkyl chains
gdw	Gram of dry weight
GIT	Gastrointestinal tract
GK	Glucokinase
GKRP	Glucokinase regulatory protein
[1,2-$^{13}C_2$]glucose	Glucose enriched with ^{13}C in carbons 1 and 2
[1,2,3-$^{13}C_3$]glucose	Glucose enriched with ^{13}C in carbons 1, 2 and 3
[U-^{13}C]glucose	Glucose enriched with ^{13}C in all carbons
[U-^{14}C]glucose	Glucose enriched with carbon 14 in all carbons
[2-^{3}H]glucose	Glucose enriched with tritium in position 2
Glut-2	Glucose transporter 2
GP	Glycogen phosphorylase
GS	Glycogen synthase
GSK3	Glycogen synthase kinase 3
^{1}H	Proton
^{2}H	Deuterium
$^{2}H_2O$	Deuterated water
HDL	High density lipoproteins
HMQC	Heteronuclear multiple quantum coherence

HPLC	High performance (or pressure) liquid chromatography
i.e.	*id est*, Latin expression meaning "that is"
i.p.	Intraperitoneal
IRS	Insulin receptor substrate
J	Internuclear scalar coupling constant
[U-^{13}C]lactate	Lactate enriched with ^{13}C in all carbons
LPL	Lipoprotein lipase
LSD	Least significant difference
m/z	Mass to charge ratio
MAG	Monoacetone glucose
[1-^{13}C]MAG	Monoacetone glucose enriched with ^{13}C in carbon 1
[1,2-$^{13}C_2$]MAG	Monoacetone glucose enriched with ^{13}C in carbons 1 and 2
[1,2,3-$^{13}C_3$]MAG	Monoacetone glucose enriched with ^{13}C in carbons 1, 2 and 3
[U-^{13}C]MAG	Monoacetone glucose enriched with ^{13}C in all carbons
MALDI-MS	Matrix-assisted laser desorption/ionization-mass spectrometry
Malonyl-CoA	Malonyl coenzyme A
MIDA	Mass isotopomer distribution analysis
mRNA	Messenger ribonucleic acid
MTP	Microssomal transfer protein
N	Number of animals
n.s.	Non significant
NADH	Nicotinamide adenine dinucleotide (reduced form)
NADP	Nicotinamide adenine dinucleotide phosphate (oxydized form)
NADPH	Nicotinamide adenine dinucleotide phosphate (reduced form)
NEFA	Non-esterified fatty acids
NMR	Nuclear magnetic resonance
OAA	Oxaloacetate
O-GlcNAcase	*N*-acetyl-β-D-glucosaminidase
OGTT	Oral glucose tolerance test
[U-^{2}H]palmitic acid	Palmitic acid enriched with ^{2}H in the aliphatic protons
PC	Pyruvate kinase
PCR	Polymerase chain reaction
PDH	Pyruvate dehydrogenase multienzyme complex
PEP	Phosphoenolpyruvate

PEPCK	Phosphoenolpyruvate carboxykinase
per se	Latin expression meaning "in itself"
PFK	Phosphofructokinase
PI	Polydispersity index
PI3K	Phosphatidylinositol 3-kinase
PK	Pyruvate kinase
PKA	Protein kinase A
PKB	Protein kinase B
PLGA	Poly-lactide-*co*-glycolide
PP2A	Protein phosphatase 2A
ppm/PPM	Parts per million
[U-^{13}C]pyruvate	Pyruvate enriched with ^{13}C in all carbons
QELS	Quasi-elastic light scattering
rcf	Relative centrifugal force
RG	Residual glycogen
RT	Reverse transcriptase
s.c.	Subcutaneous
SEM	Standard error of the mean
SM	Satellite multiplets
SREBP1c	Sterol regulatory element binding protein 1c
STZ	Streptozotocin
TCA	Tricarboxylic acid
TEM	Transmission electron microscopy
TG	Triglyceride
Tris	Tris(hydroxymethyl)aminomethane
UDPG	Uridine diphosphate glucose
[U-^{13}C]UDPG	Uridine diphosphate glucose enriched with ^{13}C in all carbons
UDPgal	Uridine diphosphate galactose
VLDL	Very low density lipoproteins
vs	*Versus*, Latin expression meaning "against"
WHO	World Health Organization

SUMMARY

Diabetes *mellitus* (DM) is a metabolic disorder that results from a dysfunction of insulin secretion (type 1) and/or sensitivity (type 2). Type 1 and in many cases type 2 diabetic patients require daily insulin injections to control blood glucose levels and retard the appearance of diabetes-related complications. The liver plays a central role in the context of whole-body glucose homoeostasis and fuel management in general. Under physiological conditions, insulin is released by the pancreas into the portal vein and reaches the liver along with the nutrient flow absorbed in the gastrointestinal tract (GIT). Under these conditions, the actions of insulin on liver metabolism play a key role in promoting glucose and lipid storage. DM is characterized by impairment of these actions resulting in abnormal levels of blood glucose and lipids that, if left untreated, provoke widespread secondary complications. With current therapies, insulin is delivered subcutaneously and this results in a predominantly peripheral uptake, in contrast with the physiological release profile. The experimental work described on this thesis addressed the pathways for glucose disposal and storage in the liver under two experimental settings representing the fasted to fed transition and the fed state. The studies were performed in non-diabetic control rats and in a rat model for type 1 DM, the streptozotocin (STZ)-diabetic rat. The delivery of insulin by alternative liver-targeted routes was also explored.

A general introduction is presented in chapter 1. Diabetes and its therapy are briefly addressed and the STZ-diabetic rat model for the study of type 1 DM is introduced. Hepatic glucose and lipid metabolism are overviewed with emphasis to its regulatory aspects, and molecular mechanisms of insulin signaling are integrated with the metabolic regulation. In the last section of this chapter the use of stable isotope tracers for the study of hepatic metabolism is briefly overviewed.

In the studies described in chapter 2, rats were challenged with a carbohydrate load after a 24-hour fast and glucose disposal was addressed by carbon 13 (^{13}C) and deuterium (^{2}H) nuclear magnetic resonance (NMR) spectroscopy. One group of animals was given a glucose load and the other a mixture consisting of 9 equivalents of glucose and 1 equivalent of galactose. Hepatic glycogen was depleted with fasting and increased 8-10 times after the carbohydrate loads. The gluconeogenic flux dominated both glycogen synthesis and endogenous glucose production (EGP). Galactose hepatic metabolization resulted in a decreased contribution of load glucose to glycogen but apparently had little effect on the clearance of load glucose from the blood.

Chapter 3 presents the glucose challenge study performed in STZ-diabetic rats after a 24-hour fast. One group of animals was injected insulin by the subcutaneous (s.c.) route prior to receiving the glucose load. In another group insulin was delivered to the intraperitoneal (i.p.) cavity to provide a higher portal/peripheral ratio and target the liver. In a last group, rats did not receive any treatment. Glucose disposal was traced by ^{13}C and ^{2}H NMR methods. There was no net hepatic glycogen synthesis during the test, not even in the insulin-treated rats. The untreated STZ-diabetic rats showed increased EGP coupled with reduced clearance of load glucose. The absolute contribution of EGP to blood glucose in the insulin-treated rats was reduced to control levels, regardless of the route of insulin administration. Glucose clearance was highly enhanced in the insulin-treated rats even when compared to controls. These studies indicate that in the context of a glucose challenge, the stimulatory effect of insulin on glucose uptake is much higher than its inhibitory effect on EGP.

The absorptive state was addressed in chapter 4, and hepatic metabolism was studied in *ad libitum* fed STZ-diabetic and non-diabetic control rats with the deuterated water ($^{2}H_2O$) tracer approach. In controls, net glycogen synthesis during an overnight feeding accounted for one third of the hepatic stores and was equally derived from the direct and indirect (gluconeogenic) pathways. The amount of glycogen synthesized by diabetic

rats was similar to controls in all stages of the disease but the hepatic glycogen content was lower 10 and 20 days after the induction by STZ, indicating that those animals had higher glycogen turnover rates. There was a progressive increase of the indirect pathway contribution to hepatic glycogen synthesis from 70% 4 days after diabetes induction to 90% at 10 and 20 days of the disease. Parallel to the disruption in glycogen synthesis, the contribution of gluconeogenesis to EGP was profoundly increased 10 and 20 days after diabetes induction but not in the earlier stage (4 days). The lipogenic pathway was promptly reduced 4 days after the induction of diabetes but the hepatic triglyceride (TG) content was similar to controls. With the progression of the diabetic condition, the contribution of the lipolytic flux increased, resulting in elevated hepatic TG content.

Chapter 5 describes the insulin replacement experiments in STZ-diabetic rats. The treatment protocol consisted in two daily injections by the s.c. or i.p. route and was carried out for 10 days. Hepatic metabolism was then addressed by the ^2H_2O method under natural feeding conditions. Gene expression and enzyme activity assays were also performed in liver samples from those rats. With both treatments there was a restoration of the direct pathway to glycogen synthesis and of the pathways to EGP. In the i.p.-treated rats glycogen stores could be recovered to control levels. The lipogenic pathway was also enhanced but was still lower than controls in both s.c.- and i.p.-treated groups. Despite the improvements on glycogen and TG synthesis in the liver, the gluconeogenic and lipolytic fluxes could not be efficiently suppressed with the insulin-replacement protocols.

Chapter 6 explores the use of novel nanoparticle-based delivery systems in insulin therapy. Experiments in control rats showed that the hypoglycemic response following s.c. injection of insulin was enhanced by the use of nanoparticles from poly-lactide-*co*-glycolide (PLGA), especially when γ-cyclodextrin esters with 10 carbon alkyl chains (γ-CDC_{10}) were present in the formulation. The oral route was also investigated but the nanoparticles were ineffective even after coating with an enteric polymer. Experiments in STZ-diabetic rats did not demonstrate any benefit of the

nanoparticle formulation relative to a standard insulin solution in terms of the hypoglycemic response following the s.c. injection nor in the context of a glucose challenge.

RESUMO

A diabetes *mellitus* constitui um perturbação metabólica que resulta de uma disfunção na secreção (tipo 1) e/ou sensibilidade (tipo 2) à insulin. Os doentes do tipo 1, e em muitos casos também do tipo 2, necessitam de injecções diárias de insulina para controlar os níveis plasmáticos de glucose e retardar o aparecimento de complicações relacionadas com a doença. O fígado é um órgão central na regulação da homeostase da glucose e na gestão energética em geral. Em condições fisiológicas, a insulina é secretada pelo pâncreas para a veia porta e chega ao fígado de forma consertada com a absorção de nutrientes no tracto gastrointestinal. Nestas condições, os efeitos da insulina no metabolismo hepático são fundamentais para promover o armazenamento de glucose e lípidos. A diabetes é caracterizada por perturbações nestes efeitos, que se refletem em níveis anormais de glucose e lípidos no sangue, os quais, não corrigidos, provocam o alastramento de complicações secundárias. Na terapêutica tradicional, a insulina é administrada por via subcutânea (s.c.), o que resulta numa insulinização predominantemente periférica, por oposição ao perfil de libertação fisiológico. O trabalho experimental descrito nesta tese estudou a captação e consumo de glucose pelo organismo e seu armazenamento no fígado em dois contextos experimentais representando a transição do jejum para o estado prandial e o estado prandial propriamente dito. Os ensaios foram realizados em ratos controlo e ratos tornados diabéticos por indução com estreptozotocina (STZ), um modelo animal para a diabetes tipo 1. Foram ainda estudadas vias alternativas para administração de insulina direccionada ao fígado.

O capítulo 1 apresenta uma indrodução geral. A diabetes e o seu tratamento são abordados de forma breve e o modelo animal de diabetes induzida por STZ é apresentado. O metabolismo hepático da glucose e dos lípidos é analizado sendo dado ênfase ao seu controlo e regulação. Aspectos

moleculares da transdução do sinal da insulina, com relevância para a regulação metabólica, são abordados. Por último, a aplicação de substratos enriquecidos com isótopos estáveis ao estudo do metabolismo hepático é apresentada.

Nos ensaios descritos no capítulo 2, os ratos receberam uma dose massiva de açúcares após 24 horas de jejum e o consumo de glucose foi seguido por espectroscopia de ressonância magnética nuclear de carbono 13 (^{13}C) e deutério (^{2}H). A um grupo de animais foi administrada uma dose de glucose e a outro uma mistura que consistiu em 9 equivalentes de glucose e 1 equivalente de galactose. As reservas de glicogénio no fígado foram consumidas no período de jejum e aumentaram 8-10 vezes após a ingestão das doses de açúcares. Tanto a produção endógena de glucose como a síntese de glicogénio hepático foram dominadas pelo fluxo da neoglucogénese. A metabolização hepática da galactose reduziu a contribuição da glucose exógena para a síntese de glicogénio mas pouco alterou a captação de glucose do sangue.

O capítulo 3 descreve a prova de tolerância à glucose realizada em ratos diabéticos por indução com STZ, após 24 horas de jejum. Um grupo de animais recebeu insulina por via s.c. antes da dose de glucose. Num outro grupo, a insulina foi injectada na cavidade intraperitoneal (i.p.) para aumentar a razão portal/periférica e direccionar a insulina para o fígado. Um último grupo não recebeu qualquer tratamento. O consumo de glucose foi avaliado por técnicas de RMN de ^{13}C e ^{2}H. Não houve síntese líquida de glicogénio no fígado, nem mesmo nos ratos injectados com insulina. Os ratos diabéticos que não foram injectados com insulina apresentaram um aumento da produção endógena de glucose acompanhado por uma redução da captação de glucose plasmática. A contribuição absoluta da produção endógena para a glucose plasmática nos ratos diabéticos injectados com insulina foi igual à observada nos controlos não diabéticos, independentemente da via de administração. O consumo de glucose proveniente da dose administrada foi bastante aumentado, mesmo em comparação com os controlos. Estes ensaios indicam que, no contexto de

uma prova de tolerância à glucose, a acção da insulina é mais notória na estimulação da captação de glucose do sangue do que na inibição da produção endógena de glucose.

O estado prandial propriamente dito foi abordado no capítulo 4. Ratos controlo e diabéticos por indução com STZ alimentados *ad libitum* foram estudados e o seu metabolismo hepático avaliado pelo método da água deuterada (^2H_2O). Nos ratos controlo, a síntese líquida de glicogénio durante uma noite de alimentação representou um terço do conteúdo hepático e seguiu as vias directa e indirecta (neoglucogénica) de forma equivalente. Os ratos diabéticos sintetizaram uma quantidade de glicogénio similar aos controlos em todos os estádios da doença avaliados, mas o conteúdo hepático total diminui 10 e 20 dias depois da indução da diabetes, significando que nestes casos houve uma maior renovação do glicogénio hepático. Verificou-se um domínio progressivo da via indirecta para a síntese de glicogénio, que aumentou de 70% 4 dias após a indução da diabetes para 90% 10 e 20 dias depois. Paralelamente às alterações no metabolismo do glicogénio, a contribuição da neoglucogénese para a produção endógena de glucose foi profundamente aumentada 10 e 20 dias após a indução de diabetes mas manteve-se igual à dos controlos aos 4 dias da doença. A via lipogénica foi imediatamente reduzida 4 dias depois da indução da diabetes mas o conteúdo hepático de triglicerídeos manteve-se igual ao dos controlos. Com a progressão da doença, a contribuição do fluxo lipolítico aumentou, levando ao aumento do conteúdo hepático de triglicerídeos.

O capítulo 5 relata as experiências de reposição da insulina em animais diabéticos. O protocolo de tratamento consistiu em duas injecções diárias por via s.c. ou i.p. durante 10 dias. O metabolismo hepático foi, então, seguido com ^2H_2O em condições de alimentação *ad libitum*. Foram ainda feitos ensaios de expressão genética e actividades enzimáticas em amostras de fígado destes animais. Ambos os tratamentos proporcionaram a recuperação das vias de síntese hepática de glicogénio bem como das vias para a produção de glucose para valores controlo. Os animais injectados

com insulina por via i.p. apresentaram níveis de glicogénio no fígado semelhantes aos controlos. A via lipogénica também foi potenciada mas manteve-se abaixo dos valores dos controlos com ambos os tratamentos. Apesar das melhorias na síntese hepática de glicogénio e triglicerídeos, os fluxos da neoglucogénese e lipólise não foram suprimidos com os protocolos de reposição de insulina.

O capítulo 6 explora o uso de novas formulações de nanopartículas na terapêutica com insulina. As experiências em ratos controlo mostraram que a acção hipoglicémica da insulina foi potenciada através do uso de nanopartículas de um co-polímero de ácido láctico e glicólico (PLGA), mormente com a inclusão de esters da γ-ciclodextrina com cadeias alquílicas de 10 carbonos (γ-CDC_{10}). A via oral também foi investigada mas a formulação não se mostrou eficaz, nem quando as nanopartículas foram revestidas com um polímero entérico. Nas experiências em ratos diabéticos por indução com STZ não ficou demonstrado qualquer benefício da formulação de nanopartículas em relação a uma solução padrão de insulina em termos de acção hipoglicémica após administração s.c. nem no contexto de uma prova de tolerância à glucose.

LIST OF PUBLICATIONS

Part of the scientific work presented in this thesis has been published in the following articles in peer-reviewed international scientific journals or is under preparation in the following manuscripts:

Soares AF, Carvalho RA & Veiga FJ (2007), Oral administration of peptides and proteins: nanoparticles and cyclodextrins as biocompatible delivery systems. Nanomedicine 2, 183-202. (doi:10.2217/17435889 2. 2.183)

Soares AF, Veiga FJ, Carvalho RA & Jones JG (2009), Quantifying hepatic glycogen synthesis by direct and indirect pathways in rats under normal *ad libitum* feeding conditions. Magnetic Resonance in Medicine 61, 1-5. (doi:10.1002/mrm.21830)

Soares AF, Carvalho RA, Veiga FJ & Jones JG (2010), Effects of galactose on direct and indirect pathway estimates of hepatic glycogen synthesis. Metabolic Engineering 12, 552-560. (doi:10.1016/j.ymben.2010.08.002)

Soares AF, Gèze A, Choisnard L, Ribuot C, Faure P, Carvalho RA, Jones JG, Veiga FJ & Wouessidjewe D, Enhancement of insulin's biological effect by PLGA-Cyclodextrin esters nanoparticles (in preparation).

Soares, AF, Alves MG, Viegas I, Gonzalez JD, Veiga FJ, Méton I, Baanante IV, Carvalho RA & Jones JG, Effect of subcutaneous and intraperitoneal insulin replacement on the hepatic metabolic disruptions in the STZ-diabetic rat (in preparation).

1
GENERAL INTRODUCTION

All life forms exist in a state of dynamic equilibrium. Life relies on the flux of matter and energy through the cellular metabolic pathways and during these processes the balance between nutrient intake and the release of excretory products must be maintained (Fell 1997). Several levels of control including biochemical, endocrine, physiological, neuronal and behavioral are involved in the interplay between energy intake, storage and expenditure (Friedman 1995). The liver is a central organ in the context of energy balance and fuel management and hence plays an important role in whole-body metabolism.

Glucose is a universal source of energy for cells in the organism. The liver is responsible both for glucose production during fasting and its disposal and storage in the fed state. Those pathways are connected to the processing of other fuels like lipids and proteins in the intricate network of whole-body metabolism. Glucose, protein and lipid metabolism are

regulated, among other factors, by the pancreatic hormone insulin. Diabetes *melittus* (DM) is characterized by a dysfunction of insulin secretion and/or sensitivity, which results in metabolic disruptions.

The following sections address briefly DM pathology and treatment as well as an experimental animal model for its study. Hepatic glucose and lipid metabolism is overviewed with focus on its regulatory aspects and integration with insulin action. Finally, tracer-based approaches to the study of these metabolic pathways are generally discussed.

1.1 Diabetes *mellitus*

The World Health Organization (WHO) describes DM as "a metabolic disorder of multiple etiology characterized by chronic hyperglycemia with disturbances of carbohydrate, fat and protein metabolism, resulting from defects in insulin secretion, insulin action or both" (WHO 1999). The WHO report from 2006 recommends as diagnosis criteria fasting plasma glucose ≥ 7.0 mM (126 mg/dL) or 2-hour[1] plasma glucose ≥ 11.1 mM (200 mg/dL) (WHO 2006).

The current classification of DM is based on the clinical stages as well as the etiology of the disease (WHO 1999). Type 1 DM results from β cell destruction secondary to idiopathic or auto-immune factors; whereas type 2 DM may range from predominantly insulin resistance with relative insulin deficiency to predominantly insulin deficiency with relative insulin resistance. The previous types constitute the basic forms of diabetes and while there may be several therapeutic options for type 2 diabetic patients, the treatment of type 1 DM relies completely on the administration of exogenous insulin. With insulin administration (to type 1 and in some cases also type 2 diabetic patients) hyperglycemia is prevented and when a strict metabolic control is followed (Atkinson *et al.* 2001), the diabetes-related

[1] Refers to the oral glucose tolerance test (OGTT) where plasma glucose is measured 2 hours after the ingestion of a 75 g oral glucose load following an overnight fast.

complications (retinopathy, nephropathy, neuropathy, heart disease, among others) are delayed, with benefits for the patients' quality of life.

1.1.1 Insulin therapy and formulation

Before the discovery of insulin in the 1920s the life span of people diagnosed with diabetes was rarely beyond childhood. Although insulin doesn't cure diabetes, its value in the treatment of diabetic patients was immediately recognized by the attribution of the Nobel Prize in Physiology and Medicine to Banting and Macleod in 1923 for "The discovery of insulin" (Nobelprize.org 2010).

Following the discovery of insulin many advances were made concerning its isolation and purification. In the 1980s the technology of recombinant deoxyribonucleic acid (DNA) allowed for the industrial production and commercial expansion of human insulin and, in the last 15 years, modified insulins (with altered amino acid sequences) produced by biotechnology engineering techniques resulted in enhanced stability and/or modulation of the duration of action (Pillai *et al.* 2001).

Despite the huge amount of improvements on insulin therapy, its administration often requires multiple daily injections via the subcutaneous (s.c.) route. This is unpleasant for the patients, thus compromising their compliance to the treatment. Furthermore, delivery by the s.c. route is unable to mimic the physiologic portal to peripheral gradient resulting in deficient hepatic insulinization. This may limit the metabolic performance of insulin-treated diabetic patients compared to that of healthy individuals, particularly in the case of hepatic-specific actions such as glycogen kinetics (Bischof *et al.* 2002).

Presently, research on insulin formulation is focused on exploring more patient-friendly routes such as the oral (*e.g.* Chalasani *et al.* 2007; Damgé *et al.* 2007; Reis *et al.* 2008) or pulmonary (*e.g.* Johansson *et al.* 2002; Aguiar *et al.* 2004). The oral route has the advantage of delivering insulin to the portal vein, resembling the physiological release and appropriately

targeting the liver. Therefore, effective oral delivery may constitute an important strategy for optimizing the metabolic effects of insulin. This can be achieved by the use of specialized delivery systems such as nanoparticles (explored in chapter 6).

Alternatively to the insulin supplementation therapy, providing diabetic patients with functional β cells constitutes the ultimate goal of DM treatment. Pancreas and isolated islet transplantation has allowed for diabetic patients to produce their own insulin (Shapiro *et al.* 2000; Sutherland *et al.* 1998). In the context of β cell replacement, the liver is commonly used as a surrogate for the pancreatic function. For example, in islet transplantation protocols the portal vein is used to graft the β cells (Shapiro *et al.* 2000). Moreover, with advances in stem cell technology, cells in the liver have been reprogrammed to express the β cell phenotype (Aguayo-Mazzucato *et al.* 2010; Halban *et al.* 2010; Wagner *et al.* 2010). In addition, using virus as gene delivery vehicles has allowed for the basal hepatic insulin expression in diabetic rats and translated into improved glycemic control (Dong *et al.* 2002).

1.1.2 The STZ-diabetic rat as a model for type 1 diabetes

The diabetogenic action of streptozotocin (STZ) was discovered in the 1960s (Junod *et al.* 1969) and ever since this drug has been widely used in the experimental setting to induce diabetes in rodents.

In rats, type 1 DM is induced by a single intravenous injection of STZ at a dose no lower than 45 mg/kg (Junod *et al.* 1969). Alternatively, STZ can be delivered to the intraperitoneal (i.p.) cavity at a dose no lower than 50 mg/kg (Szkudelski 2001). Typically, doses of 50-65 mg/kg lead to chronic hyperglycemia and higher doses cause severe ketosis and death within days (Wei *et al.* 2003). Additionally, STZ can induce type 2 DM if rats are injected a high dose of the drug (~100 mg/kg) in the first days that follow birth (Szkudelski 2001).

Structurally, STZ is a nitrosouria derivative with a hexose moiety that allows it to enter the cells by the same transporter as glucose. Uptake of STZ occurs specifically via the glucose transporter 2 (Glut-2), which is the principal glucose transporter in rodent β cells (Wollheim *et al.* 2004), and this seems to be essential for its toxic action (Hosokawa *et al.* 2001). In addition, STZ is also toxic to other tissues expressing Glut-2, like the liver or the kidney, and the damage on extra pancreatic cells may also account for the pathology that characterizes the STZ-diabetic rat (Lenzen 2008).

Several cytotoxicity mechanisms, ultimately leading to cell death, are described for the deleterious action of STZ in β cells. Streptozotocin causes direct damage on DNA by alkylation (Bolzán *et al.* 2002). In addition, STZ acts as a nitric oxide donor leading to the production of reactive oxygen species that also account for the DNA damage (Szkudelski 2001). Recently, another toxicity mechanism has been proposed in which STZ inhibits the activity of *N*-acetyl-β-D-glucosaminidase (O-GlcNAcase), the enzyme that removes *N*-acetylglucosamine from proteins, hence contributing to increase protein glycosilation in β cells (Konrad *et al.* 2001; He *et al.* 2009). Moreover, O-GlcNAcase from pancreatic islets was found to be more sensitive to STZ than that from other tissues (Konrad *et al.* 2001), providing supporting evidence for the β cell selectivity of STZ.

The STZ-induced type 1 diabetic rat model displays the typical symptoms of type 1 DM present in humans (*e.g.* polyphagia, polydipsia and polyuria). Blood glucose levels rapidly increase within hours after the administration of a diabetogenic dose of STZ to adult rats, in parallel with a decrease in insulin levels (Burcelin *et al.* 1995). Food and water consumption increase in the first days and remain elevated for several weeks while weight gain is restrained (Wei *et al.* 2003). Hence, the STZ-diabetic rat is a very popular model for experimental type 1 DM and is used recurrently in addressing the pathophysiology of the disease and in characterizing the efficacy of antidiabetic interventions (*e.g.* Ferrannini *et al.* 1990; Akirav *et al.* 2004; Iwasaki *et al.* 2005; Lo *et al.* 2006; Suthagar *et al.* 2009).

1.2 Overview of hepatic glucose and lipid metabolism

Following meal digestion in the gastrointestinal tract (GIT), nutrients are absorbed to the blood and reach the liver via the portal vein. This event is consonant with the release of insulin from the pancreatic β cells into the portal vein, in response to glucose (and also protein and fatty acid) stimulation (Utzschneider *et al.* 2004). Under physiological conditions, the liver extracts 50-80% (Radziuk *et al.* 1994; Utzschneider *et al.* 2004) of portal vein insulin with the remainder reaching the systemic circulation. In the liver, insulin suppresses hepatic glucose production, which is active in the post absorptive or fasted state, and stimulates pathways for glucose disposal and storage as glycogen and lipids. The liver alone accounts for the extraction of one third of a glucose load, muscle and fat for another third and brain and red blood cells for the remaining third (Cherrington 1999). On the other hand, during fasting, the brain takes up about 80% of the glucose produced endogenously (Baron *et al.* 1988).

1.2.1 Glucose disposal and storage

Figure 1 depicts the fates of glucose in the liver, in the postprandial or absorptive state. Glucose enters the hepatocyte through the Glut-2 transporter, which is primarily expressed in the liver but is also present in kidney, intestine and pancreatic β cells (Nordlie *et al.* 1999). Other dietary sugars like fructose or galactose also enter the liver through this transporter. The transport of glucose via Glut-2 is bidirectional; moreover Glut-2 has low affinity and high capacity for glucose facilitating both the efflux and uptake of glucose in the range of concentrations necessary for glucose homeostasis (Nordlie *et al.* 1999).

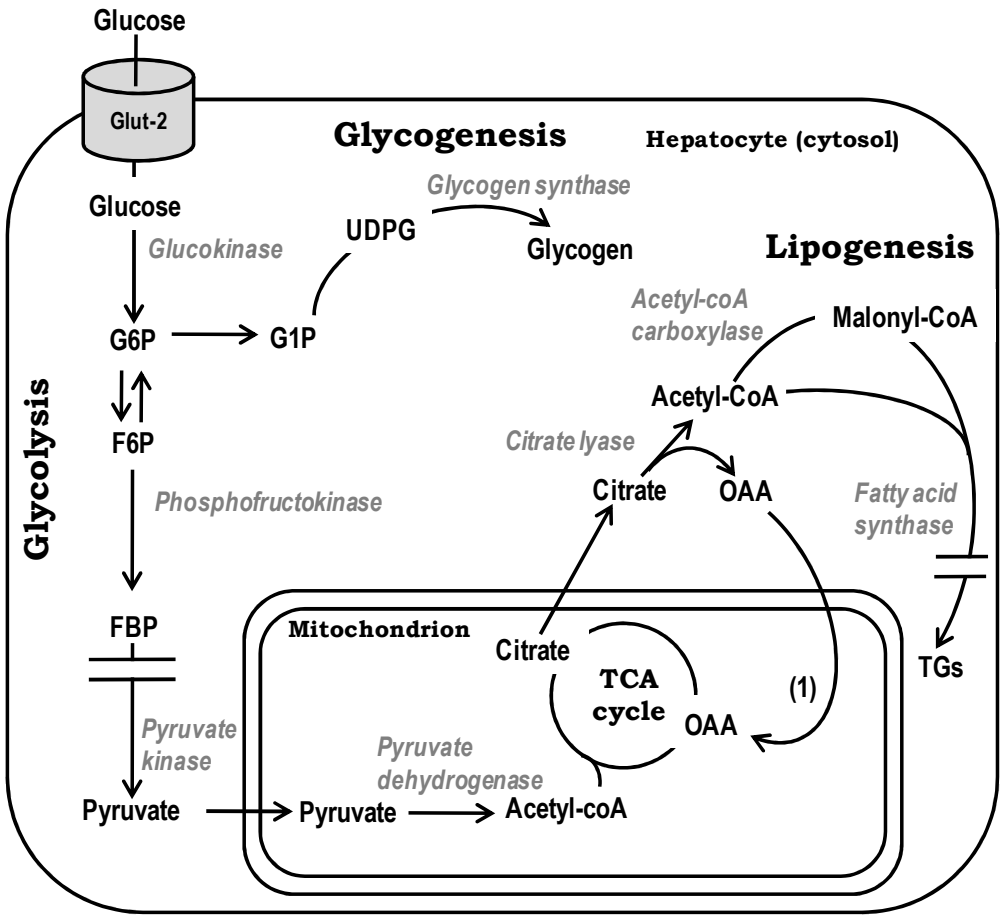

Figure 1 Schematic overview of the pathways for glucose disposal in the liver. Glycolysis, glycogenesis and *de novo* lipogenesis are presented and the key enzymes and glucose transporter involved are shown. For simplicity, some reactions in the pathways are omitted (discontinued arrows). (1) OAA is first converted to malate (and eventually further to pyruvate) in the cytosol prior to being transported back into the mitochondrion and resynthesized to OAA. Acetyl-CoA, acetyl coenzyme A; F6P, fructose-6-phosphate; FBP, fructose-1,6-bisphosphate; G1P, glucose-1-phosphate; G6P, glucose-6-phosphate; Glut-2, glucose transporter 2; malonyl-CoA, malonyl coenzyme A; OAA, oxaloacetate; TGs, triglycerides; UDPG, uridine diphosphate glucose.

In the liver, the first reaction in glucose metabolism is the adenosine triphosphate (ATP)-dependent conversion of glucose to glucose-6-phosphate (G6P) by hexokinase IV or glucokinase (GK). Glucokinase is expressed in the liver and pancreatic β cells and unlike the other

hexokinases (I, II and III) it displays low affinity for the substrate. Furthermore, GK is not inhibited by physiological concentrations of the reaction product, G6P, and this allows the feed-forward activation of subsequent disposal fluxes (Agius 2008). In the liver, the control of GK activity is dependent in a regulatory protein (GKRP) that acts as an inhibitory competitor in regards to glucose (Agius 2008). It is widely accepted that under basal conditions of 5.5 mM glucose concentration, GK exists sequestered in the nucleus in association with GKRP and that GK is released and translocated to the cytosol under high glucose or low fructose concentration (Agius *et al.* 1993; de la Iglesia *et al.* 1999; Agius 2008). Fructose-1-phosphate, whose intrahepatic levels increase in the postprandial state, binds to GKRP causing the weakening of its interaction with GK, and this results on the release of the active GK (Iynedjian 2009). On the other hand, in the postabsorptive state, fructose-6-phosphate (F6P) binds to GKRP stimulating its interaction with GK (Iynedjian 2009), which is consequently imported back to the nucleus. This way GK degradation is prevented and at the same time a large stable pool of the enzyme is conserved for recruitment upon refeeding (Newgard 2004).

Glucose uptake through Glut-2 is coordinated with its phosphorilation by GK (Figure 1) resulting in the formation of G6P, which can be directed to glycogen synthesis or glycolysis.

1.2.1.1 Glycogen synthesis

Glycogen deposition occurs in the liver after a meal. The hepatic glycogen stores represent an important source of glucose to be released in the fasted state by the liver so that plasma glucose levels remain within the physiological range and whole-body energetic demands are fulfilled. Net glycogen synthesis results from the interplay between glycogen synthase (GS) and glycogen phosphorylase (GP) activities. In the biogenesis of glycogen, G6P is first converted to glucose-1-phosphate (G1P) by phosphogluco isomerase and subsequently to uridine diphosphate glucose

(UDPG) by UDPG pyrophosphorylase. Glycogen synthase then adds glucose residues from the UDPG donor to the growing glycogen molecule via *a*-1,4 bonds.

The formation of glycogen is intimately related to glucose phosphorylation by GK. In fact, glycogen synthesis is sensitive to increases in GK activity secondary to glucose-induced translocation of GK (Agius *et al.* 1996). Furthermore, when GK translocates to the cytosol it is directed to the plasma membrane in a way that allows the coupling of glucose phosphorylation with glycogen synthesis (Jetton *et al.* 2001). The fact that GK overexpression enhances glycogen deposition (O'Doherty *et al.* 1996; Seoane *et al.* 1999; Morral *et al.* 2004), further demonstrates the dependence of glycogen synthesis on GK. The product of the GK reaction, G6P, is not only a precursor to glycogen but also a regulator itself of GS activity. Hepatic GS exists in an inactive form in the cytosol and it is activated and directed to the periphery of the cell via G6P stimulation (Ferrer *et al.* 2003). The binding of G6P to the phosphorylated (inactive) isoform of GS, causes a conformational change that makes it a better substrate for protein phosphatases, which then convert the enzyme to the active (dephosphorylated) isoform (Villar-Palasi *et al.* 1997; Ferrer *et al.* 2003). Insulin stimulates GS by increasing the protein phosphatase activity (Khandelwal *et al.* 1977; Newgard *et al.* 2000). The activity of GP, which catalyzes the breakdown of glycogen to G1P molecules, is also regulated by phosphorylation in a coordinated fashion with GS, with the dephosphorylated isoform being less active than the phosphorylated (Ferrer *et al.* 2003).

The direct conversion of glucose to glycogen via GK and GS coordinated fluxes does not account for the whole of glycogen deposition in the absorptive state and a significant contribution from gluconeogenic precursors is required for efficient glycogen synthesis to occur (Newgard *et al.* 1983; Katz *et al.* 1984; Newgard *et al.* 1984). This latter route is known as the indirect pathway, where glucose is initially metabolized to 3-carbon intermediates followed by gluconeogenic re-synthesis into hexose

phosphate (Figure 2). This route also allows non-hexose precursors such as glycerol or gluconeogenic amino acids to be converted to glycogen. The relative contributions of both pathways depend on the nutritional and pathophysiological status of the organism, with the indirect pathway contribution to glycogen synthesis increasing with fasting (Shulman *et al.* 1990; Hellerstein *et al.* 1995), type 1 DM (Hwang *et al.* 1995) or GK deficiency (Velho *et al.* 1996).

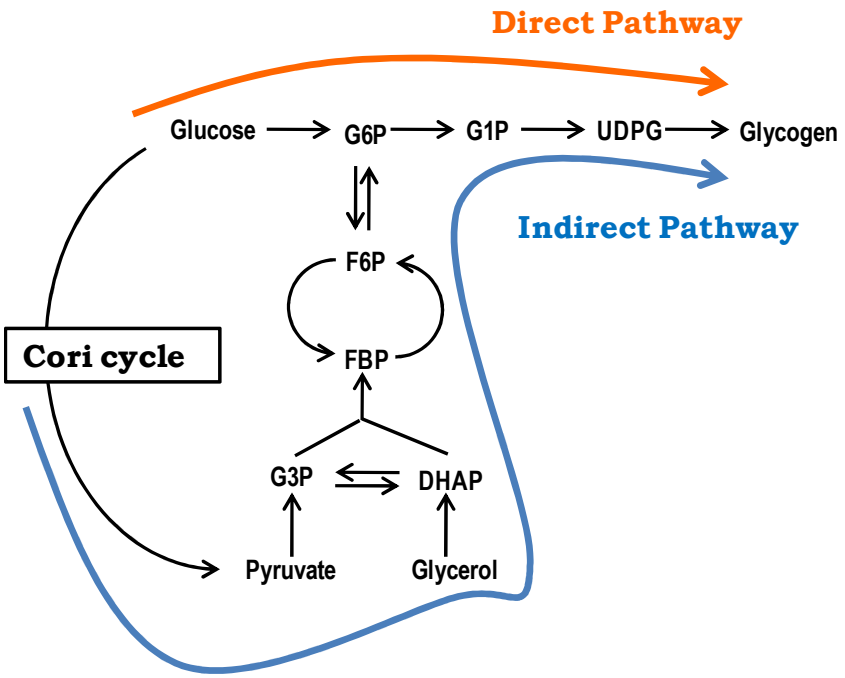

Figure 2 Pathways for glycogen synthesis in the liver. By the direct pathway (orange arrow) glucose is converted to glycogen via glucokinase and glycogen synthase coordinated activities. Alternatively, glucose can be first metabolized to 3-carbon intermediates (mostly in the muscle) that are used in the liver to generate G6P for glycogen synthesis via the indirect pathway (blue arrow). DHAP, dihydroxyacetone phosphate; F6P, fructose-6-phosphate; FBP, fructose-1,6-bisphosphate; G1P, glucose-1-phosphate; G6P, glucose-6-phosphate; G3P, glyceraldehyde 3-phosphate; UDPG, uridine diphosphate glucose.

1.2.1.2 Glycolysis and lipogenesis

Glycolysis refers to the series of cytosolic reactions that break down one glucose molecule to two pyruvate molecules. The first step in the glycolytic pathway is the highly regulated phosphorylation of glucose to G6P by GK, already overviewed. This reaction, together with the conversion of F6P to fructose-1,6-bisphosphate (FBP) catalyzed by phosphofructokinase (PFK) and the conversion of phosphoenolpyruvate (PEP) to pyruvate catalyzed by pyruvate kinase (PK) constitute the irreversible steps in glycolysis. The energy charge of the cell, as well as allosteric and transcriptional processes contribute to control the flux thourgh PFK and PK. Briefly, PFK and PK are stimulated by insulin, glucose and products from its early metabolism, while a high ratio of ATP to adenosine diphosphate (ADP) plus adenosine monophosphate decreases the activity of those enzymes (Newgard 2004).

The most important activator of hepatic PFK is fructose-2,6-bisphosphate ($F2,6P_2$), which is degraded (to F6P and inorganic phosphate) and regenerated (from F6P and inorganic phosphate) by the bifunctional enzyme, 6-phosphofructo-2-kinase/fructose-2,6-bisphosphatase. In the fed state, xylulose-5-phosphate derived from glucose metabolization via the pentose phosphate pathway stimulates protein phosphatase 2A (PP2A) that dephosphorylates the bifunctional enzyme, favoring its kinase activity and the formation of $F2,6P_2$ (Newgard 2004). Experiments in fasted rats showed that hepatic levels of $F2,6P_2$ start to increase several hours after glucose administration or refeeding, when glycogen stores in the liver are near to replenishment (Kuwajima *et al.* 1984; Kuwajima *et al.* 1986; Holness *et al.* 1988; Jin *et al.* 2003). Hence, under refeeding circumstances, stimulation of the glycolytic flux occurs after that of glycogen synthesis. Moreover, a positive correlation was observed between hepatic glycogen levels and the lipogenic rate after chow refeeding (Holness *et al.* 1988). Accordingly, when hepatic glycogen is depleted in humans by dietary intervention, excessive carbohydrate intake is disposed by high glucose oxidation rates and *de novo* lipid synthesis only after glycogen stores become saturated (Acheson *et al.*

1988). On the other hand, under natural feeding conditions, $F2,6P_2$ levels rise in parallel with glycogen in the liver (Bois-Joyeux *et al.* 1986) suggesting the sequence of events may not be the same as in refeeding conditions.

After the glycolytic phase, pyruvate enters the mitochondria and is oxidized to acetyl coenzyme A (acetyl-CoA) by pyruvate dehydrogenase multienzyme complex (PDH). This reaction links glycolysis to the tricarboxylic acid cycle (TCA cycle) and *de novo* lipogenesis (DNL). The activity of PDH is ruled by posphorylation (inhibition)-dephosphorylation (stimulation) mechanisms and inhibited by the end products acetyl-CoA and nicotinamide adenine dinucleotine in the reduced form (NADH) (Strumiło 2005). In rats, starvation, DM and low carbohydrate diet result in the inactivation of PDH whereas insulin and high carbohydrate loads activate PDH (Randle 1998). Furthermore, a decrease in circulating non-esterified fatty acids (NEFA) is observed under those conditions (high insulin, low glucagon). Since the activity of PDH is inhibited by increased mitochondrial levels of acetyl-CoA and NADH from NEFA metabolism (Randle 1998; Holness *et al.* 2003), reduced NEFA levels permit more PDH flux and a greater potencial for glycolytic acetyl-CoA generation. In rats, the decrease in hepatic DNL rate during fasting (decline in insulin and glucose levels) is accompanied by a progressive reduction of PDH activity (Holness *et al.* 1990). In contrast, the flux through PDH relative to that of the TCA cycle is increased under simultaneous hyperinsulinemia and hyperglycemia conditions (Alves *et al.* 2011).

The "first" reaction in the TCA cycle is the condensation of acetyl-CoA with oxaloacetate (OAA) to yield citrate, catalyzed by citrate synthase. Citrate is common to both pathways downstream acetyl-CoA formation. Alternatively to following the TCA cycle reactions, citrate can be exported to the cytosol where citrate lyase (CL) reconverts it to acetyl-CoA, which can be used in DNL, and OAA that returns to the mitochondria in the form of either malate or pyruvate. The cytosolic conversion of OAA to malate and further to pyruvate requires the sequential activities of malate dehydrogenase and nicotinamide adenine dinucleotine phosphate (NADP)-

malic enzyme. The latter reaction provides the majority of reducing equivalentes for DNL in the form of reduced NADP (NADPH). The remainder is produced in the pentose phosphate pathway by the activities of glucose-6-phosphate dehydrogenase (G6PDH) and 6-phosphogluconate dehydrogenase (6PGDH).

In addition to glycolytically-derived pyruvate, acetyl-CoA molecules for the lipogenic pathway may be produced from amino acid catabolism, fatty acid oxidation or acetate from intestinal fermentation. Malonyl coenzyme A (malonyl-CoA) is formed by the carboxylation of acetyl-CoA catalyzed by acetyl-CoA carboxylase (ACC). Malonyl-CoA is a physiological inhibitor of carnitine palmitoyltransferase 1 (CPT1) (Ruderman *et al.* 1999), which transports fatty acids from the cytosol to the mitochondrial matrix for β oxidation. In this way, fatty acids from DNL are directed to esterification resulting on the synthesis of triglycerides (TGs).

In humans, under normal conditions, daily hepatic DNL accounts only for a minor fraction of TG synthesis (3-7%) in the liver but this contribution is increased (up to 32%) by dietary (*e.g.* fructose, low fat-high carbohydrate diets) or hormonal intervention (*e.g.* insulin) (Hellerstein *et al.* 1996). In rodents, the contribution of DNL to the hepatic TGs ranges from 5% in 5-hour refed rats (Hellerstein *et al.* 1991) to 11% in 3-day *ad libitum* fed rats (Delgado *et al.* 2009a). Other studies report contributions up to 70% when the experiment was followed for two weeks, using a different rat specie (Lee *et al.* 2000; Bassilian *et al.* 2002).

1.2.2 Lipids disposal and storage

1.2.2.1 Brief overview of lipoprotein metabolism

Lipids are different from other nutrients since, with the exception of short-chain fatty acids, they are not directly delivered to the portal circulation upon intestinal absorption. Instead, water-insoluble dietary lipids are processed within the enterocyte and packed into chylomicrons

that are absorbed to the lymphatic circulation prior to reaching the blood. Chylomicrons are part of the specialized family of plasma lipid-carriers, lipoproteins. These structures are spherical particles composed of a hydrophobic core (cholesterol esters and TGs) and a hydrophilic surface monolayer of phospholipids, cholesterol and apolipoproteins. Lipoproteins with distinct functions and compositions arise from the dynamic crosstalk between the liver and peripheral tissues through the bloodstream.

The main function of chylomicrons is to transport diet-derived TGs to the tissues of destiny. After meals, the increase in plasma TGs is largely dependent on the chylomicron-TGs, although there is also a contribution from very low density lipoprotein (VLDL)-TGs (Frayn 2002). Chylomicron-TGs are hydrolyzed by the endothelial enzyme lipoprotein lipase (LPL) and the resulting fatty acids are taken up by the tissues and stored (adipose tissue) or used for oxidation (skeletal muscle). Also by LPL activity, VLDL secreted by the liver deliver fatty acids to extra-hepatic tissues. Insulin is a potent activator of LPL, stimulating its expression and activity in the adipose tissue (Frayn 2002; Vergès 2009). Accordingly, in insulin-deficient mice, LPL activity is reduced hampering the storage of fat in adipocytes (Pighin *et al.* 2005). In untreated type 1 diabetic patients, the lack of insulin causes hypertriglyceridemia as a consequence of the reduced catabolism of TG-rich lipoproteins (Vergès 2009) and the same is observed in insulin-deficient rats (Iwasaki *et al.* 2005).

With the further removal of TGs, VLDL remnant particles are converted to the cholesterol-enriched intermediate density lipoproteins and low density lipoproteins, which supply cholesterol to essentially all cells. Conversely high density lipoproteins (HDL) are responsible for the reverse transport of cholesterol to the liver for excretion in the bile. The liver secretes these particles as lipid-poor lipoproteins. In the circulation, nascent HDL receive phospholipids and apolipoproteins from chylomicrons and VLDL, and take up cholesterol and phospholips from the peripheral tissues (Vergès 2009).

1.2.2.2 Hepatic TG dynamics and VLDL metabolism

Besides DNL (see section 1.2.1.2), dietary and lipolytic sources contribute to the hepatic TG pool. As chylomicrons travel through the bloodstream they become depleted on TGs and the remnant particles are cleared from the blood by the liver through receptor-mediated endocytosis. Hence, dietary TGs reach the liver associated to the remnant chylomicrons. Hepatic lipase hydrolyses TGs from chylomicrons (and also other lipoproteins) releasing the fatty acids, which are re-esterified and stored as TGs in intra-hepatic lipid droplets (Sparks *et al.* 2009).

In addition, fatty acids from adipose tissue lipolysis transported by plasma albumin also contribute to the hepatic TG pool. This inflow of NEFA is particularly high during fasting and decreases rapidly after meals as a result of insulin action on suppressing hormone sensitive lipase in the adipose tissue (Frayn 2002). This event, coupled with the stimulation of LPL causes the net storage of TGs in the adipocyte in the postprandial state.

In the liver, TGs are packed along with cholesterol into VLDL and secreted to the bloodstream. A rate-limiting step in the formation of VLDL is the transfer of TGs to apolipoprotein B (apoB) by the microsomal transfer protein (MTP) (Kamagate *et al.* 2008). Insulin decreases VLDL secretion (Huang *et al.* 2009) by several mechanisms, including a direct inhibition of MTP gene expression and apoB synthesis (Sparks *et al.* 2009) and the suppression of NEFA release from adipose tissue as discussed above. Hence, and in accordance with the stimulation of DNL and of energy storage in general, insulin promotes the accumulation of TGs in the liver (Huang *et al.* 2009).

1.2.3 Glucose production

In the absence of exogenous glucose, provided by food intake, plasma glucose levels are maintained via endogenous glucose production (EGP). The liver is the main organ accounting for EGP but the kidney and

small intestine are also able to produce glucose and release it to the bloodstream (Mithieux *et al.* 2004), although their contribution only becomes significant in severe insulinopenic states such as prolonged fasting or diabetes (Mithieux *et al.* 2006). This capacity for glucose output relies on the activity of glucose-6-phosphatase (G6Pase), the enzyme that catalyzes the dephosphorylation of G6P to glucose.

In the liver, G6P can originate from the release of glucosyl units from hepatic glycogen stores (glycogenolysis) or can be synthesized *de novo* in the process of gluconeogenesis. In healthy humans the gluconeogenic contribution to EGP increases with fasting from 40-55% in the postprandial state to 95% from the 42nd hour of fasting and onward (Chandramouli *et al.* 1997; Roden *et al.* 2001). Parallel to this, hepatic glycogen stores decrease linearly in the first hours of fasting (Petersen *et al.* 1996) and are nearly depleted by the 42nd hour (Roden *et al.* 2001).

Pathways to glucose production are dependent on substrate and hormonal inputs. The fall of glucose levels and the concomitant increase in the glucagon/insulin ratio observed in the fasted state translates into an increase in glycogenolysis and gluconeogenesis (Lefèvre 2004).

1.2.3.1 Glycogenolysis

As mentioned in section 1.2.1.1, net glycogen storage or breakdown depends on the activities of GS and GP. Those enzymes are regulated by reciprocal phosphorylation/dephosphorylation mechanisms. In catabolic states such as fasting or stress, cyclic adenosine monophosphate (cAMP)-dependent protein kinase A (PKA) phosphorylates GS, inactivating it and conversely phosphorylates phosphorylase kinase that phosphorylates (activates) GP (Newgard *et al.* 2000). In addition, glycogen synthase kinase 3 (GSK3) is also activated by PKA and contributes to further inactivate GS (Jope *et al.* 2004).

1.2.3.2 Gluconeogenesis

The regulation of gluconeogenesis mainly occurs at a transcriptional level, in accordance with the slow transition from the fed to fasted state (Newgard 2004). The first step of gluconeogenesis is the conversion of pyruvate to PEP. This step actually involves the activity of two key enzymes: pyruvate carboxylase (PC) that generates OAA from pyruvate and PEP carboxykinase (PEPCK) that converts OAA to PEP. Under fasting conditions, it is the oxidation of fatty acids that fuels this energetically-expensive conversion and at the same time provides allosteric regulators that favor it. Namely, acetyl-CoA stimulates PC and along with NADH and ATP (also by-products from the oxidation of fatty acids) inhibit PDH (Newgard 2004). Furthermore, the binding of glucagon to its cell receptor results in the conversion of ATP to cAMP that acts to stimulate the PEPCK gene expression (Gurney *et al.* 1994; Newgard 2004). The expression of the G6Pase gene is also increased by cAMP and, in addition, by variables associated with the diabetic condition like hyperglycemia and hyperlipidemia (Newgard 2004). The gene expression and activity of FBPase are also increased with fasting or insulinopenic diabetes but the underlying mechanisms are still unclear (Newgard 2004).

1.3 Molecular aspects of insulin signaling

Insulin is a hormone that promotes anabolic processes. In the liver, insulin acts to stimulate glucose disposal and storage and inhibit glucose production as generally discussed in the previous sections. These effects are mediated by changes in enzyme activities or amounts as a consequence of the intracellular transduction of insulin's signal.

When insulin binds to its transmembrane receptor elicits a conformational change that results in the autophosphorylation of the receptor, which in turn mediates the phosphorylation of several intracellular substrate proteins on tyrosine residues (Garvey 2004). The

effects of insulin on cell function will depend on the substrate proteins involved and on the signaling pathways activated henceforward. Most of insulin's metabolic effects result from a signaling pathway that involves the phosphorylation of the insulin receptor substrate (IRS) proteins and the sequential activation of phosphatidylinositol 3-kinase (PI3K) and Akt or protein kinase B (Akt/PKB).

The following section introduces some of the most important signaling mechanisms and molecules implicated in insulin's metabolic effects in the liver.

1.3.1 Metabolic effects of insulin signaling in the liver

In the liver, the PI3K pathway stimulates glycogen synthesis since Akt/PKB phosphorylates GSK3, inactivating it and hence stimulating GS activity (see also section 1.2.3.1) (Peak *et al.* 1998; Saltiel *et al.* 2001; Garvey 2004).

Another important hepatic metabolic consequence of the Akt/PKB pathway is the phosphorylation of forkhead box O1 (FoxO1) and the consequent export of that transcription factor from the nucleus to the cytosol. By this mechanism, the FoxO1-dependent gene expression of gluconeogenic enzymes PEPCK and G6Pase is decreased (Foufelle *et al.* 2002; Garvey 2004; Postic *et al.* 2004). In addition, phosphorylation of FoxO1 as a result of insulin signaling also prevents its interaction with peroxisome proliferative activated receptor γ co-activator 1, which is necessary for the transcription of the PEPCK and G6Pase genes (Postic *et al.* 2004). Moreover, since the nuclear activity of FoxO1 also accounts for the expression of MTP and apoB, insulin inhibition of FoxO1 translates into a decrease of VLDL secretion in the liver (Sparks *et al.* 2009).

Conversely to the inhibition of FoxO1, insulin induces another transcription factor, the sterol regulatory element binding protein 1c (SREBP1c) probably also through the PI3K-Akt/PKB signaling pathway (Foufelle *et al.* 2002; Barthel *et al.* 2003). SREBP1c regulates gene expression

for GK, PK and most lipogenic genes, including the ones for fatty acid synthase multienzyme complex (FAS), ACC and CL (Foufelle *et al.* 2002; Garvey 2004). However, SREBP1c activity alone does not account for the stimulation of the glycolytic and lipogenic metabolic pathways and, with the exception of GK, most of the enzymes involved in those pathways are also induced by glucose via the carbohydrate responsive element binding protein (ChREBP) (Dentin *et al.* 2005). Under basal conditions, PKA phosphorylates ChREBP retaining it in the cytosol; conversely, under high glucose levels, xylulose-5-phosphate-stimulated PP2A dephosphorylates ChREBP allowing it to migrate to the nucleus (Towle 2005).

1.4 Nuclear magnetic resonance spectroscopy methods in metabolism

Metabolic phenotyping is emerging in the post-genomics and proteomics era in the context of linking cell metabolism – a fundamental parameter of cell function – to the DNA information and transcription (Chikayama *et al.* 2008). A comprehensive metabolic analysis provides an integrate profile of the pathophysiological status that results from the genomic, transcriptomic and proteomic variability, and is the basis for the development of a new field, metabonomics/metabolomics[2] (Lindon *et al.* 2007; Bain *et al.* 2009). Nuclear magnetic resonance (NMR) spectroscopy is a powerful and versatile technique for the study of cellular, tissue and whole-body metabolism. In the context of metabonomics, NMR spectroscopy represents a quantitative, non-destructive tool that requires little sample preparation for the analysis of complex biological fluids, cells or even intact tissues. For such samples, a sizable array of metabolites can be identified

[2] These two terms are used interchangeably in the scientific community. In its original definition "metabonomics" is the quantitative measurement of the dynamic multiparametric metabolic response of living systems to pathophysiological stimuli or genetic modification while "metabolomics" is the comprehensive and quantitative analysis of all metabolites in a system (Lindon *et al.* 2007).

and their concentrations measured from a single proton (^{1}H) NMR spectrum.

Moreover, NMR assessments can be performed *in vivo,* what represents a major breakthrough relative to the previously-established invasive approaches that required needle biopsies and catheterization (Roden *et al.* 2001). With *in vivo* ^{1}H, carbon 13 (^{13}C) and phosphorous 31 NMR spectroscopy experiments, the metabolic profile of diverse metabolites can be determined in several organs includind liver, brain and muscle (*e.g.* Sinha *et al.* 2002; Goforth *et al.* 2003; Gruetter *et al.* 2003; Lanza *et al.* 2006; van Zijl *et al.* 2007) and followed in longitudinal studies to assess the dynamics of metabolite pools. Most interestingly, in the context of hepatic carbohydrate metabolism, the quantification of glycogen by *in vivo* ^{13}C NMR spectroscopy is used in combination with tracer-based experiments and plasma turnover measurements providing a comprehensive insight into the metabolic fluxes (Roden *et al.* 1996; Bischof *et al.* 2002; Petersen *et al.* 2004).

1.4.1 The use of stable isotopes to trace carbohydrate and lipid metabolism

By definition, a metabolic tracer is a substance used to follow the biological transformation of an endogenous substrate (tracee). The tracer must be metabolically indistinguishable from the tracee but at the same time possess a unique property allowing for its detection. In the large majority of cases, tracers consist of synthetic substrate molecules where one or more of the atoms have been substituted by rare isotopes that can be detected by a specific technique. Stable isotopes such as ^{13}C and deuterium (^{2}H) can be detected by NMR and mass spectrometry and these approaches have largely replaced earlier tracer studies based on their radioactive counterparts (carbon 14 and tritium). In addition to being safer, stable isotope analytical methods have a key advantage over radioactive tracer detection in that they inherently provide positional labeling information. Equivalent information may be obtained with radioactive tracers, but it

involves highly tedious carbon-by-carbon degradation of the metabolite of interest.

Isotopic labels at specific positions of any given precursor substrate are transferred to metabolic intermediates and products in a highly specific manner during the biochemical reactions within the organism. Thus, the fate of the labeled precursor is highly predictable depending on the metabolic pathway that it transverses. With NMR analysis of the product labeling pattern, different metabolic routes can be discriminated and measured.

1.4.1.1 [U-^{13}C]glucose as a tracer to glucose and glycogen metabolism

Glucose kinetics can be addressed by enriching the plasmatic pool with [U-^{13}C]glucose. This is easily achieved by supplementing a meal or a glucose solution with the tracer or even by delivering it directly to the bloodstream in more invasive infusion procedures. When [U-^{13}C]glucose enters the disposal pathways, two important events occur to the plasmatic pool, (i) it becomes less enriched with the tracer as it is taken up by the cells and (ii) other ^{13}C-enriched glucose isotopomers [3] arise from the metabolization (or recycling) of the tracer. The relative contribution of each isotopomer to the plasma glucose pool can be disclosed by ^{13}C NMR spectroscopy and this information provides insight into the dynamics of whole-body glucose metabolism, which is sensitive to several pathophysiological conditions.

Uptake of [U-^{13}C]glucose is followed by its metabolization within the cells. For example, in the liver, the direct conversion of the tracer into glycogen renders [U-^{13}C]UDPG and glycogen composed of [U-^{13}C]glucosyl residues. If, on the other hand, glucose follows the glycolytic pathway, this results in the formation of two molecules of [U-^{13}C]pyruvate. The glycolytic

[3] Contraction of the words isotope and isomer, refers to molecules that differ one from the other solely by their isotopic composition. For example, considering the glucose molecule and the ^{13}C isotope, each carbon may be ^{12}C or ^{13}C. Since there are 6 carbons in glucose, there are $2^6 = 64$ possible isotopomers.

processing is especially active in peripheral tissues like the muscle, where, under anaerobic conditions, pyruvate is further converted to lactate by lactate dehydrogenase. Lactate from muscle glycolysis then enters the bloodstream and is taken up by the liver, where it is reconverted to pyruvate that serves as a gluconeogenic substrate for glucose production. This sequence of events is named the Cori cycle. As a result of the glucose resynthesis from [U-^{13}C]pyruvate, other isotopomers arise. In this process there is scrambling of the labeling due to pyruvate recycling (pyruvate → OAA → PEP → pyruvate) and racemization at the OAA/fumarate inter-conversion. In consequence, several possible populations of glucose isotopomers from [U-^{13}C]pyruvate can be predicted (Mendes *et al.* 2006) but [1,2-$^{13}C_2$]- and [1,2,3-$^{13}C_3$]glucose account for the majority (Perdigoto *et al.* 2003), and the isotopomer analysis is thus much simplified. Moreover, those isotopomers can be distinguished from the [U-^{13}C]glucose tracer by analysis of the C1 resonance in the ^{13}C NMR spectrum of a glucose derivative (method applied in chapters 2 and 3).

1.4.1.2 Deuterated water as a tracer to glucose and glycogen metabolism

Deuterated water (^2H_2O) is a relatively inexpensive tracer. Upon administration it freely distributes within the tissues and rapidly equilibrates with total body water, thus allowing to follow whole-body metabolism (Murphy 2006). Deuterated water is easily administered both to humans and animals by adding it to the common drinking water in tracer amounts. Furthermore, ^2H_2O can be delivered to animals as an i.p. bolus that results in a steady state enrichment within 10 minutes (Turner *et al.* 2003). Additionally, the subjects may be maintained under ^2H_2O administration for several days, making it suited for assessing metabolism both in short and long term studies in diverse experimental settings (Murphy 2006).

Glucose-6-phosphate is a common precursor to both glycogen and glucose. In the presence of ^2H_2O, G6P is labeled with ^2H in several positions due to the incorporation of that isotope from body water in exchange and addition reactions of the G6P production pathways. This labeling is maintained in the glucose and glycogen molecules. Thus, a given positional ^2H enrichment in glucose or glycogen reflects the reaction accounting for incorporation from ^2H_2O in that position. Moreover, the positional ^2H enrichment quantitatively reflects its respective reaction if isotopic steady state has been achieved (which occurs very fast with ^2H_2O) and the reaction is complete.

A large body of studies has been performed in the past 15 years based on the ^2H_2O method and equations established by Landau and co-workers (Landau *et al.* 1995; Landau *et al.* 1996). The exchange of protons with ^2H from the ^2H_2O at the level of the G6P/F6P keto-enolic equilibrium results in the enrichment of G6P with ^2H in position 2 (Figure 3). Because that isomerization is extensive and essentially complete, the G6P pool is enriched with ^2H in position 2 regardless of its origin. Hence, ^2H labeling of position 2 of glucose is assumed to reflect the total EGP, both via gluconeogenesis and glycogenolysis. In fact, in fasting conditions, when EGP is the only source of blood glucose, the ^2H enrichment in position 2 of glucose is essentially that of body water both in humans (Landau *et al.* 1995; Jones *et al.* 2006a) and rats (Nunes *et al.* 2009). Likewise, both direct and indirect pathway precursors of glycogen become enriched with ^2H from ^2H_2O in position 2. On the other hand, ^2H enrichment from ^2H_2O in position 5 of G6P specifically and quantitatively reflects the contribution of gluconeogenesis from both pyruvate and glycerol. Incorporation of ^2H in that position occurs at the level of the triose phosphates isomerization (Figure 3).

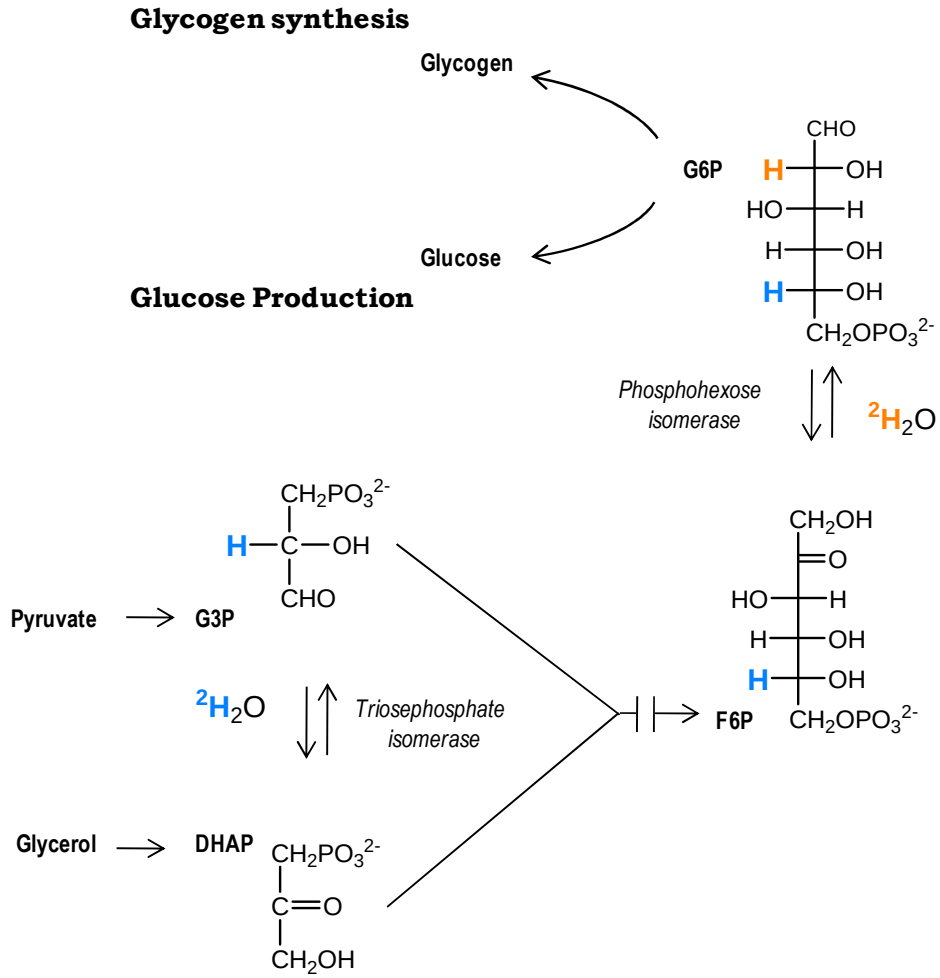

Figure 3 Reactions for glucose and glycogen labeling from ^2H_2O. Deuterium incorporation in position 2 of G3P (in blue) results in labeling of G6P in position 5. This labeling occurs when G6P is produced from either gluconeogenic precursor pyruvate or glycerol. Deuterium enrichment in position 2 (in orange) of G6P reflects both gluconeogenesis/indirect pathway and glycogenolysis/direct pathway due to the extensive G6P/F6P equilibrium. DHAP, dihydroxyacetone phosphate; F6P, fructose-6-phosphate. G3P, glyceraldehydes-3-phosphate; G6P, glucose-6-phosphate.

1.4.1.3 Deuterated water as a tracer to de novo *lipogenesis*

Fatty acid biosynthesis, as that of many other endogenous polymers, can be measured by mass isotopomer distribution analysis (MIDA). This method is based on the mathematics of combinatory probabilities and determines the true precursor enrichment by the analysis of the isotope distributions on the polymer end-product. For example, plasma VLDL isotopomer abundances can be quantified by mass spectrometry following the administration of ^{13}C-enriched acetate (Hellerstein *et al.* 1996) or $^{2}H_2O$ (Murphy 2006) and the precursor (intracellular acetyl-CoA) enrichment determined by MIDA provides an estimation of hepatic DNL. Alternatively, the hepatic pool of acetyl-CoA can be sampled *in vivo* by the administration of a xenobiotic metabolized in the liver by acetylation. This strategy was developed by Hellerstein and colleagues (Hellerstein 1991; Hellerstein *et al.* 1991) and reports DNL values comparable with those from MIDA analysis.

In the process of lipid biosynthesis, the incorporation of hydrogens (or deuterium) from the body water into the fatty acid molecule may occur directly or indirectly, through NADPH in the reduction steps or via the labeling of precursor acetyl-CoA. The methyl groups of the fatty acids in the TG molecule are derived from acetyl-CoA (Murphy 2006). Hence, a simple method for the quantification of DNL consists in determining the ^{2}H enrichment in the methyl group of TGs (by ^{2}H NMR analysis of hepatic lipids) and relate that to the precursor enrichment in the presence of $^{2}H_2O$ (Delgado *et al.* 2009a).

2
GLUCOSE PRODUCTION AND HEPATIC GLYCOGEN SYNTHESIS DURING A CARBOHYDRATE CHALLENGE IN RATS – EFFECT OF GALACTOSE

2.1 Introduction

The study of hepatic glycogen synthesis by the direct and indirect pathways is of central importance in the field of metabolic disorders like diabetes or obesity. Those contributions can be resolved in humans by supplementing a breakfast meal with ^{13}C-enriched glucose and a xenobiotic glucuronide precursor such as paracetamol (Hellerstein *et al.* 1986; Delgado *et al.* 2009b). The ^{13}C enrichment of UDPG, sampled via the urinary glucuronide, relative to that of ^{13}C-enriched plasma glucose provides a measure of direct and indirect pathway contributions. Alternatively, the enrichment of UDPG position 5 from ingested $^{2}H_2O$ can be used to determine direct and indirect pathway contributions to glycogenic flux (Jones *et al.* 2006a). To date, none of these measurements have accounted for the effects of galactose that may be present in the breakfast meal. Although

it may be a minor component of the total meal carbohydrate intake, the fact that it is metabolized by liver (while dietary glucose is mostly metabolized by peripheral tissues) amplifies its effects on postprandial hepatic carbohydrate metabolism. For example, a 300 mL portion of reduced fat milk contains about 15 g of lactose or 7.5 g galactose – about 7.5% of the total carbohydrate from a typical breakfast meal containing ~100 grams of carbohydrate. Galactose aside, the liver accounts for about 20%, or 20 grams of glucose absorption from this meal. In this setting, the contribution of galactose to total hepatic carbohydrate uptake is 7.5/27.5 g, or approximately 27%.

Galactose is metabolized to common intermediates of glucose metabolism via the Leloir pathway as shown in Figure 4 (Hellerstein *et al.* 1988; Niewoehner *et al.* 1990; Niewoehner *et al.* 1992; Wehrli *et al.* 2007). After galactose phosphorylation to galactose-1-phosphate (Gal1P), galactose-1-phosphate uridyltransferase catalyses the transference of the UDP moiety from UDPG to Gal1P, producing UDP-galactose (UDPgal) and G1P. UDPgal is then converted to UDPG by UDP-galactose 4-epimerase. UDPG may then be converted to glycogen via GS or be metabolized to G1P. The extensive equilibration between G1P and G6P coupled to G6Pase activity allows the net conversion of galactose to hepatic glucose.

All tracer measurements of direct and indirect pathway contributions to hepatic glycogen synthesis are based on the assumption that the labeled G6P precursor of one pathway is diluted by unlabeled G6P generated by the other. Thus, glucose tracers are metabolized to G6P via the direct pathway and are assumed to be diluted by G6P molecules generated by indirect pathway activity so that UDPG enrichment is less than that of the glucose precursor. With $^{2}H_2O$, G6P derived via the indirect pathway is enriched in the fifth hydrogen to the same level as body water and this enrichment is assumed to be diluted by direct pathway G6P molecules that are not enriched in this position. In the presence of galactose, these assumptions are no longer valid since the conversion of galactose to UDPG

represents a hitherto undefined capacity for diluting UDPG enrichment from either ^{13}C-glucose or $^{2}H_2O$ tracers.

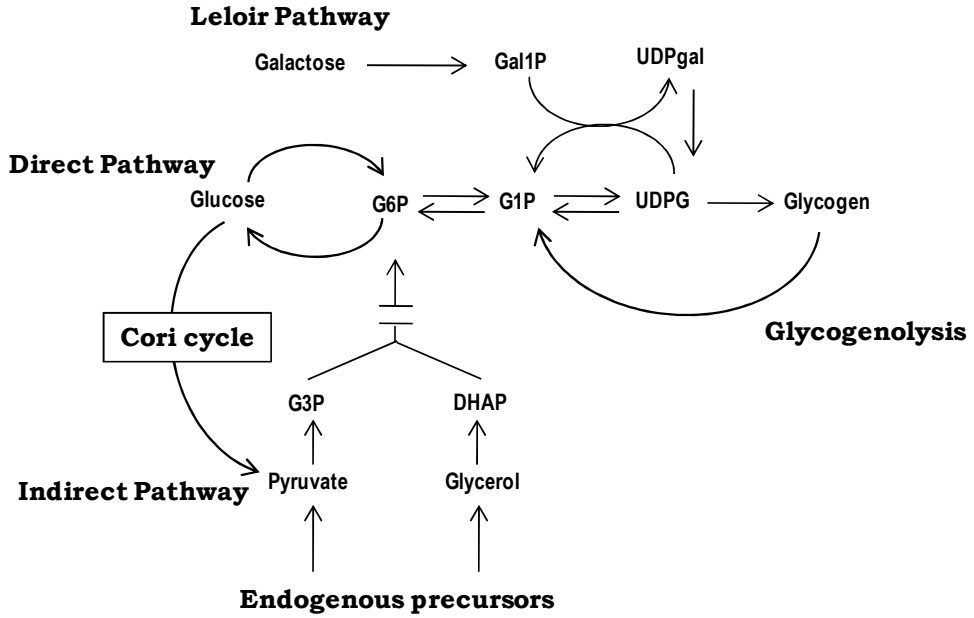

Figure 4 Schematic representation of pathways for glycogen synthesis and endogenous glucose production in the liver during a mixed glucose/galactose load. Glycogen sources include glucose (direct or indirect pathway), galactose and endogenous precursors. Sources of endogenous glucose production include gluconeogenesis (glucose load recycling plus endogenous precursors), galactose and glycogen. DHAP, dihydroxyacetone phosphate; G1P, glucose-1-phosphate; G3P, glyceraldehydes 3-phosphate; G6P, glucose-6-phosphate; Gal1P, galactose-1-phosphate; UDPG, uridine diphosphate glucose; UDPGal, uridine diphosphate galactose.

This chapter focuses on the effect of a small fraction of galactose, equivalent to that derived from a single glass of milk in a standard breakfast meal, on the estimates of direct and indirect pathways using current tracer methods. The experimental setting consisted of an oral glucose tolerance test (OGTT) performed to fasted rats, including [U-^{13}C]glucose and $^{2}H_2O$ tracers. In the galactose experiments, these tracers were accompanied by [1-^{13}C]galactose so that its conversion to glycogen could be independently monitored. Additionally, in the same experiment, the glucose clearance

from the blood could be characterized by resolving the contributions from the load glucose, galactose and endogenous sources.

2.2 Materials and methods

2.2.1 Animal studies

2.2.1.1 Animal housing

Male Wistar rats (Charles Rivers, Spain) with approximately 8 weeks were used. Animals were subjected to a 12 hour light/12 hour dark cycle (lights on from 7 am to 7 pm) with free access to a standard chow diet (60% carbohydrates, 16% proteins, 3% lipids). At least five days of acclimatization were allowed before any intervention was performed on the animals.

2.2.1.2 Animal protocols

Rats (231 ± 5g) were fasted for 24 hours with free access to water. In order to attain proper body water $^{2}H_2O$ enrichment animals were injected 2 mL of $^{2}H_2O$ in the i.p. cavity at the beginning of the study. Carbohydrate loads were also dissolved in $^{2}H_2O$. A glucose load (2 g/kg, approximately 2.6 mmol per animal) enriched to 10% with [U-^{13}C]glucose was administered to the first group (GLU, N = 6) by oral gavage. The second group (GLU+GAL, N = 6) was administered the same dose of carbohydrate as glucose-galactose mixture consisting of 9 equivalents of glucose and 1 equivalent of galactose. The glucose fraction was enriched to 10% with [U-^{13}C]glucose while the galactose fraction was enriched to 10% with [1-^{13}C]galactose. After administering the carbohydrate loads, plasma glucose was monitored from tail tip samples every 15 minutes until 180 minutes with an Accu-check Aviva (Roche, Portugal) glucometer. At 180 minutes, animals were anesthetized by injection of ketamine (100 mg/kg) in the i.p. cavity, the abdominal cavity was opened and ~5 mL of blood was collected

from the abdominal aorta. A small blood sample (0.5 mL) was reserved for determination of ^2H_2O body water enrichment and plasma insulin levels. The liver was excised and immediately freeze-clamped in liquid nitrogen. In order to determine the basal fasting liver glycogen content, 24-hour fasted animals (N = 5) were sacrificed without receiving a carbohydrate load.

2.2.2 Metabolite analyses

Whole blood was immediately treated with $ZnSO_4$ 0.15 M (1.5 mL per mL of blood) and $Ba(OH)_2$ 0.15 M (1.5 mL per mL of blood), centrifuged, and glucose on the supernatant extracted by passing through a sequential cationic and anionic ion-exchange columns. The effluent was lyophilized and glucose was derivatized to monoacetone glucose (MAG) as described below. Liver was lyophilized, and then pulverized to a fine powder and glycogen extracted by treatment with 30% KOH (8 mL per gram of liver dry weight, gdw) at 70ºC for 30 minutes. The mixture was treated with 6% Na_2SO_4 (4 mL per gdw) and 99.9% ethanol (to a final concentration of 70%, 25 mL per gdw) and glycogen was allowed to precipitate at 4 ºC overnight. After centrifugation, the upper liquid phase was discarded and the solid residue dried. The residue was resuspended in 50 mM $NaCH_3COO$ pH 4.5, and 16 units of an aqueous solution of amyloglucosidase from *Aspergillus niger* (Sigma-Aldrich, Portugal) added. The sample was incubated at 55 ºC overnight, and then centrifuged and the upper liquid collected and lyophilized. Glucose obtained from liver glycogen enzymatic hydrolysis was quantified by a standard assay kit (Invitrogen, Spain). The percent glycogen synthesized over the experimental period was determined as the difference between the quantified glycogen for each animal and the mean value determined for the 24-hour fasted controls relative to the quantified glycogen. Insulin levels were determined by ELISA enzyme immunoassay accordingly with the supplier's instructions (Mercodia, Sweden).

2.2.3 Synthesis of the glucose monoacetone derivative

In order to optimize the signal resolution in the NMR spectra, glucose was converted into its monoacetone derivative. Briefly, the dried residue either from blood or liver glycogen preparations was suspended in 10 mL (liver) or 5 mL (blood) acetone with 4% sulphuric acid. Acetone and sulphuric acid were enriched with deuterium to 2% as previously described (Jones *et al.* 2006b). The mixture was stirred overnight at room temperature to yield diacetone glucose. The acetonation reaction was quenched by adding 10 mL (liver) or 5 mL (blood) of water and adjusting the pH to 8 with 1 M $NaHCO_3$. Following acidification of the solution to pH 2.0 with 1 M HCl, diacetone glucose was hydrolysed to MAG by incubation at 40 ^{o}C for 5 hours. The solution pH was then increased to 8 with 1 M $NaHCO_3$ and the samples were dried by rotary evaporation under vacuum. MAG in the residue was extracted with 4 mL of boiling ethyl acetate. Following evaporation of ethyl acetate, the residue was saved in a desiccator until NMR analysis.

2.2.4 NMR Spectroscopy

All spectra were analyzed with the NUTS PC-based NMR spectral analysis software (Acorn NMR Inc., USA). The peak areas were quantified using the curve fitting or the integration tool and the applied line broadening was 0.5 Hz for ^{1}H NMR spectra, 1 Hz for ^{2}H NMR spectra and 0.2 Hz for ^{13}C NMR spectra.

2.2.4.1 ^{2}H NMR analysis of body water

Body water $^{2}H_2O$ enrichments were determined from plasma by ^{2}H NMR as described by Jones *et al.* (Jones *et al.* 2001) with adaptations. Briefly, 10 μL of plasma were mixed with 1 mL of acetone. After centrifugation 0.6 mL of the supernatant was collected and transferred to a 5 mm NMR tube.

^{2}H NMR spectra were obtained at 25 ^{o}C with a 11.7 T Varian Unity 500 spectrometer (Agilent, USA) equipped with a 5 mm broadband probe with the observe coil tuned to ^{2}H. Proton decoupled ^{2}H NMR spectra were acquired with a 25° pulse, 4 seconds of acquisition time and 8 seconds of pulse delay. The number of scans was 24 and spectra typically looked like the one depicted in Figure 5. In order to determine the absolute ^{2}H enrichment level of plasma samples a calibration curve was prepared from water standards enriched with 99% $^{2}H_2O$ from 1.3% to 3.3% (Figure 6).

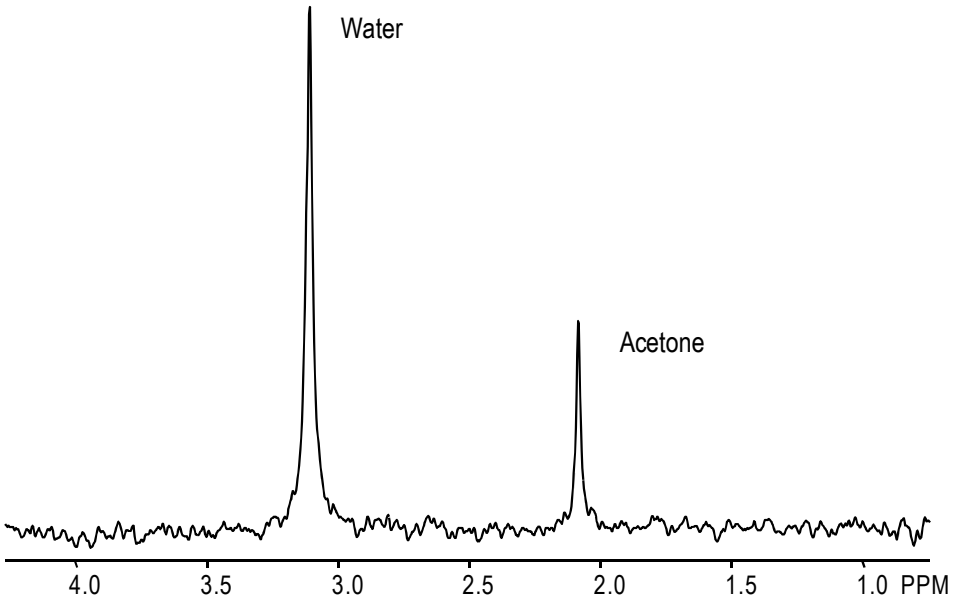

Figure 5 ^{2}H NMR spectrum showing the resonances for acetone and water. The water sample was enriched with $^{2}H_2O$ to 3.3% while acetone was used as internal standard.

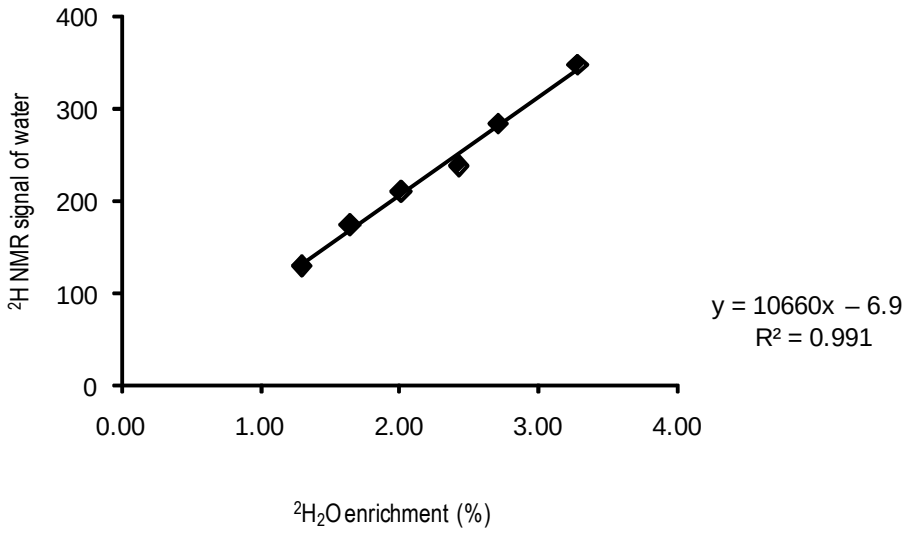

Figure 6 Plot of the area of ^2H water signals (normalized for the masses of sample and acetone; ^2H-acetone signal area was set to 100) as a function of the ^2H_2O enrichment of water standards. The linear regression equation used to determine the ^2H enrichment level of body water from plasma samples is shown.

2.2.4.2 ^2H NMR analysis of MAG

MAG was dissolved in 0.6 mL of 85% (v/v) acetonitrile in dimethyl sulfoxide (DMSO) or, alternatively, in 0.2 mL or 0.6 mL of 90% (v/v) acetonitrile in water with $NaHCO_3$ (9 mg/mL), accordingly with the probe used. Proton-decoupled ^2H NMR spectra of MAG samples were obtained at 50 ^oC with two alternative NMR spectrometers, a 11.7 T Varian Unity 500 equipped with a 5 mm broadband probe and a 14.1 T Varian 600 (Agilent, USA) equipped with either a 3 mm or a 5 mm broadband probe. In all cases the observe coil was tuned to ^2H and fully-relaxed spectra were acquired with a 90° pulse and 1.7 seconds of recycling time. The collection time ranged from 45 minutes to 12 hours according with sample size. In the Varian 600 system, field frequency stability was maintained via the Varian ^1H-Scout acquisition sequence. MAG ^2H enrichments were quantified from the ^2H NMR spectra by measuring the intensity of each signal of the MAG hexose moiety relative to the mean intensity of the two intramolecular

methyl reference signals at 1.28 and 1.40 ppm (Jones *et al.* 2006b). Each reference signal represents three equivalent hydrogens enriched to 2.5% with ^{2}H (*i.e.* corresponding to 7.5% enrichment for a single hydrogen site). After each acquisition, the solvents were immediately removed by evaporation and the dried samples saved until ^{13}C NMR analysis.

2.2.4.3 ^{1}H and ^{13}C NMR analyses of MAG

Samples were dissolved in 0.2 mL of 90% (v/v) acetonitrile-d_3 in water. Proton-decoupled ^{13}C NMR spectra were acquired at 14.1 T with the Varian 600 spectrometer equipped with a 3 mm broadband probe. Spectra were obtained at 25 ^{o}C. An acquisition time of 2.5 seconds and a pulse delay of 0.5 seconds were used and the number of acquisitions ranged from 5,000-25,000. ^{1}H NMR spectra were obtained in the same spectrometer equipped with a 3 mm indirect detection probe. Spectra were obtained at 25 ^{o}C, using an acquisition time of 1.5 seconds and a pulse delay of 0.1 second. The number of acquisitions ranged from 22 to 512.

The ^{13}C enrichment level of MAG carbon 1 ($^{13}C1$) was determined by ^{1}H NMR analysis of the hydrogen 1 signal (Figure 7). This resonance consists of a central doublet, D (from ^{1}H-^{1}H coupling to hydrogen 2 - $^{3}J_{HH}$ = 3.8 Hz), representing hydrogens bound to $^{12}C1$, and a pair of satellite multiplets, SM (from heteronuclear direct ^{1}H-^{13}C coupling to $^{13}C1$ – $^{1}J_{HC}$ = 184.5 Hz; ^{1}H-^{1}H coupling to hydrogen 2, and long range ^{1}H-^{13}C couplings to carbons 2 and 3 - $^{n}J_{HC,\ n>1}$), representing hydrogens bound to $^{13}C1$. The $^{13}C1$ enrichment level was estimated as the intensity of the SM divided by the total resonance intensity *i.e.* SM + D as follows:

$$\text{Total } ^{13}\text{C enrichment } (\%) = 100 \times \frac{\text{SM}}{\text{SM+D}}$$

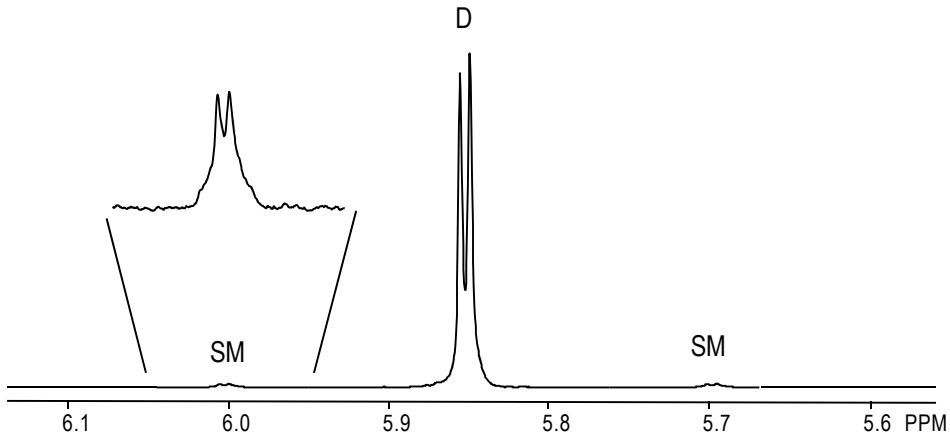

Figure 7 ^{1}H NMR spectrum of a MAG sample enriched with ^{13}C1 isotopomers. The resonance for position 1 hydrogen is shown, it consists of a central dublet (D) representing hydrogens bound to ^{12}C1 and two satellite multiplets (SM) representing hydrogens bound to ^{13}C1. The expansion for one of the satellite multiplets is also shown.

The fractional contribution of [1-^{13}C]-, [1,2-$^{13}C_2$]-, [1,2,3-$^{13}C_3$]- and [U-^{13}C]hexose isotopomers to the ^{13}C1 enrichment of MAG was determined from analysis of the carbon 1 multiplet signal in the ^{13}C NMR spectrum as follows. The 7-line multiplet (Figure 10) can be resolved into a singlet component (C1S), representing [1-^{13}C]MAG, a doublet component (C1D) representing the sum of [1,2-$^{13}C_2$]- and [1,2,3-$^{13}C_3$]MAG isotopomers, and a quartet component (C1Q), representing [U-^{13}C]MAG. The fractional contribution of each isotopomer component to the total ^{13}C1 signal (C1 total) was calculated by measuring the ^{13}C signal intensity of each component relative to that of C1 total. To obtain ^{13}C isotopomer excess enrichments, the fractional isotopomer contribution to the ^{13}C1 signal was multiplied by the total ^{13}C1 enrichment, as shown below. Since [1-^{13}C]MAG enrichment (but not the other isotopomers) has a significant contribution from the 1.1% natural abundance ^{13}C, this amount must be subtracted from the estimated [1-^{13}C]MAG excess enrichment as shown below.

$$[1\text{-}^{13}\text{C}]\text{MAG} = \frac{\text{C1S}}{\text{C1 total}} \times \text{ total } ^{13}\text{C1 enrichment} - 1.1\%$$

$$[1,2\text{-}^{13}C_2] + [1,2,3\text{-}^{13}C_3]\text{MAG} = \frac{\text{C1D}}{\text{C1 total}} \times \text{total } ^{13}\text{C1 enrichment}$$

$$[\text{U-}^{13}\text{C}]\text{MAG} = \frac{\text{C1Q}}{\text{C1 total}} \times \text{total } ^{13}\text{C1 enrichment}$$

2.2.5 Metabolic contributions parameters

The non-hexose precursors or indirect pathway contribution to hepatic glycogen synthesis includes Cori cycle intermediates from metabolism of the glucose load as well as endogenous gluconeogenic precursors. The fractional contribution of non-hexose precursors to glycogen synthesis was calculated from the ratio of position 5 enrichment relative to that of position 2 (Landau *et al.* 1997) as shown in Equation 1. The balance represents the direct pathway flux from glucose as shown in Equation 2. The contribution of gluconeogenesis to plasma glucose was also calculated by Equation 1 and the hepatic glycogen's contribution by Equation 2.

Equation 1

$$\text{Non-hexose precursors (or gluconeogenesis) (\%)} = 100 \times \frac{\text{H5}}{\text{H2}}$$

Equation 2

$$\text{Direct Pathway (or glycogenolysis) (\%)} = 100 - \text{Non-hexose precursors (or gluconeogenesis)}$$

Based on the absence of any significant levels of [1-^{13}C]glucose isotopomers derived from the metabolism of [U-^{13}C]glucose (Perdigoto *et al.* 2003; Mendes *et al.* 2006; Sena *et al.* 2007), it was assumed that the enrichment levels of [1-^{13}C]MAG derived from glycogen or blood glucose reflects the contribution from the [1-^{13}C]galactose tracer in the load.

From Equation 1 to Equation 6, hepatic glycogen synthesis from hexose and non-hexose precursors were resolved as shown in Figure 4. The hexose sources are resolved into glucose and galactose precursors while the gluconeogenic sources are resolved into recycled or indirect pathway carbons derived from the load and endogenous gluconeogenic precursors.

Since the fraction of galactose in the load was 10% enriched with [1-^{13}C]galactose, the percent contribution of galactose to total hepatic glycogen was estimated as the enrichment level of [1-^{13}C]MAG multiplied by 10 with correction for the pre-existing residual unlabeled glycogen fraction (RG), as shown in Equation 3. The RG fraction was determined as the amount of residual glycogen measured in 24-hour fasted rats divided by the hepatic glycogen level at the end of each of the tracer load administrations. As for [1-^{13}C]MAG, it was assumed that the enrichment levels of [U-^{13}C]MAG derived from glycogen reflect the direct contribution from load glucose. Since enrichment of load glucose with [U-^{13}C]glucose was also 10%, its contribution to hepatic glycogen was estimated as being 10 times [U-^{13}C]MAG enrichment, with correction for RG as shown in Equation 4.

Equation 3

$$\text{Load galactose (\%)} = [1\text{-}^{13}\text{C}]\text{MAG} \times 10 \times \frac{1}{1 - \text{RG}}$$

Equation 4

$$\text{Load direct pathway glucose (\%)} = [\text{U-}^{13}\text{C}]\text{MAG} \times 10 \times \frac{1}{1 - \text{RG}}$$

The [1,2-$^{13}C_2$]- and [1,2,3-$^{13}C_3$]MAG isotopomer pair are assumed to be derived by gluconeogenic recycling of the glucose load via the Cori cycle and/or hepatic indirect pathway (Perdigoto *et al.* 2003; Mendes *et al.* 2006; Sena *et al.* 2007). In addition to the factor of 10 to account for the 10% [U-^{13}C]glucose precursor enrichment in the load, these isotopomer levels were multiplied by an additional factor of 1.5 to account for dilution at the level of the hepatic TCA cycle (Mendes *et al.* 2006), and corrected for residual unlabeled glycogen as shown in Equation 5. Isotopomers arising from indirect pathway metabolism of [1-^{13}C]glucose formed via Leloir pathway metabolism of [1-^{13}C]galactose were assumed to have negligible contributions to glycogen.

Equation 5

$$\text{Load indirect pathway (\%)} = ([1,2\text{-}^{13}C_2]\text{MAG} + [1,2,3\text{-}^{13}C_3]\text{MAG}) \times 10 \times 1.5 \times \frac{1}{1 - \text{RG}}$$

The percent contribution of endogenous gluconeogenic sources was estimated as the difference between load contribution (Equation 3 to Equation 5) and 100 as shown in Equation 6.

Equation 6

$$\text{Endogenous gluconeogenic (\%)} = 100 - \text{Load galactose} - \text{Load direct pathway glucose} - \text{Load indirect pathway}$$

Total non-hexose precursors contribution was also determined in an alternative way to that calculated by Equation 1 as the sum of endogenous gluconeogenic and load indirect contributions:

Equation 7

$$\text{Non-hexose precursors (\%)} = \text{Endogenous gluconeogenic} + \text{Load indirect pathway}$$

Plasma glucose consists of glucose absorbed from the GIT (gastric glucose) plus glucose from EGP. The latter includes recycling of glucose from the load, glucose derived from glycogen, endogenous gluconeogenic precursors, and galactose. Except for gastric glucose, all the other sources result in ^{2}H enrichment of blood glucose in position 2. It is assumed that (i) hepatic G6P/F6P exchange is complete and (ii) there is negligible cycling of plasma glucose and hepatic G6P via GK and G6Pase. The contributions of load galactose and load glucose (both gastric and recycled) were determined similarly to those for hepatic glycogen, as shown in Equation 8 to Equation 10. Likewise, the contribution of endogenous sources was determined as the difference to 100 as shown in Equation 11.

Equation 8

$$\text{Load galactose (\%)} = [1\text{-}^{13}C]\text{MAG} \times 10$$

Equation 9

$$\text{Load gastric glucose (\%)} = [U\text{-}^{13}C]\text{MAG} \times 10$$

Equation 10

$$\text{Load recycled glucose (\%)} = ([1,2\text{-}^{13}C_2]\text{MAG} + [1,2,3\text{-}^{13}C_3]\text{MAG}) \times 10 \times 1.5$$

Equation 11

$$\text{Endogenous sources (\%)} = 100 - \text{Load gastric glucose} - \text{Load recycled glucose} - \text{Load galactose}$$

Endogenous sources can be further resolved into gluconeogenesis and glycogen by analysis of blood glucose ^{2}H enrichment from $^{2}H_2O$. The H5/H2 ratio corrected for the presence of gastric glucose (not labeled with ^{2}H) is a measure of the total gluconeogenic contribution to blood glucose (Equation 12), which includes that of the recycled load. The balance (Equation 13) represents the combined contributions of glycogen and galactose, since both originate glucose enriched with ^{2}H in position 2 but not 5. The contribution of endogenous gluconeogenic precursors (Equation 14) was determined by subtracting that of the recycled load (Equation 10) to the total gluconeogenesis (Equation 12).

Equation 12

$$\text{Total gluconeogenesis (\%)} = (100 - \text{Load gastric glucose}) \times \frac{\text{H5}}{\text{H2}}$$

Equation 13

$$\text{Glycogen \& galactose (\%)} = (100 - \text{Load gastric glucose}) \times (1 - \frac{\text{H5}}{\text{H2}})$$

Equation 14

$$\text{Endogenous gluconeogenesis (\%)} = \text{Total gluconeogenesis} - \text{Recycled load glucose}$$

2.2.6 Statistics

Data are expressed as means ± standard error of the mean (SEM). Statistical significance was determined by unpaired Student's *t* test and defined as a $p < 0.05$ except when comparing more than two groups. In that case a one way analysis of variance (ANOVA) was performed and differences among means determined by Fisher's least significant difference (LSD) test.

2.3 Results

2.3.1 Plasma glucose levels during the carbohydrate challenge

Plasma glucose levels over the experimental period are depicted in Figure 8. Baseline glycemia was not significantly different between the two groups (65 ± 4 mg/dL for animals assigned to the GLU group and 66 ± 5 mg/dL for animals assigned to the GLU+GAL group). After the carbohydrate loads, blood glucose levels increased rapidly, peaking at 30 minutes (182 ± 8 mg/dL for the GLU group and 169 ± 7 mg/dL for GLU+GAL group). Blood glucose levels returned to the normoglycemic range 75 minutes past the administration of the carbohydrate loads and at 3 hours, glycemia was 87 ± 3 mg/dL for the GLU animals and 92 ± 4 mg/dL for the GLU+GAL animals (p = n.s.).

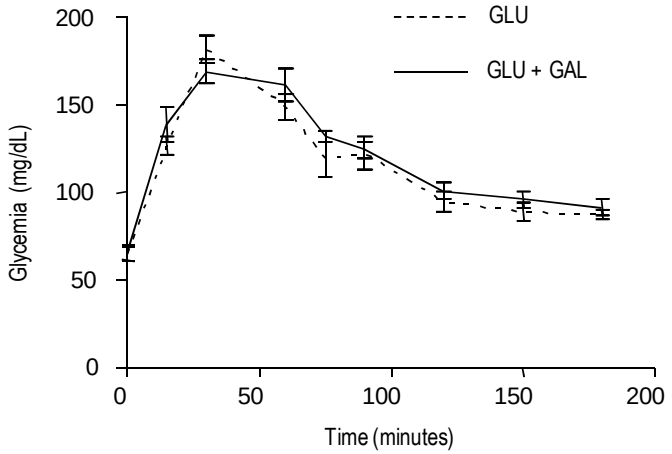

Figure 8 Changes in blood glucose over the 180-minutes tolerance test. After a 24-hour fast, rats were administeraed $^{2}H_2O$ and a 2 g/kg oral hexose load with tracer amounts of [U-^{13}C]glucose (GLU) or a 9:1 mixture of [U-^{13}C]glucose and [1-^{13}C]galactose (GLU+GAL).

The glycemic profile obtained following the oral administration of the carbohydrate loads matches other observations of conscious Sprague-Dawley rats subjected to the same fasting period and hexose dose (Jin *et al.*

2003). The glycemic response was further assessed by calculating the area under the curve (AUC) for plasma glucose levels. These values were similar in both experimental groups. At the end of the experiment, insulin levels for the GLU group were 1.1 ± 0.4 µg/L and 2.4 ± 0.4 µg/L for the GLU+GAL group (p = 0.05).

2.3.2 Hepatic glycogen content

Figure 9 shows the hepatic glycogen content of control (24-hour fasted) and experimental rats, 180 minutes after the carbohydrate challenge.

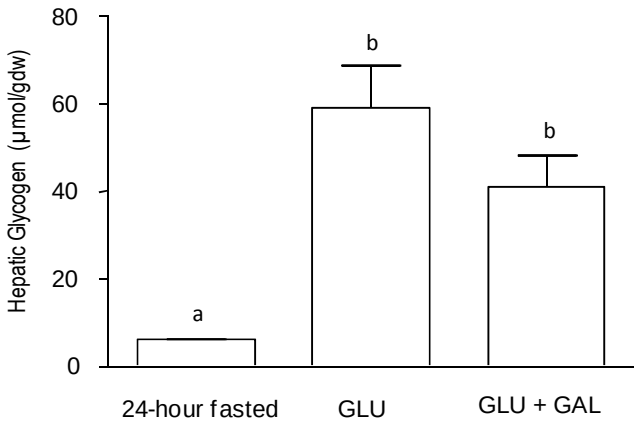

Figure 9 Hepatic glycogen content (µmol of glucosyl units per gram of liver dry weight) for 24h-fasted control rats and experimental groups. Groups are as described in the legend of Figure 8. Bars not sharing a common superscript letter are significantly different; statistical significance was accepted for a $p < 0.05$ determined by one way ANOVA with Fisher's LSD post test.

In the 24-hour fasted controls, liver glycogen amounted to 6.0 ± 0.4 µmol of glucosyl units/gdw (12 ± 0.5 µmol per liver). For animals that had been subjected to the carbohydrate challenges, hepatic glycogen levels were ~8-10 fold higher: 59 ± 10 µmol of glucosyl units/gdw in the GLU group (net glycogen synthesis of 53 ± 10 µmol/gdw) and 41 ± 7 µmol of glucosyl units/gdw in the GLU+GAL group (net glycogen synthesis of 35 ± 7

μmol/gdw, p = n.s.). These amounts were lower[4] than the range of 30 – 60 μmol per gram of tissue reported by others for Sprague-Dawley rats weighing 100 – 200 g fasted for the same period prior to receiving either the same dose of glucose (Jin *et al.* 2003) or a somewhat lower (1 g/kg) load (Niewoehner *et al.* 1992). Glycogen synthesized during the 3-hour period represented 85 ± 4% of the total hepatic content for the GLU group and 83 ± 2% for the GLU+GAL group, hence the pre-existing residual unlabeled glycogen fraction accounted for ~15% of total glycogen for both groups.

2.3.3 ^{2}H enrichments

Animals in both GLU and GLU+GAL groups attained matching ^2H_2O body water precursor enrichments (Table 1). This ~2% enrichment level, coupled with the rates of glucose production and hepatic glycogen synthesis, provided sufficient amounts of ^{2}H in the derivatized glycogen and glucose samples to generate ^{2}H NMR spectra with acceptable signal-to-noise ratios for precise quantification of positional ^{2}H enrichment levels. This is illustrated by the representative ^{2}H NMR spectra of Figure 10.

Table 1: ^{2}H enrichment levels of body water (BW) and position 2 of monoacetone glucose (MAG H2) derived from hepatic glycogen and blood glucose. Groups are as described in the legend of Figure 8. Liver and blood were collected 3 hours after the carbohydrate challenge. *Significantly different (p < 0.05) from BW in the same group (unpaired Student's t test).

	^{2}H enrichments (%)		
	BW	MAG H2	
		Blood glucose	Hepatic glycogen
GLU	2.02 ± 0.05	1.51 ± 0.13 *	1.48 ± 0.13 *
GLU + GAL	2.15 ± 0.10	1.64 ± 0.17 *	1.24 ± 0.08 *

[4] The result expressed as μmol/gdw is divided by 4 to yield the corresponding value expressed as μmol per gram of wet weight. Hence, the hepatic glycogen content after the carbohydrate loads is ~15 μmol/g for GLU group and ~10 μmol/g for GLU+GAL.

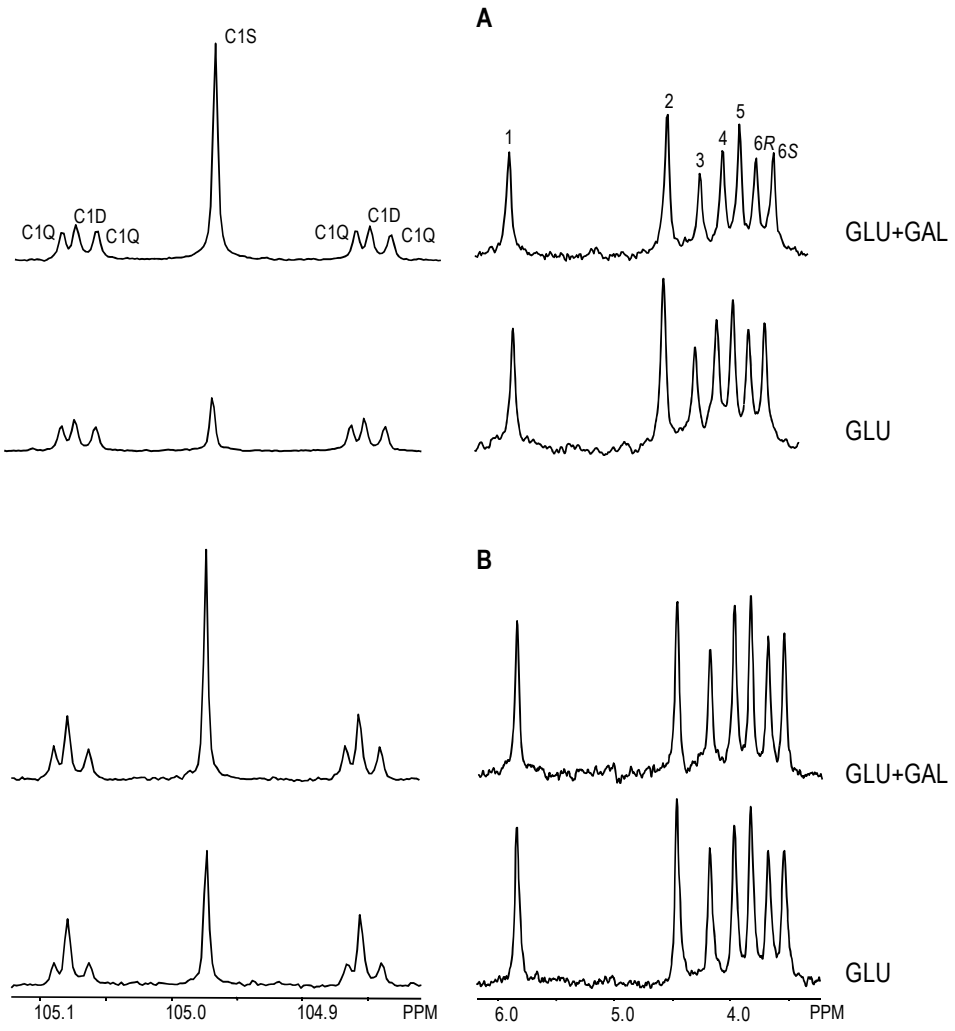

Figure 10 Representative ^{13}C (left hand side) and ^{2}H (right hand side) NMR spectra from monoacetone glucose derived from (**A**) hepatic glycogen and (**B**) blood glucose. The resonance for C1 is shown; the central singlet C1S represents [1-^{13}C]MAG, the doublet component C1D represents the sum of [1,2-$^{13}C_2$]- and [1,2,3-$^{13}C_3$]MAG isotopomers, and the quartet component C1Q represents [U-^{13}C]MAG. The ^{2}H NMR spectra depict the resonances from H1 to H6*S*. Groups are as described in the legend of Figure 8. Liver and blood were collected 3 hours after the carbohydrate challenge.

Position 2 of both glycogen- and blood glucose-derived MAG is enriched with ^{2}H from body water via its incorporation in the G6P common precursor in the G6P/F6P exchange. In both metabolites the ^{2}H enrichment level of position 2 ($^{2}H2$) was significantly lower than that of body water. This is due to the presence of unlabeled hepatic glycogen that was not completely depleted during the fasting period in the liver and of glucose from the oral load that remains in the blood at the end of the test. In the case of blood glucose the dilution effect caused by load glucose can completely account for the lower $^{2}H2$ enrichment of glucose in both experimental groups (see section 2.3.6). However, the dilution from residual glycogen doesn't completely account for the reduced $^{2}H2$ enrichments observed in hepatic glycogen, especially in the GLU+GAL group (see section 2.3.5). Moreover, in the GLU+GAL group the $^{2}H2$ enrichment in hepatic glycogen tended to be lower (p = 0.06) than that in blood glucose demonstrating that the presence of galactose provides an additional dilution of the $^{2}H2$ enrichment in glycogen.

2.3.4 ^{13}C enrichments and isotopomer analysis

The oral glucose or glucose + galactose loads enriched to 10% with [U-^{13}C]glucose and [1-^{13}C]galactose provided sufficient ^{13}C enrichment of blood glucose and hepatic glycogen to generate ^{1}H and ^{13}C NMR spectra with acceptable ^{13}C-signal intensities as shown in Figure 10. Thus, it was possible to precisely quantify ^{13}C isotopomers from both [U-^{13}C]glucose and [1-^{13}C]galactose precursors. The ^{13}C fractional enrichments and isotopomer levels derived by NMR analysis are shown in Table 2.

Total glycogen $^{13}C1$ excess enrichment was not different between GLU and GLU+GAL groups, in agreement with the similar net glycogen synthesis amounts observed for the two groups by enzymatic measurements. The GLU group had no detectable excess enrichment from [1-^{13}C]MAG isotopomer, in accordance with previous findings (Perdigoto *et al.* 2003; Mendes *et al.* 2006; Sena *et al.* 2007) while the GLU+GAL group had

significant excess enrichment of [1-^{13}C]MAG, reflecting the direct contribution of load galactose to hepatic glycogen. Excess enrichment levels of multiply-enriched glucose isotopomers ([1,2-$^{13}C_2$]- + [1,2,3-$^{13}C_3$]- and [U-^{13}C]MAG), which could not have been derived from [1-^{13}C]galactose and therefore reflect only the contribution of load glucose metabolized via indirect pathway and/or Cori cycle, were significantly reduced in the GLU+GAL compared to GLU group.

Table 2: ^{13}C Isotopomer enrichment of monoacetone glucose (MAG) derived from hepatic glycogen and blood glucose. Groups are as described in the legend of Figure 8. Liver and blood were collected 3 hours after the carbohydrate challenge. *Significantly different ($p < 0.05$) from GLU (unpaired Student's t test).

	Excess ^{13}C-isotopomer enrichments (%)							
	Hepatic glycogen				Blood glucose			
	^{13}C1	[1-^{13}C] MAG	[1,2-$^{13}C_2$]+ [1,2,3$^{13}C_3$] MAG	[U-^{13}C] MAG	^{13}C1	[1-^{13}C] MAG	[1,2-$^{13}C_2$]+ [1,2,3$^{13}C_3$] MAG	[U-^{13}C] MAG
GLU	3.89 ± 0.50	-0.06 ± 0.05	1.39 ± 0.19	2.56 ± 0.29	3.25 ± 0.10	0.16 ± 0.05	1.54 ± 0.06	1.55 ± 0.15
GLU + GAL	4.39 ± 0.49	1.87 ± 0.26 *	0.86 ± 0.08 *	1.67 ± 0.17 *	3.33 ± 0.25	0.70 ± 0.10*	1.26 ± 0.14	1.30 ± 0.07

The total ^{13}C1 excess enrichment in blood glucose was similar between GLU and GLU+GAL groups, indicating that after 3 hours the hexose load was cleared from the blood at the same extent in both cases. This observation is in agreement with the similar glycemic curves registered for the experimental groups throughout the test. Similarly to the observations for glycogen-derived MAG, the enrichment levels of the [1-^{13}C]MAG isotopomer in the GLU group were very close to the natural abundance but were significantly higher in the GLU+GAL group. This demonstrates that galactose in the load also contributed to blood glucose. The excess enrichment levels for the multiply-enriched isotopomers ([1,2-$^{13}C_2$]- + [1,2,3-$^{13}C_3$]- and [U-^{13}C]MAG) that reflect the contribution of load glucose to blood glucose were similar in both groups.

2.3.5 Hepatic glycogen synthesis

For animals that received the simple glucose load, position 2 enrichment of glycogen was significantly less than that of body water (Table 1). This is due in part to the presence of residual unlabeled glycogen prior to the introduction of $^{2}H_2O$, as already discussed. When this is taken into account, the theoretical enrichment of glycogen position 2 (*i.e.* assuming complete exchange of position 2 hydrogen via G6P/F6P exchange) is ~85 % that of body water. The measured enrichment of position 2 was only 73 ± 5% that of body water indicating that G6P/F6P exchange experienced by G6P en route to glycogen was extensive but not complete and/or that this group of animals had a higher residual glycogen content compared to the group where residual glycogen was determined. For GLU+GAL animals, glycogen position 2 enrichment relative to body water was significantly lower, amounting to only 58 ± 3% of body water ^{2}H. The incorporation of galactose into glycogen via UDPG does not involve exchange of position 2 hydrogen with body water, thus the lower position 2/body water enrichment ratios observed for the GLU+GAL compared to the GLU group are consistent with this mechanism.

From the analysis of ^{2}H and ^{13}C enrichment distributions of hepatic glycogen, the principal sources of hepatic glycogen synthesis for GLU and GLU+GAL groups were estimated. Conversion of glucose to glycogen via both direct and indirect pathways was resolved. Formally, the indirect pathway includes intra-hepatic metabolism of glucose to glycogen via 3-carbon intermediates as well as glucose metabolized via the Cori cycle. The Cori cycle can be considered as an indirect pathway where the glycolytic phase (glucose → pyruvate) occurs in peripheral tissues and the gluconeogenic phase (pyruvate → G6P) occurs in the liver. The direct pathway involves the conversion of plasma glucose to glycogen via hexose intermediates (Figure 4). Glucose absorbed from the oral load as well as unlabeled circulating glucose existing prior the carbohydrate administration contributes to the direct pathway. In addition to direct and indirect contributions of the load carbohydrates, the glycogenic contribution of

endogenous gluconeogenic precursors that were not derived from glucose recycling was also measured.

For the GLU group, the direct pathway contribution from the load, as calculated from the dilution of [U-^{13}C]glucose (Equation 4), accounted for less than one-third of all sources, see Table 3, matching the observations from Shulman *et al.* in a similar experimental setting (Shulman *et al.* 1985). The direct pathway contribution estimated by the $^{2}H_2O$ method was in excellent good agreement with that estimated by ^{13}C isotopomer analysis (Table 4). Indirect pathway flux was dominated by unlabeled endogenous gluconeogenic precursors while indirect pathway/Cori cycle metabolism of the load glucose were subsidiary contributors as seen by the low abundance of [1,2-$^{13}C_2$]- plus [1,2,3-$^{13}C_3$]glucose isotopomers.

When 10% of the oral glucose load was substituted by galactose, there were no significant changes in net glycogen synthesis, but glycogen sources were significantly modified. Although representing only 10% of the oral carbohydrate load, the galactose contributed about one-quarter of net hepatic glycogen synthesis. The ^{13}C NMR analysis of glycogen-derived MAG indicates that the conversion of galactose to hepatic glycogen displaced contributions from both direct and indirect pathways of load glucose, but had no significant effect on the apparent endogenous gluconeogenic contribution to glycogen synthesis (Table 3).

Table 3: Percent contributions of various sources to hepatic glycogen synthesis 3 hours after the carbohydrate challenge, as determined by the ^{13}C isotopomer analysis of glycogen-derived monoacetone glucose. The corresponding equations used to derive the source contributions are also indicated. Groups are as described in the legend of Figure 8. N.A., not applicable. *Significantly different ($p < 0.05$) from GLU (unpaired Student's *t* test).

	Hexose Load (%)			Endogenous Gluconeogenic (%)	Total Non-hexose precursors (%)
	Direct pathway glucose	Indirect pathway	Galactose		
	Equation 4	Equation 5	Equation 3	Equation 6	Equation 7
GLU	30 ± 3	24 ± 3	N.A.	47 ± 4	70 ± 3
GLU + GAL	20 ± 3 *	16 ± 2 *	23 ± 4	41 ± 6	57 ± 5 *

Table 4: Percent contributions of various sources to hepatic glycogen synthesis 3 hours after the carbohydrate challenge, as determined by analysis of glycogen-derived monoacetone glucose ^{2}H enrichment from $^{2}H_2O$. The corresponding equations used to derive the source contributions are also indicated. Groups are as described in the legend of Figure 8.

	Direct pathway glucose (%)	Total Non-hexose precursors (%)
	Equation 2	Equation 1
GLU	32 ± 4	68 ± 3
GLU + GAL	29 ± 6	71 ± 6

2.3.6 Blood glucose sources

Blood was collected at the end of the experimental period and the MAG derivative analysed by ^{1}H, ^{13}C and ^{2}H NMR. Total gluconeogenesis (endogenous sources plus load glucose recycling), as estimated from the H5/H2 ratio in blood-derived MAG, contributed to 92 ± 4% of EGP in the GLU group and 95 ± 2% in the GLU+GAL group. These values were corrected for the presence of glucose from gastric absorption in order to determine the contributions to the overall blood glucose pool (Table 5).

Table 5: Percent contributions of various endogenous sources to blood glucose 3 hours after the carbohydrate challenge, as determined by analysis of blood glucose-derived monoacetone glucose ^{2}H enrichment from $^{2}H_2O$. The corresponding equations used to derive the source contributions are also indicated. Groups are as described in the legend of Figure 8.

	Gluconeogenesis (%)		Glycogen & galactose (%)
	Total	Endogenous	
	Equation 12	Equation 14	Equation 13
GLU	78 ± 4	55 ± 3	7 ± 3
GLU + GAL	83 ± 1	62 ± 1	5 ± 2

The ^{2}H enrichment in position 2 of blood glucose relative to the ^{2}H enrichment in the body water provides an estimation of the EGP contribution to the circulating glucose, assuming that plasma glucose ^{2}H

enrichment by futile glucose/G6P cycling is negligible. In the GLU group this contribution was 75 ± 7%. That EGP accounted for such a large majority of plasma glucose under these conditions is surprising, since the glucose load would have been expected to suppress hepatic glucose output. In comparison, the contribution of the absorbed glucose from the load accounted for only 16 ± 1% of post-load plasma glucose (Table 6), which consistently adds up to the contribution from EGP to account for the overall blood glucose pool. Moreover, this indicates that most of the oral glucose load underwent rapid clearance. The presence of significant levels of recycled glucose isotopomers indicates that a substantial fraction of the cleared glucose was rapidly metabolized via the Cori cycle. Most surprisingly, about half of plasma glucose derived from endogenous gluconeogenesis that did not involved recycling of the glucose load (Table 5).

Table 6: Percent contributions of various sources to blood glucose 3 hours after the carbohydrate challenge, as determined by ^{13}C isotopomer analysis of blood glucose-derived monoacetone glucose. The corresponding equations used to derive the source contributions are also indicated. Groups are as described in the legend of Figure 8. N.A., not applicable.

	Hexose Load (%)			Endogenous sources (%)
	Gastric glucose	Recycled glucose	Galactose	
	Equation 9	Equation 10	Equation 8	Equation 11
GLU	16 ± 1	23 ± 1	N.A.	61 ± 1
GLU + GAL	13 ± 1	20 ± 1	7 ± 1	60 ± 3

For the animals receiving the carbohydrate mixture, the contribution of EGP to blood glucose as determined from the ratio between ^{2}H enrichment in position 2 relative to the body water was 79 ± 7%, similar to the one determined for the GLU group. Gastric glucose accounted for the remainder blood glucose with a 13 ± 1% contribution (Table 6). In this group of animals, the contribution of recycled glucose and endogenous gluconeogenic precursors was essentially the same as in the glucose-fed

rats. The combined contributions from glycogen and galactose were similar to that of galactose by itself (see Table 5 and Table 6). These observations indicate that by 3 hours after the carbohydrate load, galactose that had been metabolized to G6P did not contribute significantly to hepatic glucose output and plasma glucose levels.

2.4 Discussion

2.4.1 Effect of galactose on direct and indirect pathway estimates with [U-^{13}C]glucose and $^{2}H_2O$ tracers

In this study, sources of hepatic glycogen synthesis following a load of pure glucose were quantified and compared with those following a load where 10% of the glucose was replaced by galactose. This proportion of galactose and glucose is representative of a breakfast meal containing a glass of skimmed milk – a standard source of protein for experimental breakfast meals. Given the rapid digestion of lactose and the fact that galactose is efficiently extracted and utilized by the liver, any effects of dietary galactose on direct/indirect pathway measurements are expected to be most pronounced in the initial stages of meal absorption. Interestingly, several studies with glucose tracers have shown that direct pathway contributions measured immediately after a mixed meal are significantly smaller than those measured 4-6 hours later (Shulman *et al.* 1990; Taylor *et al.* 1996). The study of Taylor *et al.* documents the presence of milk in the meal (Taylor *et al.* 1996), while the study of Shulman *et al.* (Shulman *et al.* 1990) refers to a "standardized breakfast meal" which typically includes milk. By comparison, measurements performed during a glucose load infusion also show increases in direct pathway contributions over time (Stingl *et al.* 2006), but these changes are relatively modest when compared to those observed with meal studies. The hypothesis set for this study was that the uptake and metabolism of galactose from the breakfast meal could

account for unexpectedly low values of direct pathway fluxes in the early stages of absorption.

The experimental model adopted was able to recapitulate that effect by replacing a small fraction of the glucose load with galactose. When the direct pathway contribution was measured with [U-^{13}C]glucose, it reported a 30% contribution to hepatic glycogen synthesis for animals administered with glucose only. For animals that were administered with the glucose/galactose mixture, the direct pathway contribution reported by [U-^{13}C]glucose was significantly reduced by one-third to 20%. Since net glycogen accumulation was not significantly different to that of the glucose only group, this indicates that galactose competed against the direct pathway for glycogen synthesis. In addition, it was found that the indirect pathway contribution from load glucose was also reduced by one-third (24% to 16%). However, the apparent contribution from unlabeled gluconeogenic sources was not significantly altered by galactose metabolism.

With the $^{2}H_2O$ method, the fractional contribution of indirect pathway flux to glycogen synthesis was estimated from the ratio of position 5 enrichment to that of position 2 (H5/H2) and the direct pathway contribution is estimated as the balance. Since UDPG derived from galactose is not enriched with ^{2}H in any position, this activity will systematically dilute all positional ^{2}H enrichments of glycogen hence the H5/H2 ratio and direct/indirect pathway estimates based on this value will not be modified. In the absence of galactose, the direct pathway contribution obtained by this analysis (32%) matched the 30% estimate obtained with [U-^{13}C]glucose tracer. With galactose present, the observed H5/H2 ratio yielded an identical direct pathway contribution (29%) indicating that this analysis was insensitive to the contribution of galactose to glycogen synthesis. As predicted, the presence of galactose systematically reduced the ^{2}H enrichment in all positions of glycogen relative to that of body water. Assuming that the enrichment in position 2 of glycogen derived from glucose metabolism is equivalent to that of body water, then in theory, the

difference between the enrichment in position 2 of glycogen and that of the body water should correspond to the fraction derived from galactose. However, in this experimental setting this analysis has high uncertainty since equilibration of UDPG position 2 and body water hydrogens was incomplete and the amount of pre-existing unlabeled glycogen could not be directly determined. After adjusting for these parameters, the galactose contribution was estimated to be 18%, in fair agreement with the 23% estimate obtained directly with the [1-^{13}C]galactose tracer.

2.4.2 Dominance of the indirect pathway of glycogen synthesis

A key finding of this study was that the indirect pathway was the dominant source of hepatic glycogen synthesis even after a pure glucose load. Both [U-^{13}C]glucose and $^{2}H_2O$ tracers reported a ~70% indirect pathway contribution for the animals receiving the glucose only bolus. In a similar oral glucose test performed on 24-hour fasted rats, Jin *et al*. found an even higher indirect pathway contribution, accounting for ~90% of post-load glycogen synthesis (Jin *et al.* 2003).

In 24-hour fasted rats, hepatic glycogen is extensively depleted (Niewoehner *et al.* 1992; O'Doherty *et al.* 2000; Jin *et al.* 2003) therefore the maintenance of plasma glucose levels is almost completely dependent on gluconeogenesis. Following oral administration of a large glucose load, glucose disposal pathways must be activated while EGP from gluconeogenesis needs to be suppressed in order to maintain glucose homeostasis. In this setting, the diversion of gluconeogenic G6P flux from glucose to glycogen synthesis is a fast and effective means of suppressing EGP under these conditions. The observation that a significant fraction of synthesized glycogen was derived from endogenous gluconeogenic precursors is consistent with this mechanism. Moreover, this flux was maintained in the face of competition from galactose suggesting that under the conditions of our study, the diversion of gluconeogenic G6P to glycogen is somehow prioritized over other glycogenic fluxes. Under normal fasting-

feeding conditions where the transition from negative to positive endogenous glucose balance is less abrupt, the gluconeogenic contribution to glycogen synthesis is present, but it accounts for a smaller fraction (~50%) of hepatic glycogen synthesis (Chapter 4).

2.4.3 Conversion of the hexose load into hepatic glycogen

For both the glucose and glucose-galactose loads, the synthesis of hepatic glycogen represented a very minor fraction of the total carbohydrate disposal. For example, out of the 2.6 mmol oral glucose load, only 68 μmol, or 2.6%, was converted to glycogen by all (direct plus indirect) pathways. With glucose and galactose loads, the fractional hepatic extraction of glucose to glycogen synthesis was significantly further reduced to 1.1%, (*i.e.* 25 μmol of the 2.3 mmol load, $p < 0.01$ compared to the fraction from glucose only load). While the conversion of load galactose (~230 μmol) to glycogen was relatively more efficient, it nevertheless accounted for only 7.4% of the total, amounting to ~15 μmol.

2.4.4 Endogenous glucose production during the carbohydrate challenge

One striking feature about the glucose dynamics during this experiment was the high contribution of EGP to plasma glucose levels a short time after the administration of a large glucose bolus. This was determined by a novel method based on the ^{2}H enrichment level of plasma glucose position 2 from $^{2}H_2O$ and is dependent on the assumption that there is negligible cycling between plasma glucose and hepatic G6P. When this cycle is active, position 2 of plasma glucose can be enriched from $^{2}H_2O$ independently of EGP. Glucose/G6P cycling activity has been previously measured as an increased rate of [2-^{3}H]glucose turnover relative to that of [U-^{14}C]glucose (Dunn *et al.* 1976). In the $^{2}H_2O$ experiment, glucose/G6P

cycling activity would result in unlabeled glucose molecules, including those absorbed from the load, being enriched in position 2. This has two important and verifiable consequences on the ^{2}H and ^{13}C enrichment data. First, the EGP contribution to plasma glucose as measured by position 2 enrichment from $^{2}H_2O$ would be overestimated while the contribution of absorbed glucose would be correspondingly underestimated. Therefore, the gastric glucose contribution as directly reported by the ^{13}C tracer would be higher than that estimated by the $^{2}H_2O$ method (indeed if all plasma glucose underwent glucose/G6P cycling the apparent gastric glucose contribution would be zero). In fact, the gastric contribution reported by the [U-^{13}C]glucose tracer (13-16%) was comparable to the fraction of plasma glucose that was not labeled in position 2 from $^{2}H_2O$ (15-21%). The second consequence of glucose/G6P futile cycling would be to reduce the plasma glucose H5/H2 ratio compared to that of glycogen. Data from this experiment show that plasma glucose H5/H2 ratios were higher than those of glycogen indicating that there was no preferential enrichment of plasma glucose position 2 from $^{2}H_2O$ by glucose/G6P cycling. Based on these observations, it is conclude that in comparison to EGP activity, cycling between plasma glucose and hepatic G6P did not significantly contribute to plasma glucose enrichment from $^{2}H_2O$.

2.4.5 Estimation of gluconeogenesis and glycogenolysis with $^{2}H_2O$

In these experiments effective glycogen synthesis was accompanied by a minor contribution of glycogenolysis to blood glucose. The estimation of glycogenolysis relies on the assumption that glucose derived from glycogen is enriched with ^{2}H in position 2 but not 5. However, in this experiment the majority of glycogen was enriched in both positions 2 and 5, reflecting the high contribution from three carbon precursors and as a result, the calculations based on the ^{2}H labeling pattern of blood glucose may underestimate the actual contribution from GP activity. However, since

the glycogenolytic contributions were very minor accounting for the glycogen precursor pool enriched beforehand does not significantly change the overall source contributions to plasma glucose[5].

2.5 Conclusions

This study demonstrates that a relatively low amount of galactose, similar to what would be expected from a breakfast meal containing dairy products, has a significant effect on direct and indirect pathway estimates using current tracer methods. With ^{13}C NMR isotopomer analysis of suitable ^{13}C-enriched glucose and galactose substrates, the galactose contribution to glycogen synthesis may be resolved from those of glucose and non-hexose precursors. When this is not possible or practical, galactose should be excluded from the dietary carbohydrate load.

In terms of its overall effects on glucose metabolism and disposal, galactose utilization resulted in a decreased contribution of load glucose to hepatic glycogen synthesis but it had little effect on the clearance of glucose into peripheral tissues.

[5] For example, considering that 85% of the hepatic glycogen was synthesized during the 3-hour test and that of this fraction ~70% derived from the indirect pathway (*i.e.* non-hexose precursors), then about 60% of the total hepatic glycogen pool is labeled in both positions 2 and 5. The contribution of glycogenolysis to the plasma glucose pool corrected by this factor yields ~11% compared to the original ~7% estimation.

3
SOURCES OF BLOOD GLUCOSE AND HEPATIC GLYCOGEN SYNTHESIS DURING A GLUCOSE CHALLENGE IN DIABETIC RATS – EFFECT OF A SINGLE INSULIN DOSE.

3.1 Introduction

In the clinical setting, the OGTT is commonly used to discriminate among several pre-diabetic conditions although it is not applied to type 1 diabetic patients (WHO 2006). Nonetheless, the OGTT is widely used in experimental animal models of type 1 DM in the context of evaluating and comparing the efficacy of antidiabetic agents. Sometimes, the intravenous or the i.p. routes are also used in animals to deliver a glucose load. Generally, the aim of the test is to evaluate the glycemic response over time as a measure of glucose disposal. The glucose tolerance test represents a very straightforward approach for assessing the antidiabetic efficacy of pharmacological agents (Marti *et al.* 2001) or dietary supplementation (Akhani *et al.* 2004; Lo *et al.* 2006), for example.

By introducing [U-^{13}C]glucose and $^{2}H_2O$ in tracer amounts during the OGTT, load glucose clearance, pathways of glucose production and glycogen synthesis can be disclosed (see Chapter 2). Given that hyperglycemia in STZ-diabetic rats results in part from deficient glucose disposal (Wi *et al.* 1998) the tracer-enriched OGTT may provide insight on the underlying metabolic alterations and how they change with antidiabetic intervention. To address those questions the OGTT protocol presented in chapter 2 was performed on STZ-diabetic rats and STZ-diabetic rats previously injected with a single dose of insulin so that the effect of the drug on glucose disposal could be evaluated. Insulin was delivered by two different routes, the traditional s.c. route and the i.p. route, which results in higher hepatic insulinization (Mason *et al.* 2002). Hence, it was anticipated that any hepatic-specific insulin action in the context of glucose disposal would be detected and characterized under this experimental setting.

3.2 Materials and methods

3.2.1 Animal studies

3.2.1.1 Animal housing

As described in section 2.2.1.1.

3.2.1.2 Animal protocols

Rats (270 ± 3 g) were given a 50-65 mg/kg intra-peritoneal injection of STZ (Sigma-Aldrich, Portugal) dissolved in 10 mM citrate buffer pH 4.5 to induce diabetes. Animals that did not develop hyperglycemia 1 day after the injection were given the same dose of STZ the following days up to a total of 3 doses. Animals were considered diabetic when glycemia was > 250 mg/dL.

On the 20th and 21st days following the induction of diabetes, animals were fasted for 24 hours and then randomized into three groups. In two of the groups, rats were injected insulin (Actrapid®, Novo Nordisk, kindly donated by the Hospitais da Universidade de Coimbra) at a dose of 5 U/kg to the s.c. route (SC, N = 5) or the i.p. route (IP, N = 5). In the other group (STZ, N = 5), animals did not receive any injection. Thirty minutes after the insulin dose, all animals were administered $^{2}H_2O$ and gavaged a glucose load enriched to 10% with [U-^{13}C]glucose and glycemia monitored for a 3-hours period, as described in section 2.2.1.2. The GLU group in the experiment described in chapter 2 was used as non-diabetic control for the present experiment. In order to determine the basal fasting liver glycogen content a separate group of 24-hour fasted STZ-diabetic animals (N = 5) were sacrificed without receiving the glucose load.

3.2.2 Metabolite analyses

Glucose was extracted from the blood, hepatic glycogen isolated hydrolyzed to glucose and quantified, as described section 2.2.2. Glucose was converted to MAG as described in section 2.2.3. Exogenous (human) insulin levels were determined in the plasma obtained after centrifugation of a small blood sample by ELISA enzyme immunoassay (Mercodia, Sweden) accordingly with the supplier's instructions.

3.2.3 NMR spectroscopy

As described in sections 2.2.4, 2.2.4.1, 2.2.4.2 and 2.2.4.3.

3.2.4 Metabolic contributions parameters

As described in section 2.2.5

3.2.5 Statistics

As described in section 2.2.6.

3.3 Results

3.3.1 Induction of diabetes and performance during the OGTT

Successful induction of diabetes was confirmed 4 days after STZ injection by the presence of typical symptoms like hyperglycemia (374 ± 17 mg/mL), weight loss (weight represented ~80% of the initial), polydepsia and polyuria. On day 20, after 24 hours of fasting, the glycemia registered for the STZ was significantly higher than that found for control animals (Table 7).

Table 7: Glycemia values registered at the beginning and at the end of the oral glucose tolerance test (OGTT); area under the curve (AUC) determined for the glycemia profiles in Figure 11; exogenous insulin and hepatic glycogen determined at the end of the OGTT. After a 24-hour fast STZ-diabetic rats (STZ), STZ-diabetic rats injected a single 5 U/kg insulin dose by the subcutaneous (SC) or intraperitoneal (IP) route, and non-diabetic controls (Control) were gavaged a 2 g/kg glucose load and sacrificed 3 hours after. Insulin was injected to 30 minutes before the OGTT. Values not sharing a common superscript letter are significantly different; statistical significance was accepted for a $p < 0.05$ determined by one way ANOVA with Fisher's LSD post test. N.D., not determined.

	STZ	SC	IP	Control
Glycemia t_0 (mg/dL)	172 ± 34 ^{a}	180 ± 42 ^{a}	121 ± 40 ^{ab}	65 ± 4 ^{b}
Glycemia t_{180} (mg/dL)	297 ± 52 ^{a}	37 ± 5 ^{b}	34 ± 9 ^{b}	86 ± 3 ^{b}
AUC $t_{0\rightarrow180}$ (arbitrary units)	432 ± 51 ^{a}	181 ± 40 ^{b}	211 ± 41 ^{bc}	328 ± 34 ^{ac}
Exogenous insulin (mU/L)	N. D.	29 ± 8 ^{a}	77 ± 24 ^{a}	N. D.
Hepatic glycogen (µmol/gdw)	236 ± 65 ^{a}	221 ± 77 ^{a}	199 ± 24 ^{a}	59 ± 10 ^{b}

The glycemia variation over the OGTT experiment is depicted in Figure 11 and is expressed as percent from initial value (at time t = 0 minutes). In all groups of animals, after the oral gavage of glucose, glycemia increased more than 100% in the first 30 minutes. In the STZ, that increment followed for another 30 minutes with the peak occurring at 60 minutes. On

the other hand, in the non-diabetic controls, SC and IP the glycemia for that time corresponds to the descending phase of the curve. Moreover, the injection of insulin to the diabetic animals translated into an increase of the slope of the descending part of the glycemia curve.

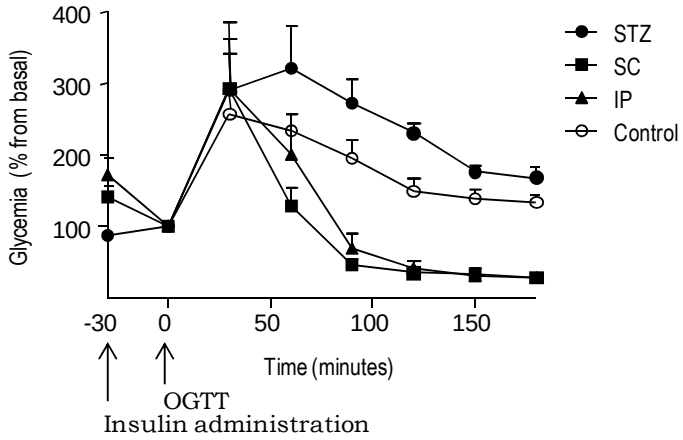

Figure 11 Glycemia profiles (expressed as % from initial value) registered during the 180 minutes of the oral glucose tolerance test. Experimental groups are as described in the legend of Table 7.

Table 7 summarizes the performance of the different experiment groups subjected to the OGTT. The overall glycemia response during the OGTT was evaluated by determining the AUC corresponding to $t_{0\rightarrow180}$. The AUC for STZ tended to be higher than that of controls ($p < 0.1$). Both IP and SC groups displayed significantly lower AUC than STZ. Furthermore, the AUC for IP was similar to that of controls whereas in the SC group it was significantly lower. This observation is in agreement with higher peripheral glucose uptake in the case of the s.c. route relative to the i.p., in the first half of the test, as indicated by the marked decrease in glycemia (Figure 11). With time, glycemia for the IP group approached that of the SC and, at the end of the test, the glycemia values observed for both the IP and SC groups were similar and under the physiological range. On the other hand, by that time, non-diabetic controls had recovered from the oral glucose load and

again displayed glycemia within the physiological range, whereas in the STZ glycemia remained elevated. Exogenous insulin was quantified from the blood collected at the time of sacrifice and there were no significant differences between the values detected for IP and SC.

All groups of STZ-diabetic rats displayed higher levels of hepatic glycogen relative to non-diabetic controls. However, contrarily to what was observed for controls (see chapter 2, section 2.3.2) after 24 hours of fasting, hepatic glycogen content was not nearly depleted in the STZ-diabetic rats, amounting to 373 ± 41 μmol/gdw. These values were not changed after the OGTT and when insulin was previously injected to the STZ-diabetic rats (SC and IP) glycogen levels in the liver were still similar to those of STZ. These observations indicate that, for the STZ-diabetic rats, there was no net glycogen synthesis in the liver in the context of the OGTT, even in the presence of insulin.

3.3.2 ^{13}C and ^{2}H metabolite enrichments

The body water ^{2}H enrichment level was determined from a small blood sample and was similar among all groups: 2.04 ± 0.06%, STZ; 1.80 ± 0.10%, IP; 1.98 ± 0.15%, SC; and 2.01 ± 0.05%, Control. With this level of enrichment, the positional ^{2}H enrichments obtained in blood glucose allowed for an adequate ^{2}H NMR analysis in non-diabetic controls and STZ as shown in Figure 12. In those groups, ^{2}H enrichment of blood glucose-derived MAG was 1.51 ± 0.13% and 1.52 ± 0.16%, respectively. However, because in IP and SC groups little glucose could be extracted from the blood due to the hypoglycemia experienced by those animals, the ^{2}H NMR spectra obtained in those cases didn't have a signal to noise ratio adequate for a confident analysis.

The ^{13}C enrichment level at C1 of MAG from blood glucose was 4.35 ± 0.10% in the non-diabetic controls, similar to that determined in the STZ: 4.62 ± 0.23%. In the diabetic animals injected with insulin prior the OGTT, the ^{13}C enrichment levels in C1 of MAG from the blood were significantly

lower than the ones observed for the STZ and control groups: 2.27 ± 0.21%, SC; and 2.06 ± 0.25%, IP.

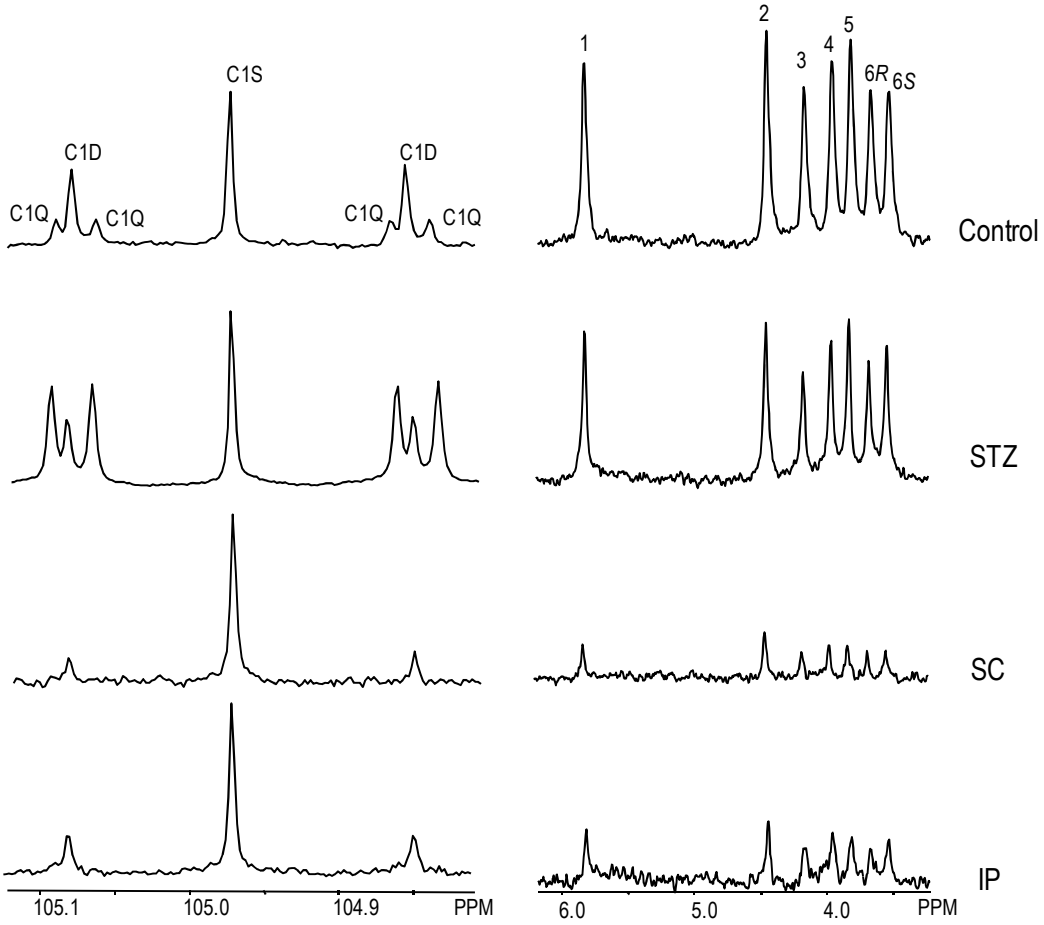

Figure 12 Representative ^{13}C (left hand side) and ^{2}H (right hand side) NMR spectra from monoacetone glucose derived from blood glucose 3 hours after the oral glucose tolerance test. Experimental groups are as described in the legend of Table 7. The oral load was enriched with $^{2}H_2O$ and [U-^{13}C]glucose tracers. The resonance for C1 is shown; the central singlet C1S represents [1-^{13}C]MAG, the doublet component C1D represents the sum of [1,2-$^{13}C_2$]- and [1,2,3-$^{13}C_3$]MAG isotopomers, and the quartet component C1Q represents [U-^{13}C]MAG. The ^{2}H NMR spectra depicts the resonances from H1 to H6*S*.

The glycogen extracted from the liver of all STZ-diabetic rats was found to have profoundly reduced ^{13}C1 enrichment levels when comparing

to those we determined in the non-diabetic controls (5.50 ± 0.49%). In fact in the STZ, IP and SC groups, the $^{13}C1$ enrichment level was very close to the 1.11% natural abundance: 1.40 ± 0.10%, in the STZ; 1.26 ± 0.06%, in the IP and 1.34 ± 0.04% in the SC. Hence, in these animals there was no efficient glycogen synthesis from the oral glucose load, in perfect agreement with the similar hepatic glycogen content prior and after the test as determined by the enzymatic measurement.

3.3.3 Sources to blood glucose

The relative contributions to blood glucose were calculated from the equations presented in section 2.2.5 and are shown in Table 8. To determine the concentration of glucose derived from each source, the percent contribution was multiplied by the glycemia registered at the end of the experiment. This analysis is depicted in Figure 13.

Table 8: Percent contributions of various sources to blood glucose 3 hours after the glucose tolerance test. Experimental groups are as described in the legend of Table 7. The oral load was enriched with $^{2}H_2O$ and [U-^{13}C]glucose tracers. The corresponding equations used to derive the source contributions are also indicated. Values not sharing a common superscript letter are significantly different; statistical significance was accepted for a $p < 0.05$ determined by one way ANOVA with Fisher's LSD post test. N.D., not detectable.

	Gastric	Recycled	Endogenous
	% (Equation 9)	% (Equation 10)	% (Equation 11)
Control	16 ± 1 ^{a}	23 ± 1 ^{a}	61 ± 1 ^{a}
STZ	23 ± 4 ^{a}	13 ± 1 ^{b}	65 ± 5 ^{a}
SC	N.D.	9 ± 1 ^{bc}	91 ± 1 ^{b}
IP	N.D.	7 ± 2 ^{c}	93 ± 2 ^{b}

3.3.3.1 Comparison between Control and STZ

In the STZ, all the absolute contributions to blood glucose were elevated when compared to controls (Figure 13). Hence, both a reduced

clearance of the oral load as well as an increased contribution from endogenous sources account for the hyperglycemic state of those animals. For this reason, the relative contributions of load glucose (gastric + recycled) and endogenous precursors to blood glucose were similar between STZ and Control (Table 8). These findings are in line with the observations from infusion studies by Wi *et al* where, one day after a 75 mg/kg STZ injection, hyperglycemia was associated with both increased glucose output and reduced clearance (Wi *et al.* 1998). Furthermore, those authors correlated the defects in glucose clearance with a decreased uptake of plasma glucose by the skeletal muscle. That mechanism also provides a good explanation for the present observations of reduced recycled glucose contribution in the STZ-diabetic rats since the apearence of recycled glucose relies largely on skeletal muscle uptake and metabolism of the parent [U-^{13}C]glucose tracer.

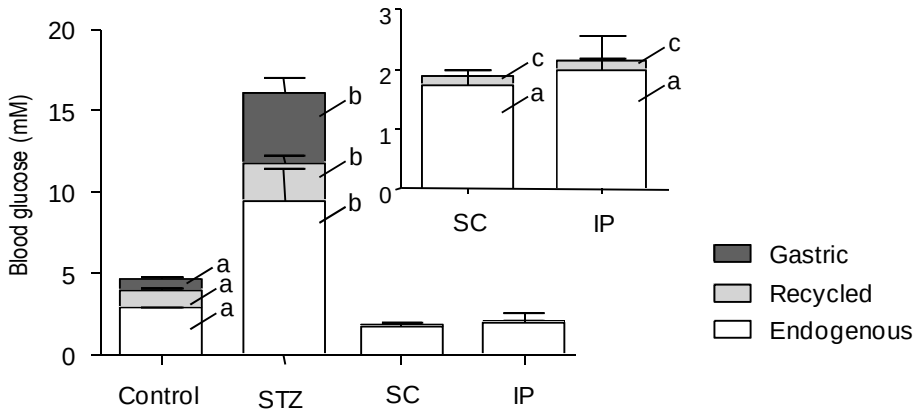

Figure 13 Contributions (expressed as glucose concentration) of gastric absorption, glucose load recycling and endogenous sources to blood glucose 3 hours after the glucose tolerance test. Experimental groups are as described in the legend of Table 7. The oral load was enriched with $^{2}H_2O$ and [U-^{13}C]glucose tracers. A zoom for SC and IP groups is shown. For each source, bars not sharing a common letter are significantly different; statistical significance was accepted for a $p < 0.05$ determined by one way ANOVA with Fisher's LSD post test.

In the STZ, the contribution of EGP to blood glucose, as estimated by the ^{2}H enrichment level of glucose position 2 relative to that of the body water was 72 ± 6%. This value is consistent with combined contributions of

endogenous precursors and recycled load (78%), determined by analysis of ^{13}C isotopomer enrichment indicating that the enrichment of position 2 from $^{2}H_2O$ was representative of net hepatic glucose output rather than futile glucose/G6P cycling. Moreover, the contribution of EGP to plasma glucose is similar to the 75 ± 7% determined for controls (see chapter 2). Finally, in both cases, gluconeogenesis dominated EGP as estimated by the H5/H2 ratio: 0.89 ± 0.03 for STZ and 0.92 ± 0.04 for Control.

3.3.3.2 Effect of the insulin dose

Insulin administration to the STZ-diabetic rats in the IP and SC groups significantly altered glucose load disposal. In those groups the [U-^{13}C]glucose isotopomer was no longer detectable in the blood 3 hours after the oral gavage (see Figure 12), indicating that almost all of the glucose load had been cleared from the circulation. Additionally, the contribution of glucose from recycling of the load was significantly reduced relative to both STZ and Control groups. These observations, together with the absence of net glycogen synthesis in the liver, suggest that glucose may have been oxidized or stored as glycogen in the skeletal muscle.

At the end of the test, more than 90% of blood glucose had derived from endogenous sources in the STZ-diabetic rats injected with insulin (Table 8). This contribution represented a glucose concentration similar to that observed in the non-diabetic controls, indicating that insulin reduced the contribution of EGP relative to the STZ-diabetic rats.

Because of the poor signal to noise ratio that characterized most of the ^{2}H NMR MAG spectra from blood glucose in SC and IP groups, the relative contributions of glycogenolysis and gluconeogenesis to EGP could not be quantified with confidence. Nevertheless, the similar intensities for H5 and H2 signals of blood glucose-derived MAG obtained from these animals (Figure 12) clearly indicate that gluconeogenesis was the main source of EGP in both cases.

3.3.4 Hepatic glycogen synthesis

Hepatic glycogen synthesis in the setting of the OGTT was fully characterized in chapter 2 for the non-diabetic controls. In the case of STZ-diabetic rats, there was no net glycogen synthesis in the liver. This was demonstrated by the similar glycogen content found in the liver of those animals before and after the OGTT, in contrast to what was observed for non-diabetic controls that had 10 times more glycogen after the test (see section 2.3.2). Insulin administration prior to the OGTT had no effect on the hepatic glycogen content. Furthermore, the percent ^{13}C excess enrichment determined in the glycogen of rats from STZ, IP and SC groups was ~0.2%, much lower than the ~4% detected in the non-diabetic controls subjected to the same protocol.

3.4 Discussion

Without food intake blood glucose levels depend on EGP derived either from glycogenolysis or gluconeogenesis. The gluconeogenic contribution increases with the time of fasting. For example, in non-diabetic rats after 6 hours of fasting, gluconeogenesis accounts for about two thirds of EGP whereas after 24 hours of fasting that contribution represents over 90% of EGP (Nunes *et al.* 2009). In the present studies (see also chapter 2) hepatic glycogen levels were highly depleted in control rats after the 24-hour fast, in good agreement with high gluconeogenic activity.

Unlike controls, the STZ-diabetic rats showed substantial levels of glycogen in the liver after the 24-hour fast. This has been previously reported by other authors (Friedmann *et al.* 1963; Ferrannini *et al.* 1990; Peroni *et al.* 1997). Apparently, these animals did not utilize hepatic glycogen stores during fasting, in accordance with the dominance of gluconeogenesis over glycogenolysis to EGP both in the post absorptive state and after 24 hours of fasting (Peroni *et al.* 1997). Interestingly, Friedmann *et al* showed that in diabetic rats, hepatic glycogen could be

depleted by prolonging the fasting period to 48 hours or by glucagon treatment and that refeeding after these interventions resulted in efficient hepatic glycogen synthesis, although the maximal glycogen levels still remain under those of non-diabetic controls (Friedmann *et al.* 1963).

As expected, gluconeogenesis also dominated EGP in the diabetic animals, contributing to more than 60% of blood glucose at the end of the test. This percent contribution was similar to that observed for controls but the respective absolute contribution was much higher. In fact, all the absolute contributions to blood glucose were increased in the diabetic rats. The tracer-enriched OGTT protocol demonstrated that after the administration of the oral glucose load to STZ-diabetic rats, the contribution of load glucose adds to that from glucose production to account for the elevated blood glucose levels observed at the end of the test. These findings are in line with elevated EGP (Blondel *et al.* 1989; Peroni *et al.* 1997; Wan *et al.* 2000) and reduced glucose clearance (Wi *et al.* 1998) in the post absorptive state in STZ-diabetic rats.

A single insulin injection prior to the glucose challenge altered the glycemia response of the STZ-diabetic rats, resulting in a rapid and pronounced decrease of plasma glucose levels. This enhanced glucose uptake from circulation resulted from two combined mechanisms. On the one hand, insulin reduced the absolute contribution of endogenous sources to the plasma glucose pool from the abnormally elevated values in the STZ-diabetic rats to control levels. In addition, insulin strongly promoted glucose clearance. This last action is most probably a consequence of peripheral uptake rather than hepatic disposal and storage as no efficient glycogen synthesis was detected. The persistent hypoglycemia observed in the final minutes of the test is in agreement with the absence of glucagon counterregulation to insulin-induced hypoglycemia in the STZ-diabetic rats injected with insulin, by opposition to the glucagon response that follows normal insulin secretion in non-diabetic rats (Zhou *et al.* 2004).

3.5 Conclusions

In STZ-diabetic rats both a deficient glucose clearance in peripheral tissues and an excessive glucose production contribute to the hyperglycemic state throughout the OGTT experiment. Hepatic glycogen serves as short-term reservoir for endogenous gluconeognenic flux when fasted controls receive an oral glucose load. In this way, EGP may be rapidly suppressed. Data from these studies show that this mechanism is inoperative in the STZ-diabetic rats. Insulin administration to STZ-diabetic rats reduced the contribution of EGP to plasma glucose and, most importantly, enhanced peripheral glucose disposal; but had no effect on diverting the gluconeogenic flux from EGP to hepatic glycogen synthesis during the OGTT.

4
GLUCOSE PRODUCTION AND HEPATIC GLYCOGEN AND LIPID SYNTHESIS DURING *AD LIBITUM* FEEDING CONDITIONS IN RATS – EFFECT OF DIABETES

4.1 Introduction

In humans, direct and indirect pathway contributions to hepatic glycogen are quantified by analysis of plasma glucose and UDP-glucose enrichment following infusion of a glucose tracer as part of an intravenous glucose load (Hellerstein *et al.* 1995) with corrections for recycling of the labeled carbon (Magnusson *et al.* 1987). Alternatively, the tracer can also be given as part of a meal (Taylor *et al.* 1996; Bischof *et al.* 2002) to study the pathways of glycogen repletion under normal feeding conditions. This approach is poorly suited to study hepatic glycogen synthesis in *ad libitum* fed rats since they tend to feed intermittently over the entire dark period of the diurnal cycle (Benavides *et al.* 1998). While there have been studies of glycogen synthesis under artificial substrate delivery conditions such as glucose infusion (Katz *et al.* 1989) or after a glucose load (Newgard *et al.*

1983; Shulman *et al.* 1985) there is no reported measurement of direct and indirect pathway activities in rats during their natural feeding routine. Since postprandial hepatic glycogen levels are sensitive to dietary composition (Gaíva *et al.* 2003; MacQueen *et al.* 2007), measurement of direct and indirect pathway activities under baseline conditions is essential for evaluating the effect of disease or other interventions on these fluxes.

To quantify hepatic glycogen repletion via direct and indirect pathways during *ad libitum* feeding, the positional ^{2}H-enrichment of hepatic glycogen was analyzed following the administration of $^{2}H_2O$ at the beginning and throughout the feeding cycle. The contribution of indirect pathways of hepatic glycogen synthesis was estimated by the ratio of glycogen ^{2}H enrichment in position 5 relative to position 2 (H5/H2), see chapter 1. Moreover, the relative contributions of gluconeogenesis and glycogenolysis to EGP could also be disclosed by determining the H5/H2 ratio in blood glucose.

With the present $^{2}H_2O$ administration protocol it was also possible to determine the contribution of DNL to the hepatic TG pool. That fraction was determined by analysis the ^{2}H enrichment in the methyl group of the hepatic TG relative to that of the body water as reported by Delgado *et al.* (Delgado *et al.* 2009a).

The key advantages of this assay are the simplicity of tracer administration (no infusion catheters required) and that it can be applied to any substrate delivery setting including clamp studies, oral or i.p. glucose load and *ad libitum* feeding. In this study, this method was applied to define the effect of STZ-induced diabetes on hepatic pathways for glucose disposal and storage as glycogen or TG and also pathways for EGP in *ad libitum* fed rats.

4.2 Materials and methods

4.2.1 Animal studies

4.2.1.1 Animal housing

As described in section 2.2.1.1.

4.2.1.2 Animal protocols

Rats (245 ± 4 g) were rendered diabetic by STZ injection as described in section 3.2.1.2. One group of animals consisted of non-diabetic control rats that were not injected with STZ (Control, N = 6). The other 3 groups consisted of STZ-diabetic rats studied at day 4 (STZ-4, N = 6), 10 (STZ-10, N = 8) or 20 (STZ-20, N = 8) after the induction of the disease. At 7 pm all animals received a loading dose of 99% ^2H_2O in saline by injection into the i.p. cavity. Assuming 70% body weight as water, the dose was calculated to enrich the body water to 2% or 3%. To maintain body water enrichment, their drinking water was enriched to 5% with ^2H_2O. At 8 am the next morning, animals were anesthetized by injection of ketamine (2 mL/kg) in the i.p. cavity, the abdominal cavity was opened and ~5 mL of blood were collected from the abdominal aorta. A small blood sample (0.5 mL) was reserved for determination of ^2H_2O body water enrichment and plasma insulin levels. The liver was excised and immediately freeze-clamped in liquid nitrogen.

A group of control rats (N = 5) was sacrificed at 7 pm without receiving the ^2H_2O tracer and the livers harvested for determining the baseline glycogen and TG content.

4.2.2 Metabolite analyses

Glucose was extracted from the blood, hepatic glycogen isolated, hydrolyzed to glucose and quantified and plasma insulin levels quantified

as described section 2.2.2. Glucose was converted to MAG as described in 2.2.3. Part of the lyophilized liver powder underwent lipid extraction accordingly with the method developed by Folch *et al.* (Folch *et al.* 1957). Briefly, approximately 1 g of powder was treated with 40 mL of chloroform:methanol (2:1, v:v). After centrifugation the liquid phase was recovered and 8 mL of NaCl (0.9%) were added, the solutions were vigorously mixed, centrifuged and the lower phase collected. Chloroform was evaporated under nitrogen flux and the lipid content stored at -20ºC until further analysis.

4.2.3 NMR spectroscopy

As described in sections 2.2.4, 2.2.4.1 and 2.2.4.2

4.2.3.1 ^{1}H and ^{2}H analysis of lipids

Lipid samples were treated as described by Delgado *et al* (Delgado *et al.* 2009a). Briefly, lipids were dissolved in 0.6 mL of chloroform and 150 µL of a pyrazine-d_4 solution were added as internal reference standard for quantification of hepatic TGs and determination of ^{2}H methyl enrichment levels. ^{1}H and ^{2}H NMR spectra were acquired at 25 ºC using the Varian 600 system equipped with a 5 mm broadband probe. ^{1}H NMR spectra of lipid samples consisted of one scan obtained using an acquisition time of 3 seconds and served for quantification of the hepatic TG content. ^{2}H NMR spectra were obtained within 3 to 12 hours (depending on the amount of sample and ^{2}H enrichment level) using a 90º pulse, an acquisition time of 5 seconds and a pulse delay of 2 seconds. The amount of ^{1}H-TG was determined by comparing the area of the methyl hydrogens with that of the pyrazine hydrogens in the ^{1}H NMR spectrum of each sample and the amount of ^{2}H-TG was determined by comparing the areas for those signals in the respective ^{2}H NMR spectrum. Hence, the hepatic TG content was

calculated as the sum of ^{1}H- and ^{2}H-TG. The absolute ^{2}H methyl enrichment was calculated as follows:

$$^{2}\text{H methyl enrichment} = \frac{^{2}\text{H-TG}}{^{2}\text{H-TG} + {}^{1}\text{H-TG}}$$

This quantification method was tested for linearity using a series of palmitic acid standards solutions prepared in chloroform from known amounts of [U-^{2}H]palmitic acid so that enrichment levels ranged from 0.035% to 0.40% (Figure 14).

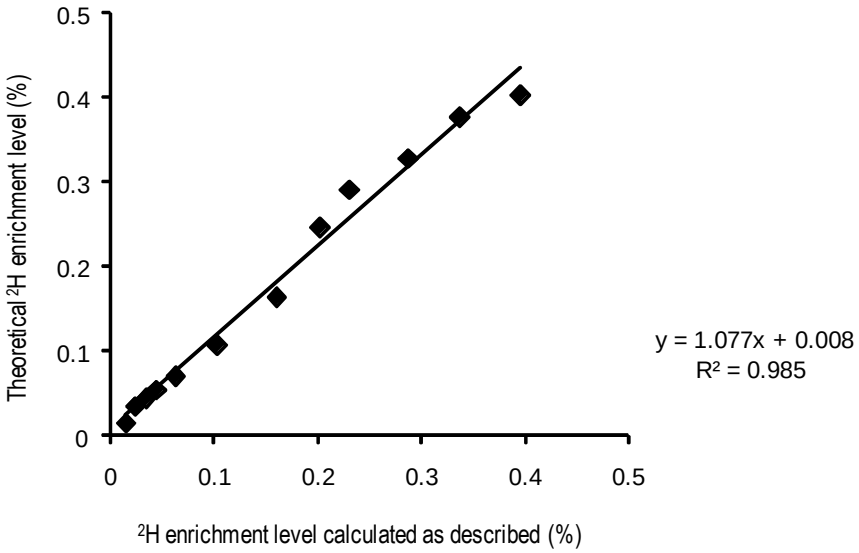

Figure 14 Plot of the theoretical ^{2}H enrichment level of a series of palmitic acid standards prepared from palmitic acid and [U-^{2}H]palmitic acid versus the ^{2}H enrichment calculated as described. The linear regression equation is shown.

4.2.4 Metabolic contributions parameters

The percent contribution of gluconeogenesis to EGP and the indirect pathway contribution to glycogen synthesis were calculated from the H5/H2 ratio in the ^{2}H NMR spectra of MAG from blood glucose and hepatic glycogen as shown in Equation 1 (page 37), while the contributions

of glycogenolysis to EGP and direct pathway to glycogen were calculated as the balance, as shown in Equation 2 (page 37).

The contribution of newly-synthesized glycogen to the hepatic glycogen pool during overnight feeding was calculated from the ratio of glycogen position 2 to body water ^{2}H-enrichments. Likewise, the contribution of newly synthesized TGs (DNL) to the hepatic TG pool was calculated as the ratio of ^{2}H methyl enrichment to body water ^{2}H enrichment.

4.2.5 Statistics

As described in section 2.2.6.

4.3 Results

4.3.1 Induction of diabetes

In this study, STZ-diabetic rats were assayed in three early stages of the disease. The first stage corresponded to 4 days after STZ injection and the other two corresponded to 10 and 20 days. In all of those stages animals were profoundly hyperglycemic (Table 9). This observation is in agreement with the reduced levels of plasma insulin determined for STZ-10 and STZ-20. Moreover, the hepatic glycogen content was reduced and the TG levels increased with the induction of diabetes by this method, in accordance with reports from other authors for SZT-diabetic rodent models (Pighin *et al.* 2005; Fernandes *et al.* 2010). These alterations were observed 10 and 20 days after the injection of STZ, but not at 4 days. Hence, 4 days after STZ injection, although rats develop hyperglycemia they still have hepatic glycogen and TG levels comparable with controls.

Table 9: Glycemia, plasma insulin, hepatic glycogen and triglyceride content determined after an overnight feeding under ^2H_2O administration in non-diabetic controls (Control) and STZ-diabetic rats assayed 4 (STZ-4), 10 (STZ-10) and 20 days (STZ-20) after induction of diabetes. For each parameter, values not sharing a common superscript letter are significantly different; statistical significance was accepted for a $p < 0.05$ determined by one way ANOVA with Fisher's LSD post test. N. D. not determined.

	Plasma Insulin (µg/L)	Glycemia (mg/dL)	Hepatic Glycogen (µmol/gdw)	Hepatic Triglycerides (µmol/gdw)
Control	5.3 ± 1 [a]	114 ± 4 [a]	907 ± 84 [a]	212 ± 22 [a]
STZ-4	N. D.	385 ± 31 [b]	816 ± 61 [a]	216 ± 7 [a]
STZ-10	0.5 ± 0.1 [b]	445 ± 31 [b]	407 ± 120 [b]	406 ± 39 [b]
STZ-20	0.7 ± 0.2 [b]	549 ± 25 [c]	344 ± 52 [b]	358 ± 31 [b]

4.3.2 Metabolite ^2H enrichment levels

Animals were kept under ^2H_2O administration overnight (~12 hours). The body water ^2H enrichment level was determined from a plasma sample at the end of that period and matched the target values (Table 10). For both blood and liver metabolites of interest, ^2H NMR spectra with sufficient signal to noise for a reliable quantification of ^2H excess enrichment were obtained (Figure 15 and Figure 17). This includes the hepatic TGs obtained for STZ-10 and STZ-20 groups, where the excess ^2H enrichment levels were very low due to a vastly decreased DNL activity.

Table 10: Body water (BW) and metabolite absolute ^2H enrichment levels observed after an overnight feeding under ^2H_2O administration. Experimental groups are as described in the legend of Table 9.

	^2H enrichement (%)				
	Target BW	BW	H2 Blood Glucose	H2 Glycogen	Methyl-TG
Control	3	2.90 ± 0.14	1.21 ± 0.15	0.99 ± 0.20	0.48 ± 0.06
STZ-4	3	3.37 ± 0.26	1.05 ± 0.06	0.91 ± 0.15	0.24 ± 0.05
STZ-10	2	1.63 ± 0.07	0.88 ± 0.09	1.19 ± 0.06	0.04 ± 0.007
STZ-20	2	1.99 ± 0.08	0.78 ± 0.02	1.12 ±0.09	0.04 ± 0.004

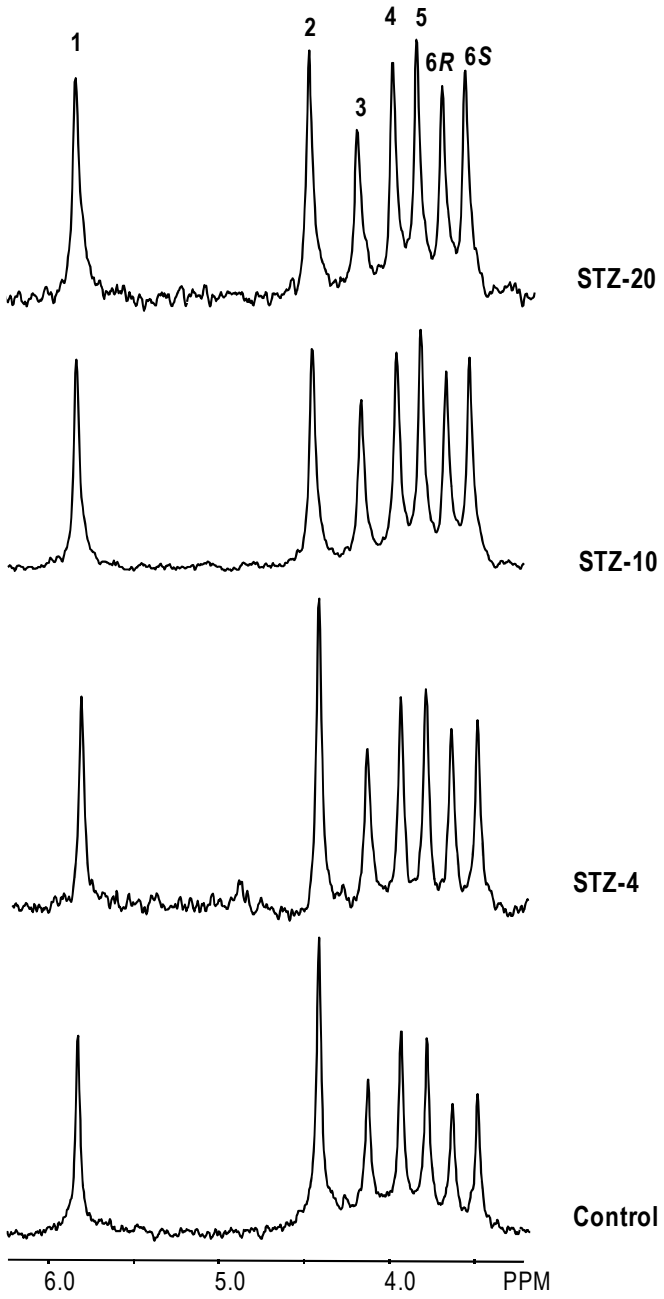

Figure 15 Representative ^{2}H NMR spectra of monoacetone glucose (MAG) showing the resonances for positions 1 to 6*S*. Blood was collected after an overnight feeding under $^{2}H_2O$ administration and glucose extracted and derivatized to MAG. Gluconeogenesis was estimated as the signal area of position 5 relative to position 2. Experimental groups are as described in the legend of Table 9.

4.3.3 Metabolic parameters

4.3.3.1 Sources of glucose production

The ^{2}H enrichment of position 2 of blood glucose relative to that of body water reflects the contribution of EGP to the circulating glucose. The remainder originates from absorption in the GIT. In non-diabetic controls, EGP accounted for 40 ± 4% of blood glucose and was similar to that determined in all STZ groups. Since STZ animals were hyperglycemic, they probably displayed higher rates of EGP coupled with increased food intake due to diabetes-related hyperphagia. Interestingly, the contribution of EGP to blood glucose in STZ-10 and STZ-20 was significantly higher than that observed for STZ-4, 46 ± 2% and 44 ± 5% *vs* 32 ± 2%, respectively. This likely reflects a weaker control (*i.e.* suppression) of EGP in animals that had been diabetic for a longer period. The STZ-10 and STZ-20 groups were additionally characterized by a significantly higher gluconeogenenic contribution to EGP compared to the STZ-4 group, which presented values comparable with non-diabetic controls (Figure 16).

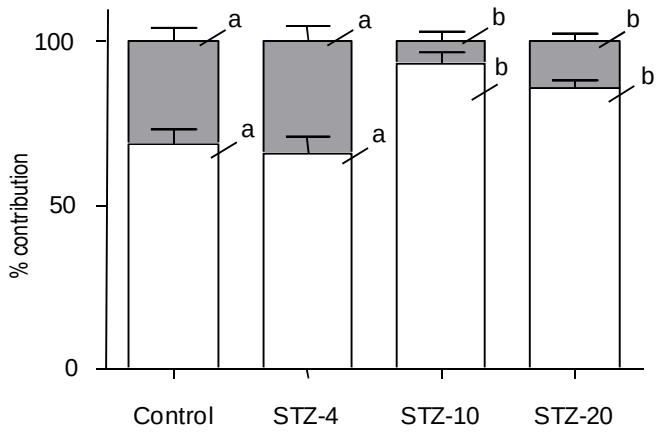

Figure 16 Relative contributions of gluconeogenesis (white bars) and glycogenolysis (grey bars) to endogenous glucose production determined after an overnight feeding under $^{2}H_2O$ administration. Experimental groups are as described in the legend of Table 9. For each source, bars not sharing a common letter are significantly different; statistical significance was accepted for a $p < 0.05$ determined by one way ANOVA with Fisher's LSD post test.

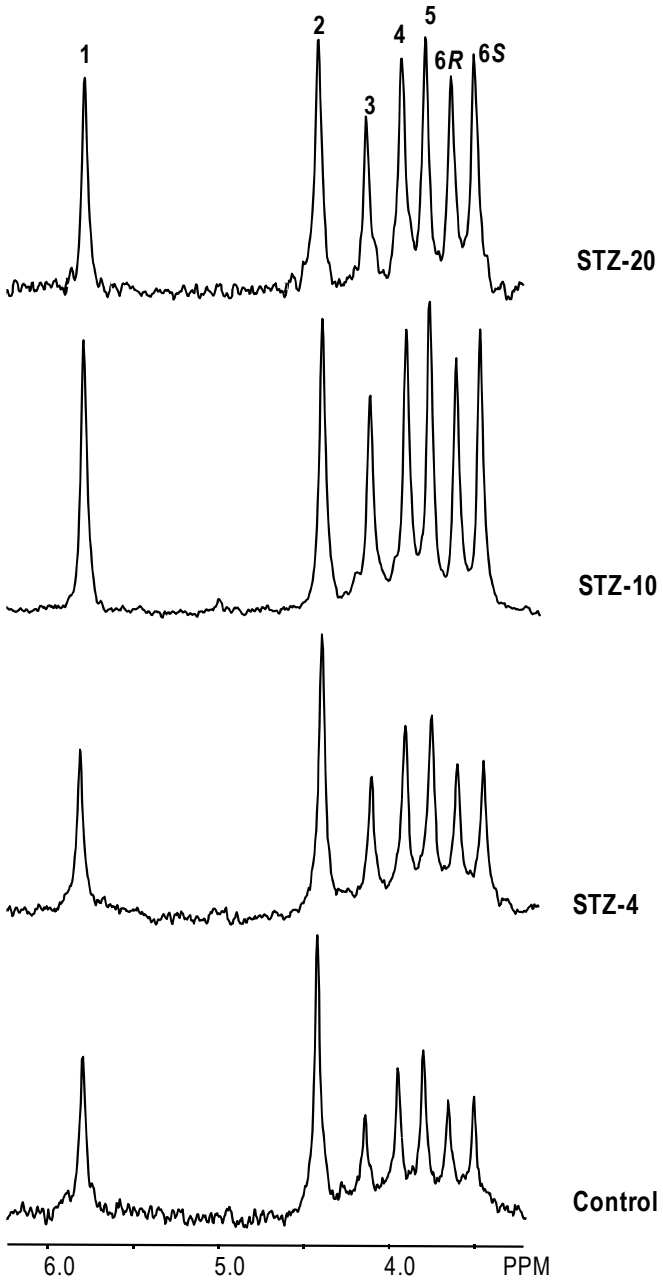

Figure 17 Representative ^{2}H NMR spectra of monoacetone glucose (MAG) showing the resonances for positions 1 to 6*S*. Livers were harvested after an overnight feeding under $^{2}H_2O$ administration and glycogen extracted, hydrolyzed to glucose and derivatized to MAG. Indirect pathway was estimated as the signal area of position 5 relative to position 2. Experimental groups are as described in the legend of Table 9.

4.3.3.2 Hepatic glycogen synthesis

In order to confirm that, under normal conditions, rats efficiently accumulate glycogen in the liver during feeding, hepatic glycogen content was quantified in non-diabetic controls at the beginning of the dark phase. In that group of animals, glycogen levels were 613 ± 75 μmol/gdw, significantly lower than the 907 ± 84 μmol/gdw determined in the morning (Table 9). This finding is in line with the circadian rhythm of hepatic glycogen, which increases during the dark phase and is consumed during the light phase under normal *ad libitum* feeding conditions (Lanza-Jacoby *et al.* 1986; Benavides *et al.* 1998). The net glycogen synthesis overnight represented about one third of the total hepatic glycogen content determined at the beginning of the light phase. This value is in excellent agreement with the estimation of glycogen synthesis from the ^{2}H enrichment in glycogen position 2 relative to that in body water, which reported a 34 ± 7% contribution in controls (Table 11). In the STZ-4 group this contribution was similar to controls but it increased significantly in STZ-10 and STZ-20, representing in those cases more than half of the glycogen. The higher fractional synthesis values detected for the STZ-10 and STZ-20 groups are consistent with the smaller glycogen pool observed for those animals. In fact, the amount of glycogen synthesized during the experiment (total amount of glycogen × $^{2}H2$-Glycogen/^{2}H-body water) was similar among the several groups.

Table 11: Contribution of newly synthesized glycogen to the hepatic pool and amount of glycogen synthesized overnight determined after an overnight feeding under $^{2}H_2O$ administration. Experimental groups are as described in the legend of Table 9. For each parameter, values not sharing a common superscript letter are significantly different; statistical significance was accepted for a $p < 0.05$ determined by one way ANOVA with Fisher's LSD post test.

	Control	STZ-4	STZ-10	STZ-20
Glycogen synthesis (% contribution)	34 ± 7 [a]	27 ± 4 [a]	63 ± 5 [b]	57 ± 8 [b]
Overnight-synthesized glycogen (μmol/gdw)	322 ± 87 [a]	212 ± 28 [a]	171 ± 31 [a]	206 ± 43 [a]

Despite the fact that the same amount of glycogen was synthesized overnight, the pathways for glycogen synthesis in the liver were altered in all STZ groups (Figure 18). In the STZ-4 group the indirect pathway was increased relative to controls and in STZ-10 and ST-20 groups it completely dominated glycogen synthesis in the liver.

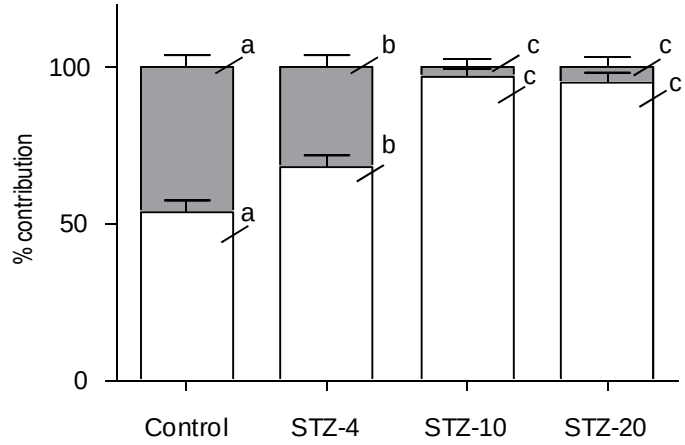

Figure 18 Direct (grey bar) and indirect (white bar) pathways for hepatic glycogen synthesis after an overnight feeding under ^2H_2O administration. Experimental groups are as described in the legend of Table 9. For each pathway, bars not sharing a common letter are significantly different; statistical significance was accepted for a $p < 0.05$ determined by one way ANOVA with Fisher's LSD post test.

4.3.3.3 Hepatic triglycerides and de novo *lipogenesis*

Figure 19 depicts a representative ^1H NMR spectrum obtained after the extraction of hepatic lipids by the Folch method. The resonance at ~0.8 ppm represents the terminal methyl groups of fatty acid chains (Noula *et al.* 2000; Ren *et al.* 2008) and was used to quantify the hepatic TG content by comparison with the internal pyrazine standard. In control rats, the amount of hepatic TGs at the beginning of the dark phase was 168 ± 17 μmol/gdw. After an overnight feeding the hepatic TG content was 212 ± 22 μmol/gdw (Table 9), which is not significantly different from that determined in the group of rats sacrificed at the beginning of the dark phase.

During feeding, TGs synthesized *de novo* are enriched with ^2H from ^2H_2O whereas those derived from the diet or adipose tissue lipolysis are unlabeled and therefore contribute to the dilution of the ^2H labeling from DNL. To the extent that the hepatic TG pool has not turned over during the overnight feeding phase, the presence of unlabeled TGs in the liver prior to the administration of ^2H_2O also contributes to that dilution. The ^2H-enriched TGs were quantified from analysis of the ^2H NMR spectra of hepatic lipids (Figure 20).

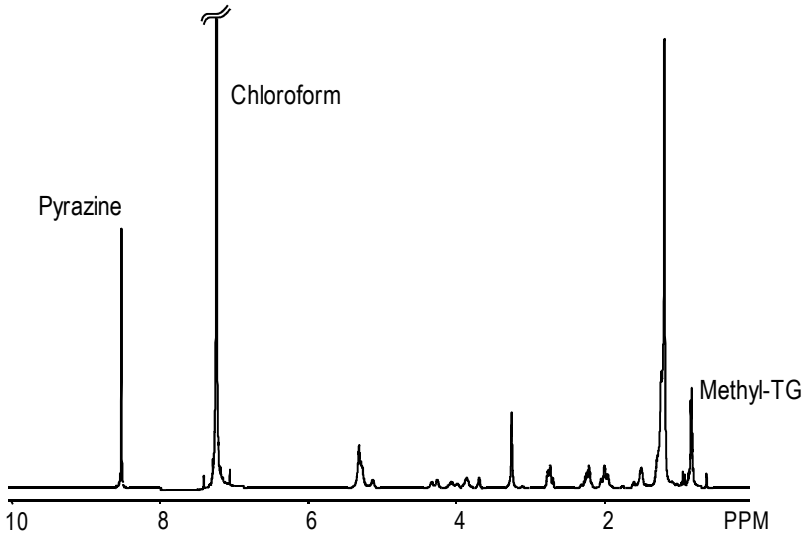

Figure 19 Representative ^1H NMR spectrum of hepatic lipids obtained by Folch extraction from a diabetic rat 4 days after STZ injection. The solvent chloroform, the standard pyrazine and the methyl groups of TG are assigned to the respective resonances.

As shown in Table 12, the contribution of DNL to the hepatic TG pool in the STZ-4 group was half of that determined for controls. In STZ-10 and STZ-20 groups DNL represented no more than 2.5% of the hepatic TG pool. These findings indicate that the dietary and/or lipolytic contribution to hepatic TGs is increased in all STZ groups especially in the STZ-10 and STZ-20, in which the hepatic TG levels were about the double of those determined for the other groups (Table 9).

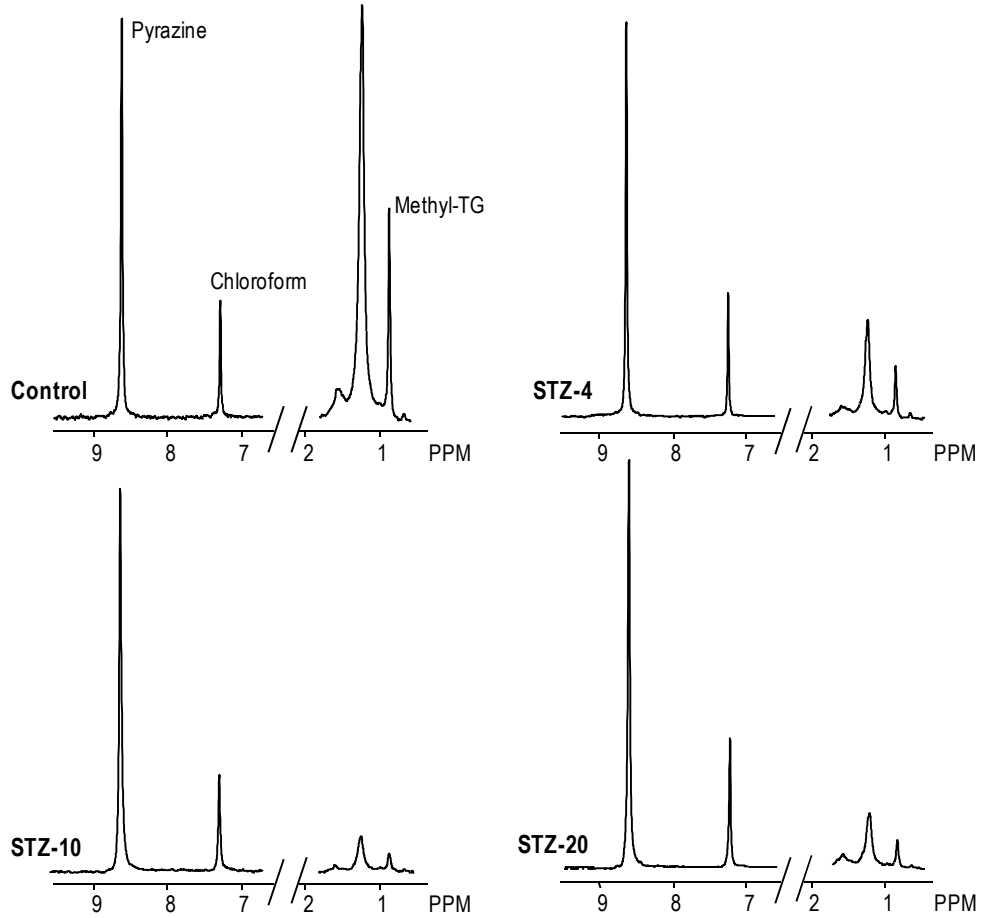

Figure 20 Representative ^{2}H NMR spectra of hepatic lipidic extracts after an overnight feeding under $^{2}H_2O$ administration. The spectral regions show the solvent chloroform, the standard pyrazine and the methyl groups of TGs assigned to the respective resonances. Control, non-diabetic controls; STZ-4, STZ-10 and STZ-20, STZ diabetic rats assayed 4, 10 and 20 days after diabetes induction, respectively.

Table 12: Contribution of *de novo* lipogenesis (DNL) to the hepatic triglyceride (TG) pool and amount of newly synthesized TGs determined after an overnight feeding under $^{2}H_2O$ administration. Experimental groups are as described in the legend of Table 9. For each parameter, values not sharing a common superscript letter are significantly different; statistical significance was accepted for a $p < 0.05$ determined by one way ANOVA with Fisher's LSD post test.

	Control	STZ-4	STZ-10	STZ-20
DNL (% contribution)	16.3 ± 1.7 [a]	7.3 ± 1.7 [b]	2.5 ± 0.4 [c]	2.0 ± 0.2 [c]

4.4 Discussion

4.4.1 Addressing the absorptive state

The circadian rhythm of the organism rules many biological functions. In the light cycle of rodents, the dark phase is characterized by high locomotive activity and oxygen consumption (Williams *et al.* 2000; Yamaoka *et al.* 2008) parallel to an increase in insulin levels (Benavides *et al.* 1998) and food and water intakes (Armstrong *et al.* 1980; Johnson *et al.* 1990; Benavides *et al.* 1998). Perhaps not surprisingly, gene array experiments performed over a 24-hour period clearly demonstrate that rat liver gene expression oscillates accordingly with the light cycle, including the expression of enzymes involved in carbohydrate and lipid metabolism (Almon *et al.* 2008). Hence, during feeding, pathways for glucose disposal and storage must be favoured against glucose production.

The studies described on this chapter were designed to follow several metabolic insulin-dependent pathways during the natural feeding cycle of rats. The protocol consisted on keeping the animals under ^2H_2O administration overnight so that pathways for glucose production, hepatic glycogen and TG synthesis could be simultaneously traced in one single experimental setting by ^2H NMR methods. With this methodological approach there is no interference with the animals' natural feeding behaviour and hence the data obtained reflect the metabolic performance in the absorptive state under *ad libitum* conditions. The baseline measurements determined in non-diabetic rats were sensitive to the STZ-induced type 1 DM, making this a valuable protocol for addressing the effect of any intervention in the context of diabetes.

4.4.2 Sources to blood glucose and hepatic glycogen synthesis

During the absorptive phase, blood glucose may be derived from both dietary absorption and endogenous production. In the present experimental setting, assuming the G6P/F6P exchange is complete and

there is no substancial glucose/G6P cycling, glucose from EGP is enriched with ^2H in position 2 to the same level as body water and that enrichment is diluted by glucose derived from absorption. In the STZ-diabetic rats, the relative contributions of EGP and dietary sources to blood glucose were similar to those determined for non-diabetic controls, despite much higher glycemia values for the STZ-diabetic animals. Insulin deficiency is expected to result in higher endogenous contributions to feeding plasma glucose levels as a result of impaired EGP suppression. However, STZ-diabetic rats also eat more than controls (see also chapter 915, Table 14), due to the hyperphagia associated with the lack of hypothalamic insulin and leptin signalling (Sindelar *et al.* 1999; Akirav *et al.* 2004). This would translate into an increased uptake of dietary glucose. Therefore, the observation that EGP and dietary contributions to blood glucose levels in the hyperglycemic STZ rats were similar to those of normoglycemic controls may be explained by systematic increases in both EGP and glucose absorption rates for the STZ-diabetic rats.

In the non-diabetic controls, the ^2H_2O method indicated that immediately after an overnight feeding, gluconeogenesis accounts for the majority (approximately two thirds) of EGP. This is similar to estimates obtained after 6 hours of fasting in the same rat specie and using the same methodology as that described in these experiments (Nunes *et al.* 2009). Saadatian *et al.* report a somewhat lower (~50%) contribution of gluconeogenesis to EGP (Saadatian *et al.* 2000), using mass spectrometry methods. Taken together, these observations demonstrate that gluconeogenesis is continually active in non-diabetic free-feeding rats and does not appreciably change during the fed to fasted transition.

In control rats only ~30% of the hepatic glycogen was synthesized overnight and of that fraction ~50% was enriched with ^2H from ^2H_2O-enriched body water in both positions 5 and 2. The ^2H_2O method relies on the assumption that only glucose derived from gluconeogenesis is enriched with ^2H from ^2H_2O in both positions 5 and 2. But, because under the present experimental protocol 15% (30% × 50%) of the total hepatic glycogen was also

enriched with ^2H in both positions 5 and 2, the contribution of glycogenolysis may be underestimated, but to a minor degree. Applying the 15% correction factor yields a 35% (instead of the 30%) contribution of glycogenolysis to EGP. Hence, under these circumstances, the ^2H_2O method is fairly reliable. However, in the case of diabetic rats studied 10 and 20 days after STZ injection, because of the high glycogen turnover (~60%) and the complete dominance of the indirect pathway (~95%), the majority of the glycogenolytic contribution to blood glucose is indistinguishable from the gluconeogenic contribution because the glucose derived from glycogen is labeled in both 5 and 2 positions. Furthermore, since the amount of glycogen synthesized overnight was apparently the same in all groups, the reduced glycogen levels observed in the later stages of STZ-diabetes must be a consequence of excessive glycogen breakdown. Taken together, these observations indicate that, at least 10 days after induction of diabetes by STZ injection to rats, there was extensive glycogen degradation with simultaneous synthesis during the absorptive state (*i.e.* glycogen cycling).

4.4.3 Estimation of *de novo* lipogenesis

With the induction of diabetes there was a drastic reduction on the DNL contribution to the hepatic TG pool and this was immediately detected 4 days after STZ injection. These observations are in line with Cohen's (Cohen 1987) experiments in perfused livers from control and STZ rats reporting that in the latter case the flux through pyruvate carboxylase is increased relative to that through pyruvate dehydrogenase resulting, amongst other things, in the recruitment of pyruvate into gluconeogenesis, rather than its oxidation to acetyl-CoA molecules for lipogenesis.

The synthesis of TG *de novo* in the liver was estimated by ^2H NMR analysis of the hepatic lipid content as the ratio of the ^2H-methyl enrichment relative to that of body water. Although this estimation provides valuable insight on the hepatic lipid kinetics it is not an accurate quantification of the contribution of DNL to the hepatic TG content. Ideally, the ^2H enrichment in

the methyl-TG should be compared to that of the precursor acetyl-CoA pool but that intermediate is scarce and difficult to isolate. Therefore, a necessary simplifying assumption is that the hepatic ^{2}H acetyl-CoA enrichment is equivalent to that of body water. It is not know to what extent the acetyl-CoA methyl hydrogens directly exchange with those of water in the cellular environment, but it is well know that many of the key acetyl-CoA precursors – notably pyruvate – exchange extensively (Kuwajima *et al.* 1986) while others, such as fatty acids, involve the direct adition of water hydrogens to the methyl group when undergoing *β*-oxidation to acetyl-CoA.

Under feeding conditions, pyruvate is considered to be the main source of acetyl-CoA (Cohen 1987) and the incorporation of ^{2}H from body water in pyruvate is extensive (Kuwajima *et al.* 1986) but not necessarily complete (Silva *et al.* 2011). To the extent that the true acetyl-CoA ^{2}H enrichment is less than that of body water, DNL contributions to the hepatic TG pool are systematically underestimated.

Another factor affecting the estimations of DNL is the turnover of the hepatic TG pool. After 12 hours under $^{2}H_2O$ administration it is possible that the TGs did not turn over completely and hence pre-existing TGs may be accounting for the dilution of the ^{2}H labelling in addition to the contribution of dietary and/or adipose tissue-derived TGs. Nonetheless, the DNL contribution determined in this experiment for non-diabetic controls was in the range of that found by Delgado *et al.* after 72 hours of $^{2}H_2O$ administration (Delgado *et al.* 2009a), suggesting the TG pool turned over during the overnight $^{2}H_2O$ protocol. In the case of the STZ diabetic rats, TG turnover may take longer given the higher hepatic pool.

4.4.4 Progressive metabolic disruption in STZ-diabetes and relationship between carbohydrate and lipid metabolism

Experimental diabetes was induced by injection of STZ in the i.p. cavity and rats studied 4, 10 and 20 days afterwards. In all cases, rats were profoundly hyperglycemic. This finding is consistent with the rapid

development of diabetic symptoms in the STZ-diabetic rat model (Burcelin *et al.* 1995; Sindelar *et al.* 1999; Wei *et al.* 2003). Furthermore, data from this study indicate that some metabolic pathways are altered in the first days following STZ injection and that those alterations are sustained afterwards. For example, at day 4 , the relative pathways to EGP were similar to controls and the contributions of the direct pathway to glycogen and DNL to hepatic TG – although reduced compred to controls – were not as low as those observed for the other STZ groups. In the later stages of diabetes (10 and 20 days after STZ injection), the complete dominance of gluconeogenesis to both glycogen synthesis and glucose production correlates with the profound reduction of the lipogenic flux. Moreover, the elevated levels of TGs in the livers from 10- and 20-day STZ-diabetic rats suggest adipose tissue lipolysis is likely to be the dominant source for hepatic TGs. Among other things, the increased abundance of hepatic lipids helps to sustain high rates of gluconeogenesis and EGP.

4.5 Conclusions

The ^2H_2O protocol for the study of the absorptive phase under natural feeding conditions was successfully applied to both non-diabetic controls and STZ-diabetic rats. With one single experiment, it identified early alterations in hepatic carbohydrate and lipid metabolism following β cell destruction by STZ. Namely, DNL was profoundly reduced as early as 4 days after the induction of diabetes. By that time the indirect pathway to glycogen synthesis was already increased relative to controls but the contributions of glycogenolysis and gluconeogenesis to blood glucose were normal. In the later stages of STZ-diabetes, gluconeogenesis was the major source of both EGP and glycogen synthesis. The dominance of the gluconeogenic (indirect) pathway to glycogen synthesis and the rapid turnover of the hepatic pool via glycogen cycling translated into an extensive enrichment of hepatic glycogen positions 5 and 2 from ^2H_2O. This likely resulted in an underestimation of the

glycogenolytic contribution to EGP as determined by the overnight $^{2}H_2O$ method.

5
GLUCOSE PRODUCTION AND HEPATIC GLYCOGEN AND LIPID SYNTHESIS DURING *AD LIBITUM* FEEDING CONDITIONS IN RATS – EFFECT OF INSULIN REPLACEMENT

5.1 Introduction

Type 1 diabetic patients have insufficient pancreatic insulin secretion and thus must rely on exogenous insulin supply to avoid persistent hyperglycemia and related complications. With the conventional s.c. insulin treatment the peripheral tissues are the ones that receive most of the insulin dose. On the other hand, i.p. insulin administration is able to mimic the physiological insulin release, maintaining a portal/peripheral gradient concentration with insulin absorption occurring evenly through splanchnic and peripheral routes (Radziuk *et al.* 1994). In fact, under physiological conditions, insulin is secreted by the pancreas to the portal vein and the liver accounts for the extraction of a 50-80% fraction (Radziuk *et al.* 1994; Utzschneider *et al.* 2004).

There are some studies highlighting the relevance of i.p. insulin delivery in the context of diabetes treatment. Implanted insulin pumps that deliver insulin by i.p. infusion reduce the risk of hyperglycemia, and offer a better metabolic control compared with s.c. infusion pumps (Catargi 2004). Intraperitoneal insulin has also been administered to diabetic patients with end-stage renal disease undergoing continuous ambulatory peritoneal dialysis and this allowed for improving the glycemic control over conventional s.c. delivery (Nevalainen *et al.* 1997).

Experiments in STZ-diabetic rats have demonstrated the beneficial effect of i.p. insulin on reducing glucose production, peripheral hyperinsulinemia, and improving glucose disposal relative to s.c. insulin (Mason *et al.* 2000; Wan *et al.* 2000). However, those studies were performed in post-absorptive conditions (after 5-6 hours of fast) and it would be of interest to evaluate the effect of i.p. insulin in natural feeding rats.

During feeding, insulin stimulates the usage of glucose and its storage as glycogen and lipids in the liver. This is accomplished by diverse mechanisms through changes in enzyme activities and/or expression (overviewed in section 1.3.1). Since the liver is the organ targeted with i.p. insulin delivery, it can be hypothesized that the hepatic metabolic pathways will respond differently to the s.c. or i.p. insulin therapies. This chapter describes and discusses the experiments set to test that hypothesis. The methodological approach was the same described in chapter 4 to address hepatic insulin-dependent metabolic pathways during the absorptive state in rats. In addition, gene expression and enzyme activities for some key metabolic enzymes involved in those pathways were also assessed. The alterations detected in STZ-diabetes were recapitulated and in parallel the effect of insulin replacement during a short period was addressed. Insulin therapy began two weeks after the induction of diabetes, when the pathways for glucose production, hepatic glycogen and lipid synthesis were already severely disrupted (see chapter 4).

5.2 Materials and methods

5.2.1 Animal studies

5.2.1.1 Animal housing

As described in section 2.2.1.1.

5.2.1.2 Animal protocols

Rats (280 ± 2 g) were rendered diabetic by STZ injection as described in section 3.2.1.2. Eight days after diabetes induction animals were assigned at random into 3 groups: one group of animals was administered a s.c. insulin injection at a dose of 15 U/kg twice a day at 8 am and 7 pm (group I-SC, N = 9); a second group of animals received an i.p. insulin injection at the same dose and times as the I-SC group (group I-IP, N = 9); finally, a third group of animals received no treatment at all (group D, N = 7). Animals were kept under the insulin treatment protocol for 9 or 10 days. Blood glucose and TG levels were monitored throughout the experimental period with an Accu-check and Accutrend (Roche, Portugal) meters, respectively. At the end of the treatment period, 30 minutes after the night insulin injection, animals received a loading dose of 99% ^2H_2O in saline by injection into the i.p. cavity and the experiment proceeded as described in section 4.2.1.2. Animals were sacrificed the next morning. Blood was collected for glucose extraction and NMR analysis and a small blood sample was reserved for determination of ^2H_2O enrichment levels, insulin and NEFA in the plasma. The liver was excised, immediately freeze-clamped in liquid nitrogen. A small liver sample was reserved for enzyme activities assays and real-time polymerase chain reaction (PCR) and the remainder lyophilized. Epididymal white adipose tissue (EWAT) was collected and weighted.

The control group in the experiments described in chapter 4 was used in this study for sake of comparison.

5.2.2 Metabolite analyses

Glucose was extracted from the blood, hepatic glycogen isolated, hydrolyzed to glucose and quantified and plasma insulin levels quantified as described section 2.2.2. Exogenous (human) insulin was quantified in the plasma as described in 3.2.2. Glucose was converted to MAG as described in section 2.2.3. Hepatic lipids were extracted as described in section 4.2.2. Plasma NEFA were determined enzymatically with NEFA-HR assay kit (Wako chemicals, Germany).

5.2.3 NMR spectroscopy

As described in sections 2.2.4, 2.2.4.1, 2.2.4.2 and 4.2.3.1

5.2.4 Metabolic contributions parameters

As described in section 4.2.4.

5.2.5 Enzyme activities assays

Enzyme activities assays were carried out as previously described (Metón *et al.* 1999; Caseras *et al.* 2000), with some modifications. Crude extracts for assaying enzyme activities were obtained by homogenization of the powdered frozen liver (1/5, w/v) using a PTA-7 Polytron (Kinematica GmbH, Switzerland) mixer (position 3, 30 seconds), and centrifugation at 15,800 rcf for 40 minutes at 4 ^{o}C. The homogenization buffer used in the assays for PFK, PK, G6PDH and 6PGDH activities consisted of 50 mM tris(hydroxymethyl)aminomethane (Tris)-HCl pH 7.5, 4 mM ethylenediaminetetracetic acid, 50 mM NaF, 0.5 mM phenylmethylsulfonyl fluoride, 1 mM 1,4-dithiothreitol and 250 mM sucrose. In the homogenization buffer used in the assay GK activity 100 mM KCl was also included and the crude extract filtered through a 1 mL Sephadex G 25

column after centrifugation. Assays for enzyme activities and total protein were adapted for automated measurement using a Cobas Mira S spectrophotometric analyzer (Hoffman-La Roche, Switzerland). All enzyme assays were carried out at 4 ºC and followed at 340 nm. For determining GK activity 5 µL of filtered sample extract were assayed in a final volume of 200 µL containing 100 mM Tris-HCl pH 7.75, 7.5 mM $MgCl_2$, 100 mM KCl, 1 mM NADP, 2.5 mM 2-mercaptoethanol, 100 mM glucose and 1 mU/mL G6PDH. The reaction was triggered with the addition of 60 mM ATP and 100 mM or 0.5 mM glucose. The GK activity was determined by subtracting the activity measured at 0.5 mM glucose from that measured at 100 mM glucose. PFK activity was assayed in a final volume of 200 µL containing 100 mM Tris HCl pH 8.25, 5 mM $MgCl_2$, 50 mM KCl, 0.15 mM NADH, 4 mM ammonium sulfate, 12 mM 2-mercaptoethanol, 10 mM F6P, 30 mM G6P, 0.675 U/mL fructose bisphosphate aldolase, 5 U/mL triose-phosphate isomerase, 2 U/mL glycerol-3-phosphate dehydrogenase and 4 µL crude extract. The reaction was triggered after addition of 10 mM ATP. The specific assay conditions for PK activity were: 250 µL of final volume containing 70 mM glycylglycine pH 7.4, 10 mM $MgCl_2$, 100 mM KCl, 0.15 mM NADH, 2.8 mM phosphoenolpyruvate, 21 U/mL lactate dehydrogenase and 4 µL of sample. ADP (2.5 mM) was added to monitor the PK reaction. G6PDH activity was measured using 4 µL sample in a final volume of 200 µL containing 77.5 mM imidazole-HCl pH 7.7, 5 mM $MgCl_2$, 1 mM NADP and 1 mM G6P. The assay conditions for 6PGDH activity were: 82.7 mM imidazole-HCl pH 7.7, 3 mM $MgCl_2$, 0.5 mM NADP, 2 mM 6-phosphogluconate and 4 µL crude extract in a final volume of 200 µL. The total protein content was determined in Cobas Mira S at 600 nm by the Bradford method (Bio-rad, Spain) at room temperature in liver crude extracts using bovine serum albumin as a standard.

5.2.6 Real-time PCR

Total messenger ribonucleic acid (mRNA) was isolated from frozen liver samples using the Speedtools Total RNA Extraction Kit (Biotools, Spain). Single strand complementary DNA (cDNA) templates for PCR amplification were synthesized from 1 µg of total mRNA by incubation with moloney murine leukemia virus reverse transcriptase (RT) (Promega Biotech Iberia SL, Spain) at 37 ^{o}C for 1 hour, accordingly to supplier's instructions. The RT reaction product was diluted 1/20 in milli-Q water and real-time quantitative PCR was performed in an ABI Prism 7000 Sequence Detection System (Applied Biosystems, Spain) using 0.4 µM of each primer, 10 µL of SYBR Green (Applied Biosystems, Spain) and 1.6 µL of diluted cDNA. The temperature cycle protocol for amplification was: 50 °C for 2 minutes, 95 °C for 10 minutes, followed by 48 cycles with 95 °C for 15 seconds and 62 °C for 1 minute.

The primer pairs used are listed in table 1 and were designed with Oligo Explorer 1.2 (Gene Link) except for PEPCK, reproduced from (Okamoto *et al.* 2008) and 18S, reproduced from (Palou *et al.* 2008). Ribosomal subunit 18 was chosen as the housekeeping gene to normalize expression levels of targets between different samples. Variations in gene expression were calculated by the standard ΔΔCt method. For all pairs of primers linearity was confirmed with consecutive dilutions (from 1/10 to 1/500) of a cDNA test sample.

5.2.7 Statistics

As described in section 2.2.6.

Table 13: Sequence of primers used for the real-time PCR experiments. Genes: GK, glucokinase; PFK, phosphofructokinase; PK, pyruvate kinase; G6PDH, glucose-6-phosphate dehydrogenase; G6Pase, glucose-6-phosphatase; FBPase, fructose-1,6-biphosphatase; PEPCK, phosphoenolpyruvate carboxykinase; CL, citrate lyase; ACC1, acetyl-CoA carboxylase 1; FAS, fatty acid synthase; CPT1a, carnitine palmitoyltransferase 1a; SREBP1c, sterol regulatory element-binding protein 1c; ChREP, carbohydrate responsive element-binding protein; 18S, ribosomal subunit 18.

Gene	Primer sense (5'-3')	Primer anti-sense (5'-3')
Glycolysis and Pentose		
Phosphate Pathway		
GK	ACCGACTGCGACATTGTGCG	ACGTCCTCACTGCGGCTTTC
PFK	TGATGTCTACCGCAAAGGGC	ACCGAACTGAAGGCCACCAC
PK	CTGGATGGGGCTGACTGTAT	TCAAACAACTGGCGGTGGTA
G6PDH	CTATGCCCGCTCACGACTCA	GGGCAAAGAACTCCTCTAGC
Gluconeogenesis		
G6Pase	TGTGGTTGGGATACTGGGCT	GATGGGGAAAGTGAGCCGCA
FBPase	GCTCAGCTCTATGGCATCGC	CCGACACAAGGACACAGGTA
PEPCK	ATCGAAGGCATCATTTTTGG	TGACCTTGCCCTTATGCTCT
Lipid metabolism		
CL	GGTTACTCCCGACACAGACT	TCCATCCAGAGAGAGGTTGA
ACC1	GGGCGTTGGGGGATAAGATT	GGAAGAGTGGGGATACCTGC
FAS	CGGCGAGTCTATGCCACTAT	ACACAGGGACCGAGTAATGC
CPT1a	ACCAACCCCAACATCCCTAA	CCAAAAGACTGGCGCTGCTC
Transcription factors		
SREBP1c	GCCATCGACTACATCCGCTT	CACTTCGCAGGGTCAGGTTCT
ChREBP	CCTGGAACCTGTCTTTGGGC	TGGGTGGACTGGCTTTTCGT
Housekeeping		
18S	CGCGGTTCTATTTTGTTGGT	AGTCGGCATCGTTTATGGTC

5.3 Results

5.3.1 Induction of diabetes and animals' performance during the insulin treatment protocol

Eight days after the injection of STZ, the body weight of the animals was significantly reduced to 261 ± 3 g (representing 93% of their initial weight) and blood glucose levels ranged from 394 to over 600 mg/dL, indicating the successful induction of type 1 DM. This was further confirmed by the reduced endogenous insulin levels determined at the end of the experiment for group D relative to the healthy controls (Table 14).

Throughout the experimental follow-up, the animals in group D continued to lose weight, while the ones kept under insulin treatment tended to gain weight (Figure 21). At the end of the insulin replacement protocol, the body weight of untreated diabetic animals was 234 ± 10 g, significantly lower than the 288 ± 7 g and the 270 ± 5 g observed for I-SC and I-IP, respectively (p = 0.06, I-SC *vs* I-IP). Furthermore, the weight variation was quantified by the AUC in the weight *vs* time plot (Table 14), and was significantly increased for groups I-SC and I-IP relative to group D. Taken together, these observations demonstrate the positive effect of insulin on weight gain. Consistent with this finding, EWAT also increased with insulin treatment.

As presented in Table 14, food and water consumption determined at the end of the experiment, were sensitive to the diabetic condition and also insulin treatment. In non-diabetic controls food consumption was 23 g/day, and water intake 35 mL/day, in good agreement with reports from several other authors (Havel *et al.* 1998; Dib 1999; Wei *et al.* 2003). As expected, diabetic animals ate and drank significantly more than controls. Insulin replacement decreased food ($p < 0.05$, D *vs* I-IP and p = 0.06 D *vs* I-SC) and water intakes in the treated diabetic rats, but the observed values were still higher than control levels.

Table 14: Biochemical and physiological parameters determined during the insulin replacement study in untreated STZ-diabetic rats (D), STZ-diabetic rats treated with insulin by subcutaneous (I-SC) or intraperitoneal (I-IP) injection twice a day at a dose of 30 U/kg/day and non-diabetic controls (C). Glycemia and plasma triglyceride measurements were performed 2 hours after the morning insulin injection on the 8th day of insulin treatment. Food and water consumption were measured in the last 24 hours prior to the sacrifices. Weight evolution is expressed as the area under the curve (AUC) in the weight *vs* time plots, from days 0 to 10. All the other parameters correspond to post mortem measurements. For each parameter, values not sharing a common superscript letter are significantly different; statistical significance was accepted for a $p < 0.05$ determined by one way ANOVA with Fisher's LSD post test. N. D., not determined, NEFA, non-esterified fatty acids, EWAT, epididimal white adipose tissue.

	D	I-SC	I-IP	C
Glycemia (mg/dL)	534 ± 22 [a]	90 ± 10 [b]	114 ± 22 [b]	105 ± 2 [b]
Triglycerides (mg/dL)	249 ± 31 [a]	133 ± 10 [b]	116 ± 10 [b]	124 ± 7 [b]
NEFA (mM)	0.586 ± 0.076 [a]	1.523 ± 0.176 [b]	1.150 ± 0.140 [b]	0.308 ± 0.047 [a]
Exogenous insulin (mU/L)	1.18 ± 1.15 [a]	4.19 ± 1.02 [b]	3.87 ± 1.4 [b]	N. D.
Endogenous insulin (µg/L)	0.5 ± 0.2 [a]	N. D.	N. D	5.3 ± 1.1 [b]
Hepatic glycogen (µmol/gdw)	320 ± 51 [a]	680 ± 56 [b]	814 ± 73 [bc]	907 ± 84 [c]
Hepatic triglycerides (µmol/gdw)	319 ± 20 [a]	301 ± 15 [a]	287 ± 11 [a]	212 ± 22 [b]
EWAT (g/100g)	0.30 ± 0.07 [a]	0.78 ± 0.09 [b]	0.92 ± 0.14 [b]	N. D.
Food intake (g/day)	40 ± 1 [a]	36 ± 2 [ab]	34 ± 0.3 [b]	23 ± 1 [c]
Water intake (mL/day)	184 ± 14 [a]	113 ± 15 [b]	119 ± 10 [b]	35 ± 3 [c]
Weight evolution ($AUC_{0\rightarrow10day}$)	229 ± 15 [a]	280 ± 6 [b]	268 ± 5 [b]	N. D.

Glycemia determined in the 8th day of the insulin treatment protocol, 2 hours after the morning dose, was successfully reduced to control values in both I-SC and I-IP groups. However, glycemia observed after an overnight feeding (*i.e.* ~12 hours after the night insulin injection) was similar between treated and untreated STZ-diabetic rats and was on the hyperglycemic range (D, 563 ± 14 mg/dL; I-SC, 525 ± 38 mg/dL; and I-IP, 551 ± 20 mg/dL). Nonetheless, exogenous insulin was still detected in the plasma of animals from I-SC and I-IP groups in the morning.

For the animals kept under insulin treatment, plasma TG levels were similar to control values whereas the untreated diabetic rats showed

significantly elevated plasma TGs, in agreement with reports from other authors (Dong *et al.* 2002; Mason *et al.* 2002; Iwasaki *et al.* 2005). The effect of insulin replacement on lowering the plasma TG levels may be a consequence of the enhanced chylomicron-TGs clearance by stimulation of LPL in the adipose tissue. This is consistent with the accumulation of fat as demonstrated by the higher content of EWAT in the insulin-treated diabetic animals relative to the untreated ones. In addition, insulin may also contribute to lower plasma TGs by inhibiting their hepatic secretion in VLDL.

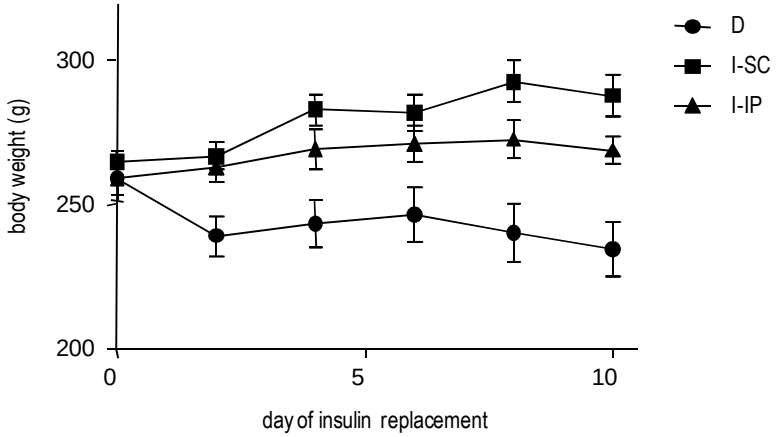

Figure 21 Plot of the animals' body weight as a function of time during the insulin replacement period. Eight days after STZ injection, diabetic rats were left untreated (D) or injected a 15 U/kg insulin dose twice a day by the subcutaneous (I-SC) or intraperitoneal (I-IP) route.

On the other hand, the concentration of NEFA in the plasma was similar between non-diabetic controls and untreated STZ-diabetic rats, and unlike reports from other authors (Wan *et al.* 2000; Dong *et al.* 2002), insulin replacement did not cause a reduction of NEFA values. Instead, and surprisingly, plasma NEFA concentration increased in the insulin-treated groups. This observation can be related to the larger mass of adipose tissue those animals presented. Actually, if plasma NEFA concentration is normalized for the mass of EWAT, the values for insulin treated rats tend to be lower than those for the STZ-diabetic rats.

Similarly to the findings from the experiments described in chapter 4, hepatic glycogen content was reduced and TG levels increased in the untreated diabetic rats relative to controls. Insulin replacement in the I-IP group increased glycogen levels back to control values. On the other hand, in the I-SC group, although hepatic glycogen content was significantly higher than that observed for untreated diabetic rats, it was still lower than control levels. In contrast with observations from other authors (Shimomura *et al.* 1999), hepatic TG content remained elevated in the diabetic rats receiving the insulin replacement treatments.

5.3.2 ^{2}H enrichment levels and metabolic parameters

After the insulin replacement period (9 or 10 days) all the animals were administered $^{2}H_2O$ and left to feed *ad libitum* overnight to trace the absorptive metabolism. The accurate body water $^{2}H_2O$ precursor enrichment was determined by ^{2}H NMR analysis of plasma samples and reached the target value of 2% (Table 15). With these range of values, plasma glucose, hepatic glycogen and lipids were also enriched with ^{2}H to levels that, coupled with the amount of sample recovered, allowed precise analysis by ^{2}H NMR. All the STZ-diabetic rats had comparable $^{2}H_2O$ precursor enrichment levels. However, the insulin-treated rats, ^{2}H enrichment in position 2 of blood glucose was higher than that of untreated STZ-diabetic rats, indicating insulin enhanced glucose turnover. On the other hand the $^{2}H2$ enrichment in glycogen was lower in the rats experiencing the insulin replacement protocol, consistent with the bigger hepatic glycogen pool. Insulin increased the absolute ^{2}H enrichment in the methyl-TG, indicating a stimulation of the lipogenic pathway and reduction of the dietary and/or lipolytic contribution since the hepatic TG content was similar among all STZ-diabetic rats.

Table 15: Body water and metabolite absolute ^2H enrichment levels observed after an overnight feeding under ^2H_2O administration. Groups are as described in the legend of **Table** 14. For each parameter, values not sharing a common superscript letter are significantly different; statistical significance was accepted for a $p < 0.05$ determined by one way ANOVA with Fisher's LSD post test.

	^2H enrichement (%)				
	Target BW	BW	H2 Blood Glucose	H2 Glycogen	Methyl-TG
C	3	2.90 ± 0.14	1.21 ± 0.15	0.99 ± 0.20	0.48 ± 0.06
D	2	1.93 ± 0.06 [a]	0.83 ± 0.06 [a]	1.21 ± 0.05 [a]	0.04 ± 0.01 [a]
I-SC	2	1.97 ± 0.05 [a]	1.44 ± 0.05 [b]	0.66 ± 0.10 [b]	0.14 ± 0.01 [b]
I-IP	2	1.96 ± 0.07 [a]	1.36 ± 0.06 [b]	0.72 ±0.13 [b]	0.16 ± 0.02 [b]

5.3.2.1 Sources of glucose production

Deuterium-enriched glucose molecules derive from EGP whereas unlabelled ones originate from the diet and subsequent gastrointestinal absorption to the blood stream. Hence, the contribution of EGP to blood glucose was assessed by the ^2H enrichment of position 2 of blood glucose relative to that of body water ($^2H2/^2H$-BW). In non-diabetic control animals EGP accounted for 40 ± 4% of blood glucose. This contribution was similar to that observed for group D (44 ± 4%) because in these animals the increased food intake is parallel to higher rates of EGP (see discussion in chapter 4, section 4.4.2). In the cases where the animals were subjected to the insulin treatment protocols, the contribution of EGP to blood glucose was significantly higher reaching 73 ± 3% in group I-SC and 71 ± 5% in group I-IP. The fact that insulin administration by both s.c. and i.p. routes translated into a higher contribution of EGP to blood glucose relative to that coming from the diet is consistent with the reduction on food intake and thus on the contribution of unlabeled dietary glucose. However, apparently, insulin did not efficiently reduce the rates of EGP under feeding conditions.

Figure 22 represents the glycogenolytic and gluconeogenic contributions to EGP as determined by ^2H NMR analysis of MAG derivative

from blood glucose. The H5/H2 ratio, which reflects the contribution of gluconeogenesis, was 0.95 ± 0.03 for the untreated diabetic animals, significantly higher than the 0.69 ± 0.04 observed for non-diabetic controls. When the STZ-diabetic animals were treated with insulin, the H5/H2 ratio was significantly reduced relative to group D and similar to that of healthy controls: 0.60 ± 0.03 for group I-SC and 0.62 ± 0.03 for group I-IP.

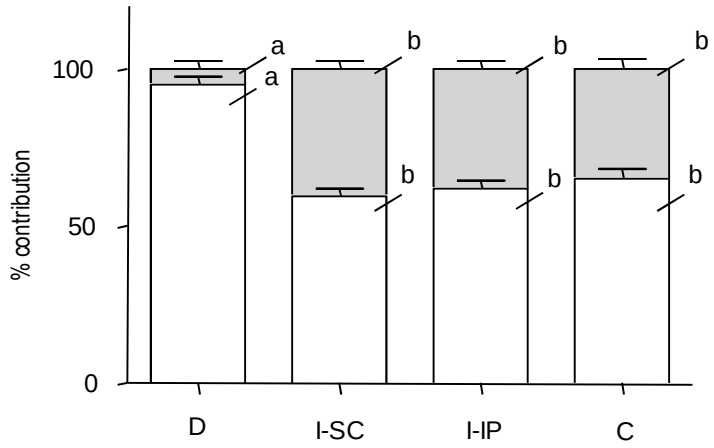

Figure 22 Relative contributions of gluconeogenesis (white bars) and glycogenolysis (grey bars) to EGP determined after an overnight feeding under ^2H_2O administration. Groups are as described in the legend of Table 14. For each contribution, values not sharing a common letter are significantly different; statistical significance was accepted for a $p < 0.05$ determined by one way ANOVA with Fisher's LSD post test.

5.3.2.2 Hepatic glycogen synthesis

The contribution of glycogen synthesized during the ^2H_2O administration protocol to the total hepatic glycogen pool is reflected in the ^2H enrichment in position 2 of glycogen relative to the body water's. With insulin administration, the $^2H2$ enrichment in glycogen was significantly reduced (Table 15).

Table 16 shows the data concerning hepatic glycogen synthesis during an overnight feeding after the insulin replacement protocol an also for non-diabetic controls. In the untreated STZ-diabetic rats more than half

of the hepatic glycogen was synthesized overnight, reproducing the observations from the experiments described in chapter 4. On the other hand, when the STZ-diabetic animals were treated with insulin, only one third of the hepatic glycogen was synthesized overnight, similar to the findings for the non-diabetic control animals. Because non-diabetic controls and insulin treated STZ-diabetic animals have higher glycogen levels the amount of glycogen synthesized overnight is actually similar in all groups.

Table 16: Contribution of newly synthesized glycogen to the hepatic pool and amount of glycogen synthesized after an overnight feeding under ^2H_2O administration. Groups are as described in the legend of **Table** 14. For each parameter, values not sharing a common superscript letter are significantly different; statistical significance was accepted for a $p < 0.05$ determined by one way ANOVA with Fisher's LSD post test.

	D	I-SC	I-IP	C
Glycogen synthesis (% contribution)	58 ± 3 [a]	34 ± 5 [b]	35 ± 7 [b]	34 ± 7 [b]
Overnight-synthesized glycogen (µmol/gdw)	192 ± 35 [a]	236 ± 47 [a]	299 ± 64 [a]	322 ± 87 [a]

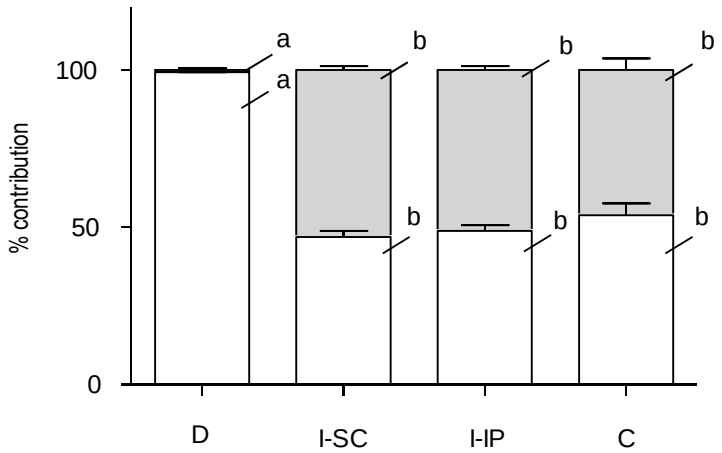

Figure 23 Relative contributions of indirect (white bars) and direct (grey bars) pathways to hepatic glycogen synthesis determined after an overnight feeding under ^2H_2O administration. Groups are as described in the legend of **Table** 14. For each pathway, values not sharing a common letter are significantly different; statistical significance was accepted for a $p < 0.05$ determined by one way ANOVA with Fisher's LSD post test.

The pathways for glycogen synthesis are depicted in Figure 23 and were altered by the induction of diabetes with the indirect pathway increasing from 54 ± 4% in the non-diabetic controls to 99 ± 1% in the untreated STZ-diabetic animals. Insulin treatment restored the direct/indirect pathways contributions to control levels with the indirect pathway accounting for 47 ± 2% in group I-SC and 49 ± 2% in group I-IP.

5.3.2.3 Hepatic triglycerides and de novo *lipogenesis*

In agreement with the observations from the experiments described in chapter 4, DNL was significantly reduced in group D when comparing to controls but the hepatic TG content was higher. This observation indicates that the contribution of dietary and/or lipolytic sources is increased in the diabetic rats. Insulin replacement to the diabetic rats significantly increased the contribution of DNL to the hepatic TG pool. The observation that the hepatic TG content was similar between the untreated and insulin-treated diabetic rats implies that the contribution of unlabeled dietary and/or lipolytic sources decreased with insulin treatment. Despite the enhancement of lipogenic TG synthesis, insulin replacement to diabetic rats did not translate into a complete restoration of the TG dynamics in the liver.

Table 17: Contribution of *de novo* lipogenesis (DNL) to the hepatic triglyceride (TG) pool after an overnight feeding under ^2H_2O administration. Groups are as described in the legend of **Table** 14. For each parameter, values not sharing a common superscript letter are significantly different; statistical significance was accepted for a $p < 0.05$ determined by one way ANOVA with Fisher's LSD post test.

	D	I-SC	I-IP	C
DNL (% contribution)	2.2 ± 0.3 [a]	7.3 ± 0.7 [b]	8.2 ± 1.0 [b]	16.3 ± 1.7 [c]

5.3.3 Changes in the gene expression and enzyme activities

Table 18 shows the enzyme activities for GK, PFK, PK, G6PDH, and 6PGDH measured from liver samples after the overnight feeding period

and the insulin replacement protocols. Figure 24 summarizes the changes in the expression of several hepatic genes involved in glucose and lipid metabolism relative to non-diabetic controls.

Table 18: Enzyme activities (mU per mg of protein) determined in liver samples after an overnight feeding. Groups are as described in the legend of **Table** 14. For each enzyme activity, values not sharing a common superscript letter are significantly different; statistical significance was accepted for a $p < 0.05$ determined by one way ANOVA with Fisher's LSD post test. GK, glucokinase; PFK, phosphofructokinase; PK, pyruvate kinase; G6PDH, glucose-6-phosphate dehydrogenase; 6PGDH, 6-phosphogluconate dehydrogenase.

	D	I-SC	I-IP	C
Glycolysis				
GK	0.050 ± 0.021 [a]	8.79 ± 0.27 [b]	7.48 ± 0.38 [b]	7.19 ± 0.96 [b]
PFK	15.17 ± 1.02 [a]	16.93 ± 0.67 [a]	17.81 ± 1.15 [a]	22.48 ± 0.49 [b]
PK	79.00 ± 15.69 [a]	463.6 ± 43.81 [b]	333.6 ± 33.88 [c]	814.7 ± 48.65 [d]
Pentose Phosphate Pathway				
G6PDH	10.73 ± 0.56 [a]	20.96 ± 3.23 [a]	19.65 ± 1.70 [a]	97.88 ± 12.07 [b]
6PGDH	11.49 ± 0.69 [a]	22.44 ± 1.62 [b]	19.71 ±0.76 [b]	43.24 ± 3.06 [c]

5.3.3.1 Enzymes involved in glucose metabolism

The relative mRNA levels of GK were significantly reduced in the STZ-diabetic animals but in both insulin-treated groups (I-SC and I-IP) the GK expression was similar to control levels. However, expression of the GK gene in the I-SC and I-IP groups was only modestly increased and thus was not significantly different from that of untreated diabetics. While the expression of the GK gene in the liver was not completely recovered with the insulin treatments, GK activity on the other hand, increased significantly to levels similar to controls (Table 18). PFK gene expression was similar among all study groups and its activity was similar for groups D, I-SC and I-IP. Moreover, in all the latter cases PFK activity was significantly lower than that measured for group C. The expression of the PK gene was significantly reduced in the STZ-diabetic animals but was completely

recovered to control levels in the I-SC and I-IP groups. Accordingly, the PK activity was significantly reduced in group D, relative to controls. Both insulin treatments resulted in significantly higher PK activities when comparing to diabetics, with the PK activity in the I-SC group being significantly higher than the one measured for I-IP, but these were however still significantly less than activities of controls.

The hepatic gene expression of G6PDH was similar among all study groups. On the other hand, the activities of both G6PDH and 6PGDH were altered with diabetes and insulin replacement. In group D, both dehydrogenases' activities were reduced when comparing to controls. Insulin replacement by both s.c. and i.p. routes resulted in a significant increase of G6PDH and 6PGDH activities, but these were still well below control levels.

Considering the gluconeogenic enzymes in the untreated diabetic animals, PEPCK and FBPase gene expression was increased, while the expression of G6Pase remained similar to that of non-diabetic controls. Insulin treatment did not translate into a reduction on the expression of gluconeogenic enzymes. Instead, in the I-SC and I-IP groups, the expression of PEPCK, FBPase and G6Pase was similar to that determined for untreated diabetic rats.

5.3.3.2 Enzymes involved in lipid metabolism

The gene expression of CL was reduced in group D and recovered to control levels in I-SC and I-IP. This behaviour was also observed for the expression of the FAS gene. On the other hand, the ACC1 gene expression was similar between diabetics and controls. Insulin treatment resulted in a significant increase on the expression of the ACC1 gene in the I-IP group. In the I-SC group the ACC1 gene expression was similar to I-IP but not statistically different from groups D and C.

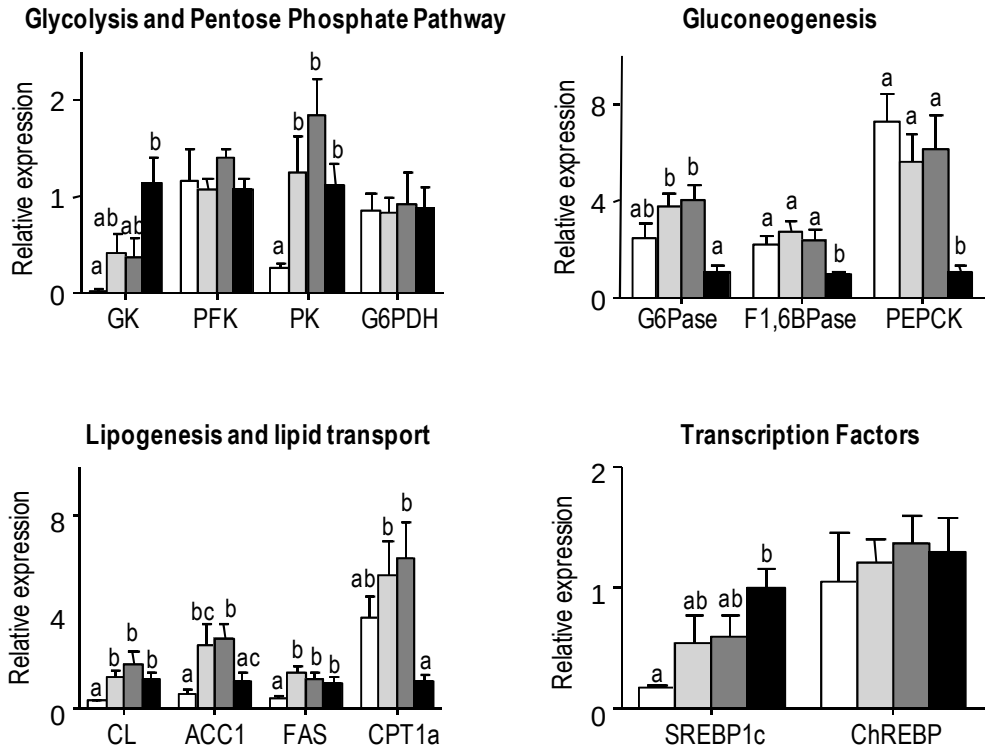

Figure 24 Gene expression (normalized for 18S and relative to controls, group C) of enzymes and transcription factors involved in carbohydrate and lipid metabolism determined after an overnight feeding in liver samples from groups D (white bars), I-SC (light grey bars), I-IP (dark grey bars), and C (black bars). Groups are as described in the legend of Table 14. Genes are as described in legend of Table 13.For each gene, values not sharing a common superscript letter are significantly different; statistical significance was accepted for a $p < 0.05$ determined by one way ANOVA with Fisher's LSD post test.

The gene expression of CPT1a, the protein that transports fatty acids from the cytosol to the mitochondria for β-oxidation was increased in group D relative to controls ($p < 0.05$, unpaired t test). This observation, together with the reduced expression of the lipogenic genes CL and FAS suggests that the STZ-diabetic animals are experiencing a catabolic state, characterized by the oxidation of fatty acids by opposition to their synthesis via the lipogenic route. Furthermore, these data are in accordance with the upregulation of the gluconeogenic pathway, as determined by the elevated PEPCK and FBPase gene expression. In contrast to what was observed for

the regulation of the lipogenic genes expression, the expression of the CPT1a transporter did no approach control values with insulin treatment. Instead, CPT1a gene expression in the I-SC and I-IP groups was similar to that observed for diabetics.

5.3.3.3 Transcription factors

SREBP1c and ChREBP are two transcription factors involved in carbohydrate and lipid metabolism responding to insulin and glucose, respectively. While the mRNA levels for ChREBP were similar among all study groups, the ones for SREBP1c were significantly reduced in group D: With either insulin treatment, SREBP1c gene expression was restored to control levels but the observed levels were still not significantly different from those of group D. The induction of SREBP1c by insulin is in good agreement with the increased expression of the glycolytic and lipogenic enzymes in the insulin-treated diabetic rats.

5.4 Discussion

Chapter 4 established a $^{2}H_2O$-based protocol for the study of the absorptive state. Those experiments pointed out the metabolic disruptions that take place with the induction of diabetes by STZ injection in regards to glucose production, hepatic glycogen and lipid synthesis. The study described in this chapter recapitulated those alterations and assessed the effect of insulin replacement on those pathways in two groups of rats receiving treatment for 9 or 10 days to the i.p. or s.c. route. In addition, modifications on the gene expression and activities of several key enzymes were evaluated. Hence, these experiments allowed for a comprehensive study of hepatic metabolism by measuring the overall metabolic performance with the tracer-based approach and disclosing some regulatory aspects of hepatic glucose and lipid metabolism by gene expression and enzymology techniques. With these

methods it was possible to identify the benefits and limitations of the insulin replacement protocol adopted.

5.4.1 Alterations underlying the dominance of gluconeogenesis in STZ-diabetic rats

In STZ-diabetic rats, both EGP and glycogen synthesis were dominated by the gluconeogenic flux. This was determined by the analysis of plasma glucose and hepatic glycogen ^{2}H enrichment profile from $^{2}H_2O$ and confirmed by the increased expression of hepatic PEPCK and FBPase. The expression of G6Pase, although higher in the case of STZ-diabetic rats, was not statistically different from control levels. However, other authors (Hidaka *et al.* 2002) report that, in addition to PEPCK, G6Pase mRNA levels are increased in fed STZ-diabetic rats in a similar stage of the disease, relative to non-diabetic controls. The finding that in the present experimental setting, PEPCK gene expression was highly sensitive to insulinopenic STZ-diabetes (mRNA levels in diabetics were 7× higher than in controls) is consistent with the idea that insulin has a dominant action on the transcriptional regulation of PEPCK gene (Scott *et al.* 2003; Yabaluri *et al.* 2010).

Gluconeogenesis from pyruvate is an energy-expensive pathway that is dependent on ATP and NADH. These can be derived from the β-oxidation of fatty acids in mitochondria. High rates of hepatic β-oxidation are supported by the increased expression of the CPT1a transporter and also by the increased availability of NEFA as a result of insulin deficiency in the STZ-diabetic rats.

5.4.2 Alterations in hepatic lipid metabolism in STZ-diabetic rats

Insulin deficiency impaired lipid uptake into adipose tissue in the STZ-diabetic rats as demonstrated by the reduced EWAT content and the elevated plasma TG levels. As a result, TGs not cleared by the adipocytes

accumulated in the liver. The prevalence of hepatic TGs as a consequence of abnormal lipid metabolism by the adipose tissue rather than of hepatic *de novo* production was further demonstrated by the down regulation of the lipogenic enzymes (CL and FAS) and, consistently, the residual contribution of DNL to the hepatic TG pool as estimated by the ^2H_2O method. In this setting, it was anticipated that the NEFA flux from adipose tissue lipolysis would be increased, in agreement with the reduced levels of circulating insulin. The similar plasma NEFA concentration between diabetics and controls may be explained by the highly depleted TG stores in the adipose tissue. In accord with this, the EWAT content of diabetic rats represented only ~0.3% of the animals' body weight, compared to the 0.6-1.2% range reported for non-diabetic controls (DiGirolamo *et al.* 1998; Wren *et al.* 2001; Takada *et al.* 2008).

5.4.3 Metabolic control and limitations of the insulin replacement therapy

Several biochemical and physiological parameters were improved by the insulin replacement protocols. For example, there was an increase in the animals' body weight, in similar fashion to what was observed by other authors for STZ diabetic rats under a similar twice-daily insulin administration protocol (Suthagar *et al.* 2009) or under continuous insulin delivery by the use of infusion pumps (Wan *et al.* 2000). Likewise the deposition of fat in adipose tissue was increased as demonstrated by the higher content of EWAT. Moreover, the insulin-treated diabetic rats showed an alleviation of the symptoms associated with the disease, such as the hyperphagia and polydepsia.

However, the metabolic evaluation by both the ^2H_2O tracer approach and gene expression and enzyme activities analyses suggests that the insulin treatment was in many aspects unable to revert the performance of diabetic animals back to that of controls. Insulin was administered as a rapid-acting formulation in two equal doses, one at the beginning of the dark phase (7 pm)

and the other at the beginning of the light phase (8 am). Prior to the administration of the morning insulin dose, glycemia was similar to that of untreated diabetic rats, in the hyperglycemic range. This indicates that the twice-daily insulin injection posology failed to afford normoglycemia throughout the complete day course. Under these circumstances, insulin action is no longer observed at the beginning of the light phase, in agreement with increased gluconeogenesis, fatty oxidation in the liver, and adipose tissue lipolysis as discussed below.

Insulin replacement was able to normalize the relative contributions of gluconeogenesis and glycogenolysis to EGP. This finding is in line with reports from studies on controlled type 1 diabetic patients (Bischof *et al.* 2002). However, in the present experiment, the absolute fluxes of glycogenolysis and gluconeogenesis must remain elevated even after the treatment of the diabetic rats, accounting for the hyperglycemia observed in the morning. The gene expression analysis showed that, after an overnight feeding, the gluconeogenic enzymes were upregulated, supporting the increased absolute flux of gluconeogenesis in the insulin-treated diabetic rats.

Despite the abnormalities in EGP the glycogenic and lipogenic pathways responded efficiently to insulin replacement in the diabetic rats, even in face of the incomplete insulinization throughout the day course. The restoration of GK gene expression and activity to control levels correlates very well with the increase in glycogen content in the liver. This effect is in accordance with the enhancement of glycogen synthesis in hepatocytes (O'Doherty *et al.* 1996; Seoane *et al.* 1999) and diabetic rats (Morral *et al.* 2004) overexpressing GK. In addition, in the diabetic rats, there was a complete recovery of the direct pathway flux with both insulin replacement protocols, contrarily to the observations for human type 1 diabetic patients that underwent intensive long-term insulin therapy where the fraction of glycogen synthesized by the indirect pathway remained dominant (Bischof *et al.* 2002).

The stimulation of GK gene expression and activities parallel to those of PK and to the gene expression of several lipogenic enzymes, supports the coupling of glycolytic and DNL fluxes. With insulin treatment, the mRNA

levels of CL, ACC and FAS were increased to control levels or even higher (in the case of ACC). The increased gene expression of lipogenic enzymes in insulin-treated diabetic rats is in good agreement with the enhancement of DNL determined by ^{2}H NMR methods and also with the stimulation of the dehydrogenases activities in the pentose phosphate pathway that generate NAPDH molecules for DNL.

Nonetheless, DNL was not completely restored to control levels. In part, this was due to an important contribution from adipose tissue lipolysis to the hepatic TG pool, consistent with the elevated levels of circulating NEFA in the STZ-rats undergoing insulin replacement therapy. With both increased contribution from *de novo* production and adipose tissue lipolysis it was surprising that the hepatic TG content did not increase relative to the untreated diabetic rats. This finding can only be explained by concurrent lipogenesis and β-oxidation, which is actually supported by CPT1a expression levels in the range found for untreated diabetic rats and lower than those of controls. Evidence demonstrating the loss of reciprocal regulation between DNL and β-oxidation has been reported in hepatocytes overexpressing wild type and malonyl-CoA-insensitive (at a greater extent) CPT1a, even under feeding-like conditions of high insulin and high glucose (Akkaoui *et al.* 2009). Moreover the sensitivity of CPT1a to malonyl-CoA is decreased in diabetic rats and is only modestly reverted by acute administration of high insulin doses (Grantham *et al.* 1988). The present study provides additional evidence that lipogenesis and β-oxidation may occur simultaneously and furthermore insulin replacement may promote the cycling of lipids between those two pathways in the diabetic rats.

5.4.4 Relevance of the intraperitoneal route

Under physiological conditions, the liver receives insulin and nutrients by the portal vein during the absorptive phase. In these studies, the i.p. route was chosen as a strategy to target insulin to the liver and the absorptive phase was addressed after the insulin replacement period. It was anticipated that the

hepatic metabolic pathways would respond differently to the i.p. and s.c. routes of insulin administration. However, most of the effects observed in the fed state were independent of the route of administration. The only apparent difference was that when insulin was delivered to the i.p. route hepatic glycogen synthesis was further enhanced relative to the s.c. route. However, this observation was not supported by differently altered gene expression or enzyme activity of GK, which exerts high positive control over glycogen synthesis (Ferrer *et al.* 2003). It is possible that the lag phase between the last insulin injection and liver harvesting time prevented route-related effects to be noticed at the level of enzyme regulation. With continuous insulin diffusion pumps, the i.p. route resulted in increased stimulation of GK activity relative do s.c. and even non-diabetic controls (Mason *et al.* 2000). Interestingly, another study from the same group reports the activity of lipogenic enzymes is enhanced to the same extent by both routes (Mason *et al.* 2002). Hence, at least in the in the absorptive state, portal insulin is more relevant in the normalization of glycogen synthesis, probably via GK regulation.

5.5 Conclusions

Delivering insulin in two daily doses to either the s.c. or i.p. route was beneficial to the overall condition of STZ-diabetic rats. Glycolytic and lipogenic fluxes in the liver were highly responsive to the treatment but gluconeogenesis and lipid degradation could not be normalized, probably as a consequence of the insufficient insulinization throughout the whole day. Preferential hepatic action could not be clearly demonstrated for the i.p. route except for the higher glycogen content in the liver that, nonetheless, was not accompanied by other differential improvements.

6
POLYMERIC NANOPARTICLES FOR INSULIN DELIVERY

6.1 Introduction

An important issue regarding the current insulin therapy is that its delivery by the s.c. route fails to recapitulate the hormone's physiological release profile, since the portal to peripheral gradient is unmet under those circumstances. Oral insulin delivery would mimic the normal secretion of insulin because the drug would be largely absorbed to the portal vein. However, because of its peptide nature, oral insulin administration is hampered. Poor absorption and high enzymatic degradation of peptide and protein agents are the main barriers compromising their efficacy by the oral route (Pauletti *et al.* 1996; Uekama *et al.* 1998; Pinto Reis *et al.* 2006). Even after reaching circulation, these drugs are rapidly cleared from the blood, and their presence may also lead to immunological complications (Uekama *et al.* 1998). In this context, nanoparticles arise as specialized delivery systems being developed by several research groups with encouraging

results in regards to enhancing the oral efficacy of peptide drugs (*e.g.* Allémann *et al.* 1998; Bilati *et al.* 2005a; Pinto Reis *et al.* 2006).

Nanoparticles are colloidal carriers ranging in size from 10 to 1000 nm. They are used in drug formulation for facilitating the passage of drugs through the biological membranes, protecting drugs against degradation, controlling drug release and targeting to specific sites of action. Once in the body, nanoparticles are recognized as strange entities, undergo opsonisation (coating with opsonin protein) that flags them to phagocyte cells and are eventually delivered to organs of the reticuloendothelial system. Unloaded biodegradable nanoparticles are mainly taken up by the liver (42 to 80% of the administered dose), spleen (0,6 to 2%), lungs (0,7 to 3%) and to a less extent by the bone narrow (Allémann *et al.* 1993). This extensive uptake is advantageous when the therapeutic agent is intended to act on those organs and can thus be used as means of passive targeting drugs to the liver, for example.

Concerning the above mentioned, a hypothesis can be set that physiological/portal delivery of insulin may be achieved by the nanoparticle strategy if: (i) the drug is successfully absorbed by the oral route; (ii) or passive liver targeting occurs even under the traditional s.c. administration. To test this hypothesis, nanoparticles with high insulin association were prepared from biodegradable and biocompatible materials and assayed for efficacy against the administration of free insulin. In the following paragraphs, some methodological considerations regarding the materials chosen to develop the nanoparticles are addressed.

From the wide variety of polymers available for preparing nanoparticles, poly-lactide-*co*-glycolide (PLGA) has the advantage of being biodegradable.

Among the various methods available for preparing nanoparticles, the nanoprecipitation technique employs mild conditions and is the most simple and straightforward. In this procedure a polymer is dissolved in an organic medium (typically acetone) and, upon contact of this solution with a non-solvent phase (typically water), the polymer immediately suffers

desolvation resulting in the formation of nanoparticles. In a second step the organic solvent is removed by evaporation and the nanoparticles are obtained as an aqueous colloidal suspension. The most common way to associate drugs to nanoparticles prepared by this methodology is to add the drug along with the polymer to the organic solvent. While this is a good procedure for hydrophobic molecules, it is not very suited for the formulation of hydrophilic compounds, such as insulin. Nonetheless, nanoprecipitation has been successfully used to prepare insulin-loaded PLGA nanoparticles by dissolving the drug in hydrochloride acid and then adding that solution to the polymer-containing acetonic phase (Barichello *et al.* 1999a, 1999b; Cui *et al.* 2007). Alternatively, Bilati *et al* using a modified nanoprecipitation method have obtained insulin-loaded PLGA nanoparticles by dissolving the drug and the polymer in DMSO or *N*-methylpyrrolidone (Bilati *et al.* 2005b). In the authors' method, the nanoparticles are recovered after centrifugation and successive washes with distilled water.

Cyclodextrins (CD) are cyclic oligosaccharides consisting of several D-glucopyranose units linked to each other by *a*-1,4 bonds (Figure 25A). Natural occurring CDs are obtained from the enzymatic breakdown of starch by bacterial amylase cyclodextrin-glucosyl-tranferase and the most abundant are *a*-, *β*- and *γ*-CD, consisting of 6, 7 and 8 glucopyranose residues respectively. Cyclodextrins assume a cone shaped form (Figure 25B) with the polar hydroxyl groups facing the outside, primary hydroxyl residues linked to C6 are in the narrowest face while secondary ones linked to C2 and C3 are localized on the wider face. These hydroxyl groups can suffer chemical modifications and be conjugated with other functional groups to alter the physicochemical properties of parent CD. Hence, CD and their derivatives cover a wide range of pharmaceutical applications and have been largely used in drug delivery as adjuvant to improve drug solubility, stability, and bioavailability (Loftsson *et al.* 2007).

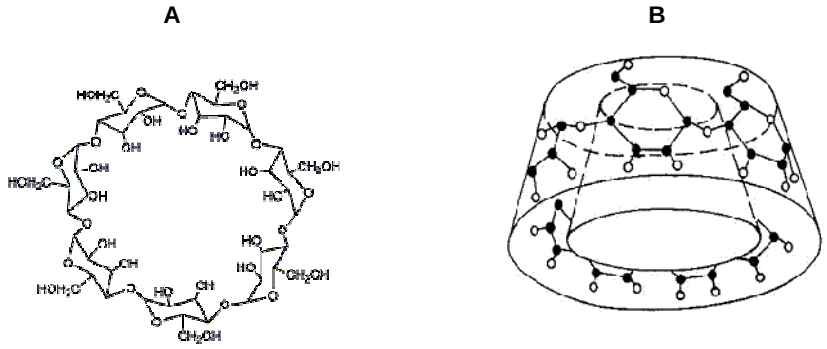

Figure 25 The chemical structure of *β*-CD. (**A**) Seven D-glucopyranose units linked by α-1,4 bonds. (**B**) The cone shape configuration of *β*-CD, black dots represent carbon atoms and white dots oxygen atoms, hydrogen atoms are omitted. Reproduced from Loftsson *et al.* (Loftsson *et al.* 1996**)**.

About twenty years ago, new CD derivatives with amphiphilic character were synthesized by Zhang and co-workers (Zhang *et al.* 1991). Similar to polymers, these molecules are able to self-assemble into nanoparticles by the nanoprecipitation technique. This new amphiphile class of CD has extended the pharmaceutical potential of CD to the domain of the nanocarrier systems. Several chains can be grafted to the CD parent molecule at different positions (Duchêne *et al.* 1999), and recently, the thermolysin catalyzed transesterification of CD with vinyl esters allowed the synthetic procedure to be simplified to a quantitative one-step reaction (Pedersen *et al.* 2005; Choisnard *et al.* 2006).

This chapter describes the preparation of insulin-loaded nanoparticles from PLGA and amphiphilic CD. The aim was to develop a new nanoparticle-based carrier for oral and/or s.c. administration of insulin that would translate in benefits with respect to the pharmacological response. From the most common *a*- *β*- and *γ*-CD, the latter is the less toxic (Loftsson *et al.* 2007) and was hence chosen to prepare an amphiphilic derivative to be included in the nanoparticle formulation. The amphiphilic CD consisted of a *γ*-CD backbone grafted with C_{10} chains from vinyl decanoate and was synthesized by enzyme catalysis. Insulin was not added to the polymer/amphipilic CD-containing solvent but rather to the non-

solvent aqueous phase. Still, good association of insulin to the nanoparticles could be observed. The relevance of the nanosystem for insulin delivery *in vivo*, was studied in several experimental settings that aimed to evaluate the hypoglycemic response upon oral and s.c. administration to non-diabetic and STZ-diabetic rats.

6.2 Materials and methods

6.2.1 Synthesis and characterization of amphiphilic cyclodextrins

Parent γ-CD (Roquette, France) was grafted C_{10} alkyl chains by a thermolysin-based catalysis as previously described (Choisnard *et al.* 2006). Briefly, ~1 g of γ-CD dissolved in 7.5 mL of DMSO plus 2.3 mL of vinyl decanoate (99%; TCI Europe nv, Interchim, France), were let to react at 45 °C for 8 days in the presence of 1 g of thermolysin (Sigma Aldrich, France) previously immobilized in celite. At the end of the reaction, the celite-thermolysin deposit was eliminated by centrifugation and cyclodextrin esters in the supernatant were precipitated by adding 20 mL of 35% (v/v) methanol in water. After centrifugation, the supernatant was discarded, the product solubilized in tetrahydrofuran and further purified by successive acetonitrile precipitation, filtration and re-solubilization in tetrahydrofuran. This procedure was repeated three times. Finally the γ-CD capric esters (γ-CDC_{10}) were dissolved in acetone and recovered as a white powder after drying under vacuum. MALDI-MS: *m/z* = 2399.11 (relative intensity, 33%; decanoate γ-CD ester with 7 chains + Na^+); *m/z* = 2553,31 (relative intensity, 100%; decanoate γ-CD ester with 8 chains + Na^+); *m/z* = 2707.48 (relative intensity, 54%; decanoate γ-CD ester with 9 chains + Na^+); *m/z* = 2861.66 (relative intensity, 15%; decanoate γ-CD ester with 10 chains + Na^+). ^1H NMR (600 MHz; DMSO-d_6): δ (ppm) = 0.85 (─CH_2─CH_2─$(CH_2)_6$─CH_3), 1.24 (─CH_2─CH_2─$(CH_2)_6$─CH_3), 1.53 (─CH_2─CH_2─$(CH_2)_6$─CH_3), 2.32 (─CH_2─CH_2─$(CH_2)_6$─CH_3), 3.49 (H4), 3.60 (H6), 3.66 (H5), 3.79 (H3), 4.43

(H2), 5.20 (H1). ^{13}C NMR (600 MHz; DMSO-d_6): δ (ppm) = 13.5 (─CH_2─CH_2─$(CH_2)_6$─CH_3), 22.0, 28.5 and 31.0 (─CH_2─CH_2─$(CH_2)_6$─CH_3), 24.0 (─CH_2─CH_2─$(CH_2)_6$─CH_3), 33.2 (─CH_2─CH_2─$(CH_2)_6$─CH_3), 59.8 (C6), 69.5 (C3), 71.0 (C5), 72.7 (C2), 77.3 (C4), 172.7 (─CO─). This product was further characterized by heteronuclear multiple quantum coherence (HMQC) spectroscopy.

6.2.2 Preparation of nanoparticles suspensions

Nanoparticles were prepared by nanoprecipitation followed by solvent evaporation (Fessi *et al.* 1992). Typically, 5 mL of acetone containing the nanoparticle-forming material was poured over 6.5 mL of a polysorbate 80 (Montanox® 80, Seppic, France) aqueous solution (0.015% m/v) under magnetic stirring, in a closed system thermostatized at 25 ^oC. Nanoparticles were spontaneously formed, the organic solvent and part of the water were removed by evaporation under vacuum and particles were recovered as an aqueous colloidal suspension (approximately 5 mL). To prepare insulin-loaded nanoparticles, 300 µL of an insulin commercial preparation (Actrapid®, Novo Nordisk, France) equivalent to 30 U of insulin were added to the aqueous phase prior nanoprecipitation to prevent possible denaturation resulting from contact with acetone. The organic solutions consisted of: (i) 5 mg of PLGA with a lactide-glycolide ratio of 50:50 (Boehringer Ingelheim, Germany) per mL of acetone; (ii) 1 mg of γ-CDC_{10} synthesized as previously described per mL of acetone; (iii) a mixture consisting of 5 mg PLGA plus 1 mg of γ-CDC_{10} per mL of acetone. To prepared coated nanoparticles, ethyl acrilate-methacrilic acid copolymer (Eudragit® L30D-55 30% aqueous dispersion, Evonik Röhm GmbH, Germany) was dissolved in acetone to prepare a 40 mg/mL mother solution and 1 mL of this solution was added to the nanoparticle suspension after the addition of the organic phase (iii) to the aqueous phase and prior to the evaporation of the solvents.

6.2.3 Nanoparticles characterization

Particle size was determined in triplicate by quasi-elastic light scattering (QELS) using a Zetasizer 3000 instrument (10 mW HeNe laser at 632.8 nm, K7132 correlator, Malvern). Nanosphere samples were diluted in distilled water in order to obtained adequate kcount readings for size measurements. The analyses took place at 25 ^{o}C, at a reference angle of 90°, viscosity of 0.899x10^{-3} Pa.s, refractive index of 1.330. The polydispersity index (PI), which is a dimensionless measure of the broadness of the size distribution, and *Z*-average mean hydrodynamic diameter (Dh) of the particles were calculated using a cumulant algorithm with Zetasizer 3000 software version V. 1.51. Dh was derived from the measured translational diffusion coefficient of the particles moving under Brownian motion.

Morphology of the particles was address by transmission electron microscopy (TEM).

6.2.4 Insulin quantification

Insulin was quantified by high performance liquid chromatography (HPLC) with a method adapted from Sarmento *et al.* (Sarmento *et al.* 2006) as described. The samples were centrifuged at 17,000 rcf for 30 minutes at 20 ^{o}C. The supernatants were diluted in HCl 0.01 M to a final volume of 2 mL and filtered through 0.22 µm polyvinylidene fluoride filters[6] prior to HPLC analysis. The chromatographic equipment consisted of a Prostar 230 ternary solvent delivery module (Agilent, USA) equipped with a reverse phase X-Terra C-18 column, 5 µm, 4.6 mm × 250 mm (Waters, France) and a Interchrom C-18, 5 µm precolumn (Interchim, France) maintained at 31 ^{o}C. A Prostar autosampler 400 (Agilent, USA) fitted a 50 µL loop was used for injections. Mobile phase A consisted of tri-distilled water with 0.1%

[6] These filters were chosen because they display low protein retention by adsorption. Since standard insulin solutions used in the preparation of the calibration curve were also subjected to the same centrifugation-filtration procedure, any eventual insulin loss during the process is accounted for.

trifluoroacetic acid and mobile phase B of acetonitrile with 0.1% trifluoroacetic acid. Each analysis was performed over 18 minutes with a flow rate of 1 mL/minute, a linear gradient from 70:30 (A:B) to 60:40 (A:B) was applied in the first five minutes, the 60:40 (A:B) was maintained for another 8 minutes; system returned to the initial conditions in the final 5 minutes. Insulin was detected at 210 nm with a Varian 9050 variable wavelength UV/Vis detector (Agilent, USA) and peak area integrated with Star Chromatography Workstation version 5.52 software. A typical chromatogram is depicted in Figure 26 and a calibration curve for insulin was set to determine insulin concentration in the supernatant (Figure 27).

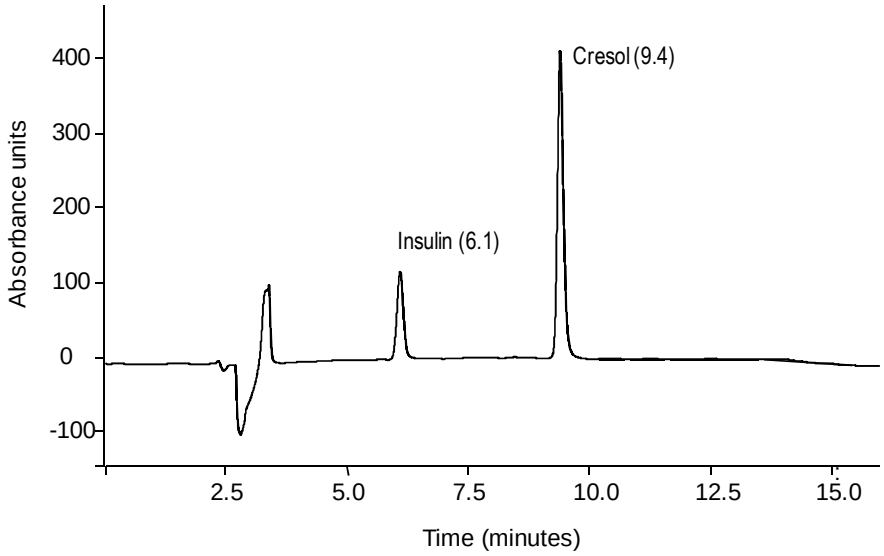

Figure 26 Typical chromatogram obtained for the 35 µg/mL insulin standard prepared by dilution of Actrapid® in HCl 0.01 M. The peaks were detected at 270 nm and correspond to insulin and cresol (included in the commercial preparation) as indicated.

Standard solutions were prepared by dilution of the insulin commercial formulation in HCl 0.01 M. Insulin Association Efficacy (AE) was calculated indirectly as a difference of the amount found in the supernatant from the theoretical amount initially added as shown in Equation 15. This method was also used to determine the %AE after

dilution of the nanoparticle suspensions 1/5 in water and in the release studies in HCl 0.1 M.

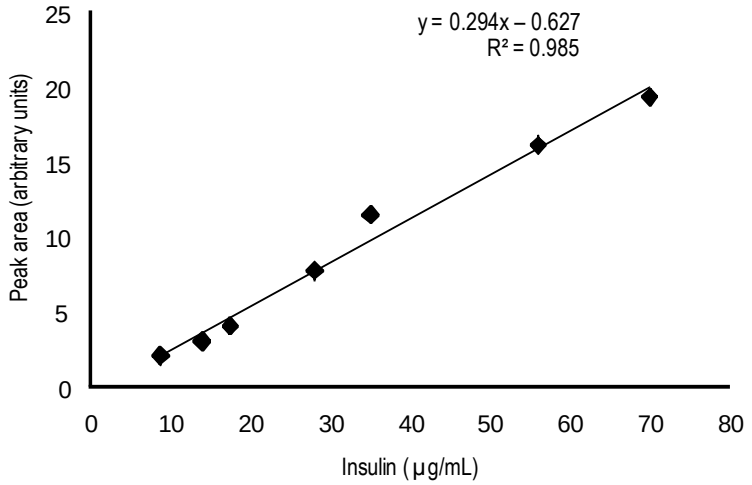

Figure 27 Calibration curve used for quantifying insulin in the supernatant of nanoparticles by HPLC. Standards were prepared from dilutions of a commercial insulin solution (Actrapid ®) in HCl 0.01M. The equation for the linear regression is show.

Equation 15

$$\%\ AE = 1 - \frac{\text{Insulin in supernatant } \left(\frac{\mu g}{mL}\right) \times \text{total volume of NS (mL)}}{\text{initially added insulin } (\mu g)} \times 100$$

A batch of nanoparticles from the PLGA-γ-CDC_{10} blend displaying 93% AE was used to determine the amount of insulin that could be recovered from the formulations. A 200 µL aliquot was diluted 1/20 in HCl 0.05 M, then 2 mL of this suspension was treated as described for the supernatant HPLC analysis and 95% of the theoretical amount of insulin added to the formulation could be recovered at the end of the procedure.

6.2.5 Release assays in HCl 0.1 M

Nanosphere suspensions were diluted 1/4 in centrifuge tubes with HCl (0.1 M, pH 1.2) and incubated in a water bath with the temperature set at 37 ^{o}C. Every 30 minutes samples were centrifuged (5,500 rcf for 10

minutes) and the supernatants collect for HPLC analysis. The solid residue was resuspended in fresh HCl solution and again placed in the thermostatized bath. The release study followed for 2 hours.

6.2.6 Animal procedures

6.2.6.1 Animal housing

As described in section 2.2.1.1.

6.2.6.2 Study I. Non-diabetic controls, s.c. route

Non-diabetic control rats (245 ± 9 g) were fasted overnight prior to the experiments and randomized into six groups (N = 5 per group) receiving the following treatments: CTRL, no treatment; ACTR, s.c. injection of Actrapid® solution in polysorbate 80 (0.015% m/v); PL-I, s.c. injection of insulin-loaded nanoparticles from PLGA; PL, s.c. injection of nanoparticles from PLGA; CDPL-I, s.c. injection of insulin-loaded nanoparticles from the PLGA-γ-CDC_{10} blend; CDPL, s.c. injection of nanoparticles from the PLGA-γ-CDC_{10} blend. The formulations were administered at an insulin dose of 2.3 U/kg or equivalent volume of placebo. Glycemia was monitored from the tail vein with a glucometer (Accu Check Performa, Roche Diagnostics, France) before treatment and henceforward at 0.25, 0.5, 1, 2, 4, 6 and 8 hours. Animals were allowed one week of recovery from this experiment and re-randomized into groups for the next study.

6.2.6.3 Study II. Non-diabetic controls, oral route

In this assay animals were fasted overnight and assigned to the following groups: CTRL, oral gavage of tap water (N = 6); ACTR, oral gavage of Actrapid® solution in polysorbate 80 (0.015% m/v) (N = 8); PLCD, oral gavage of nanoparticles from the PLGA-γ-CDC_{10} blend (N = 8);

PLCD-I, oral gavage of insulin-loaded nanoparticles from the PLGA-γ-CDC_{10} blend (N = 8). The formulations were administered at an insulin dosage of 100 U/kg or equivalent volume of placebo. Glycemia was monitored as described in study I, section 6.2.6.2 before treatment and henceforward at 0.5, 1, 2, 4, 6, 8, 10 and 24 hours.

After reformulation experiments, this assay was applied to a separate group of animals (275 ± 3 g) to assess the efficacy of the Eudragit®-coated nanoparticles. In this case, after an overnight fast, animals received an oral dose (100 U/kg) of insulin-loaded Eudragit®-coated nanoparticles from the PLGA-γ-CDC_{10} blend (NPL30D-I, N = 8) or alternatively an equivalent volume of placebo Eudragit®-coated nanoparticles from the PLGA-γ-CDC_{10} blend (NPL30D, N = 8).

6.2.6.4 Study III. STZ-diabetic rats, s.c. route

Diabetes was induced in a separate group of rats by STZ injection as described in section 3.2.1.2. Fifteen days after diabetes induction by STZ injection, animals (226 ± 6 g) were fasted overnight and randomized in two groups. One group (ACTR, N = 4) received an s.c. injection of an Actrapid® solution in polysorbate 80 (0.015% m/v) and the other (CDPL-I, N = 5) was injected insulin-loaded nanoparticles from the PLGA-γ-CDC_{10} blend. The insulin formulations were administered at a dose of 2.3 U/kg and glycemia monitored as described in study I, section 6.2.6.2.

6.2.6.5 Study IV. STZ diabetic rats, OGTT

Diabetes was induced in a separate group of rats by STZ injection as described in section 3.2.1.2. Twenty days after the induction of diabetes, animals (190 ± 7 g) were fasted for 24 hours and randomized in three groups. In two of the groups, rats were injected with insulin formulations 30 minutes before the OGTT while another group was not given any injection, STZ (N = 5). Insulin was administered at a dose of 5 U/kg as a solution of

Actrapid® in polysorbate 80 (0.015% m/v), ACTR (N = 4) or as a suspension of insulin-loaded nanoparticles from PLGA-γ-CDC_{10} blend, CDPL-I (N = 4). The glucose load was prepared at a dose of 2 g/kg and glycemia was monitored over a 3-hour period as described in chapter 2.

6.2.7 Statistics

As described in section 2.2.6. A two-way ANOVA with Bonferroni post tests was used to analyze glycemia profiles. The area above the curve (AAC) was calculated by setting a cutoff at 100%.

6.3 Results

6.3.1 Synthesis of amphiphilic cyclodextrin

Cyclodextrin esters were obtained by enzymatic synthesis as a mixture of over- and under-acylated species with the substitution degree ranging from 7 to 10 acylations (*m/z*, 2399.11–2861.66). The signals in the MALDI-MS analysis were separated by 154 mass units, corresponding to the molecular mass of the decanoate chain. The most abundant species in the mixture was acylated with 8 C_{10} chains. This profile may represent one or more acylations per glucopyranose unit that composes the CD. The presence of species with 9 and 10 acylations indicates some glucopyranose units were acylated in at least three carbons. Acylation can occur via the primary C6 hydroxyl or the secondary C2 and C3 hydroxyls. Enzymatic catalysis is reported to lead mainly to acylation in C2 however, the grafting of other positions is not to be excluded (Pedersen *et al.* 2005; Choisnard *et al.* 2006). The NMR analyses of the γ-CDC_{10} product (Figure 28 and Figure 29) further clarified the substitution profiles in the mixture, namely in what concerns the positions that were attacked during the transesterification reaction.

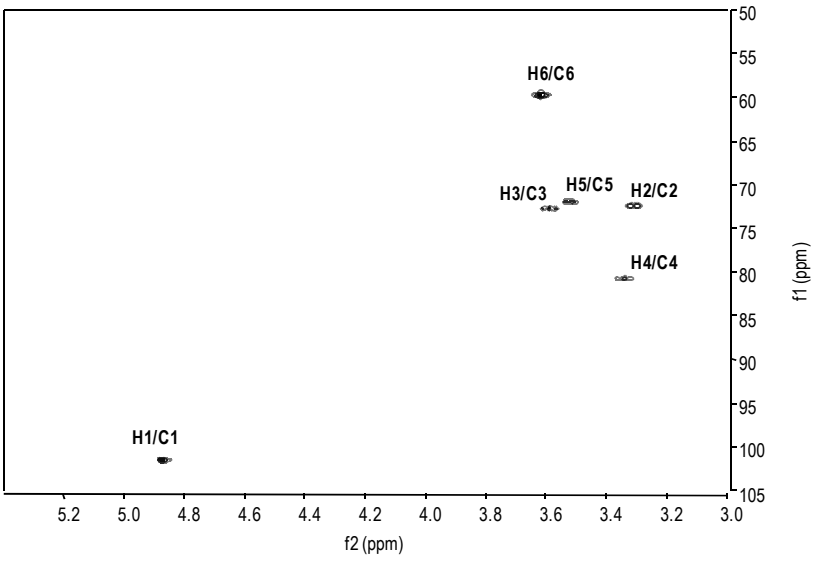

Figure 28 HMQC spectrum of γ-CD in DMSO-d6. The $^{1}H/^{13}C$ correlations are identified for each position of the hexose unit.

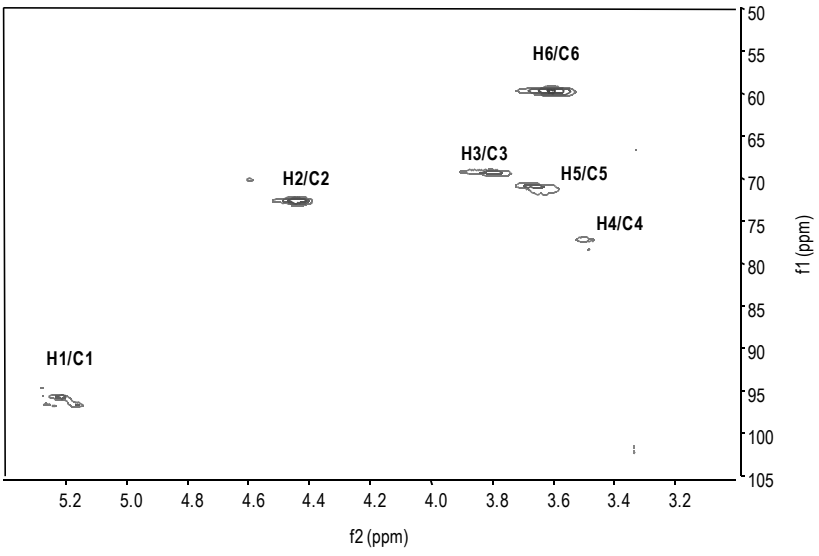

Figure 29 HMQC spectrum of γ-CDC_{10} ester mixture in DMSO-d6. The hexose moiety of the esters is shown and the $^{1}H/^{13}C$ correlations are identified for each position of the hexose unit.

The H6/C6 correlaction in the HMQC spectrum of the the γ-CDC_{10} ester mixture was similar to the one observed for the parent γ-CD. Hence, substitution in position 6 is unlikely to have occurred. The most significant shift from the parent γ-CD was observed for the H2 resonance, which moved downfield from 3.30 to 4.42 ppm, translating in an altered H2/C2 correlation. This downfield shift is consistent with a strong deshielding effect due the ester function in the C2 position. All the other positions experienced a modest downfield shift in ^1H, which indicates the presence of an additional electronegative environment in the vicinity of H3, H4 and H5 and is consistent with the C2 acylation. Nonetheless, the presence of species with 9 and 10 acylations implies that C3 was also acylated at least to some extent. The presence of an extra correlation peak at 4.59/70.43 ppm supports the presence of species acylated in C3, with the H3 moving downfield from 3.59 ppm in the parent γ-CD and from 3.78 ppm in the C2 acylated species.

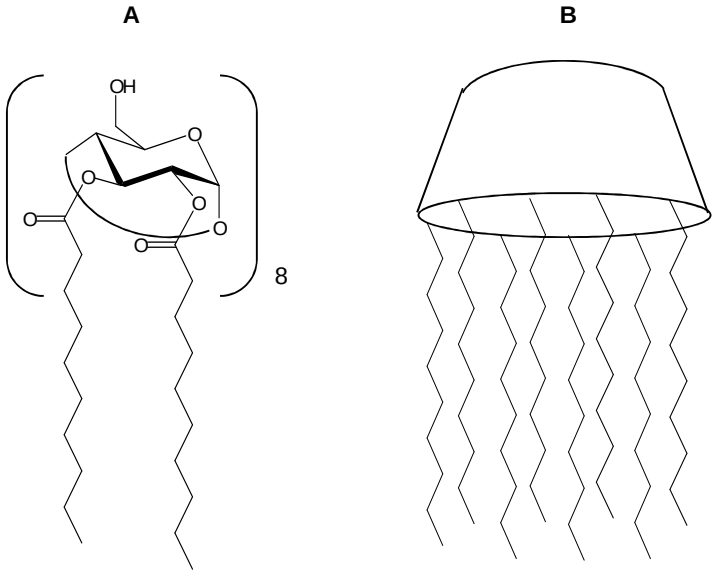

Figure 30 (**A**) Chemical structure of the γ-CDC_{10} amphiphilic cyclodextrin. By enzyme catalysis 10-carbon alkyl chains were grafted in positions 2 and 3. (**B**) Three dimensional representation of the amphiphile, consisting of a hydrophilic head (primary face of the CD cone) and 8 hydrophobic tails in the secondary face.

In sum, the γ-CDC_{10} product consisted of a mixture of esters derived from acylation of the parent γ-CD mainly in C2 and at less extent also in C3.

The proposed structure is depicted in Figure 30. This product showed self-assembly properties compatible with the formation of nanoparticles as presented in section 6.3.2.

6.3.2 Nanoparticle preparation and characterization

Nanoparticles were prepared by the solvent displacement procedure. The nanoparticle-forming material was dissolved in acetone and upon contact of this organic solution with the aqueous phase nanoparticles immediately assembled as a consequence of the desolvation process. This observation was verified for all three organic solutions: PLGA (5 mg/mL), γ-CDC_{10} (1 mg/mL) and the PLGA-γ-CDC_{10} (5:1 mg/mL) blend. Size measurements by QELS (Table 19) confirmed the presence of monodisperse particle size distributions in the nano range. Despite the differences on the composition of the organic phase, all the uncoated formulations rendered nanoparticles of similar sizes. The average mean diameter ranged from 112 to 126 nm. Moreover, these observations indicate that PLGA and γ-CDC_{10} co-nanoprecipitated in formulation from the PLGA-γ-CDC_{10} blend and this was further confirmed by TEM photographs (Figure 31) that show spherical particles in good agreement with the size measurements by QELS.

As described in section 6.2.2, insulin-loaded nanoparticles were prepared by adding a commercially available insulin formulation (Actrapid®) to the system. This formulation consists of an aqueous neutral solution of insulin and because its contact with acetone resulted in immediate turbidity observed by the naked eye, suggesting the integrity of the protein to be compromised, Actrapid® was added to the aqueous phase. When the nanoparticles were prepared from γ-CDC_{10} alone, ~80% of the insulin added to the system could be recovered in the aqueous supernatant after centrifugation, with less than 20% remaining associated to the particles (Table 19). On the other hand, excellent association efficacy (~90%) was observed for the PLGA formulation, which was maintained for the PLGA-γ-CDC_{10} blend (Table 19).

Table 19: Particle sizes (mean diameter in nm), polydispersity indexes (PI) and insulin association efficacy (% from initial, %AE) for the three organic phases studied, which consisted of the following acetonic solutions: 5 mg/mL PLGA with a lactide-glycolide ratio of 50:50 (PLGA); 1 mg/mL γ-CD esters from 10 carbon-alkyl chains (γ-CDC_{10}); and 5 mg/mL PLGA plus 1 mg/mL of γ-CDC_{10} (PLGA-γ-CDC_{10}). (1) Coating was performed with Eudragit® L30D55 after nanoparticle assembly using the specified organic phase. (2) Insulin was not detected in the supernatant after centrifugation of the nanoparticle suspensions.

	Placebo Nanoparticles		Insulin-loaded Nanoparticles		
	Size	PI	Size	PI	% AE
Uncoated Nanoparticles					
PLGA	117.4 ± 3.3	0.1 ± 0.01	112.4 ± 5.8	0.1 ± 0.001	88.1 ± 5.1
γ-CDC_{10}	118.3 ± 0.6	0.09 ± 0.03	126.5 ± 7.3	0.07 ± 0.01	19.0 ± 1.4
PLGA-γ-CDC_{10}	122.7 ± 3.5	0.09 ± 0.007	115.8 ± 5.4	0.1 ± 0.007	92.0 ± 1.0
Coated nanoparticles (1)					
PLGA-γ-CDC_{10}	167.5 ± 2.5	0.1 ± 0.01	186.5 ± 0.5	0.09 ± 0.007	N.D. (2)

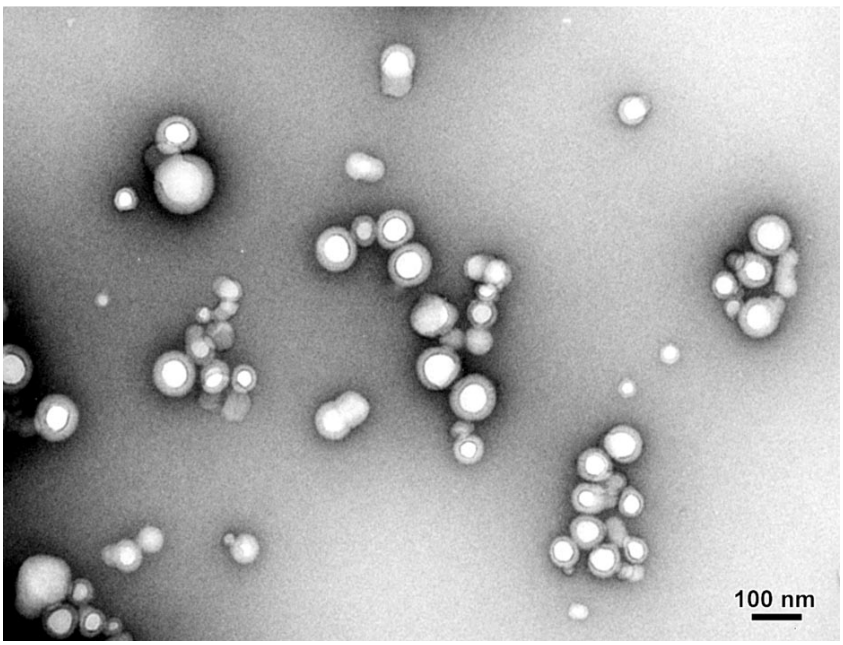

Figure 31 TEM photography for insulin-loaded nanoparticles prepared from the PLGA-γ-CDC_{10} blend.

When Eudragit® was added to the preformed nanoparticles there was a slight increase in particle size but the monodispersity of the population distribution was maintained, supporting the efficient coating of the nanoparticles. Moreover, coating seemed to strengthen the interactions between insulin and the nanoparticles since the %AE was virtually 100 as a result of no insulin being detect in the supernatants after centrifugation of the suspensions.

6.3.3 Dilution and release assays

When the uncoated nanoparticle suspensions were diluted in water, the %AE was maintained relative to that initially determined (Figure 32). This indicated that the interaction between insulin and the carrier was not disrupted upon simple dilution. These results, together with the particle size measurements and %AE determinations before dilution suggest that both formulations from PLGA and the PLGA-γ-CDC_{10} blend have similar characteristics in regards to the interaction with insulin.

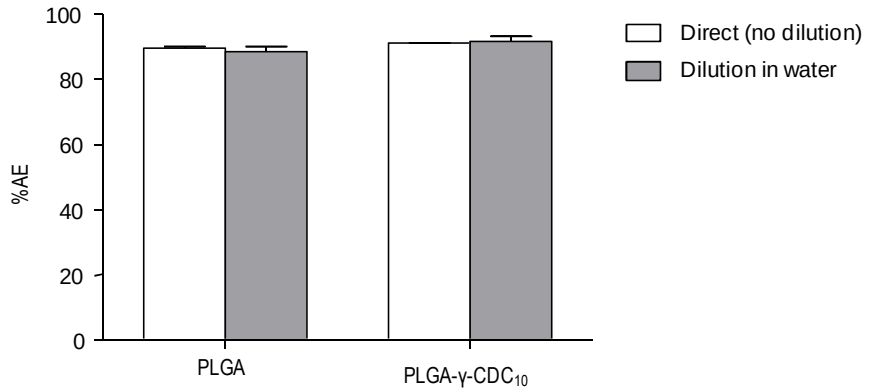

Figure 32 Percente association efficacy (%AE) after dilution of the nanoparticle suspensions in water. Nanoparticles were prepared by nanoprecipitation followed by solvent evaporation, the organic phase consisted of PLGA (5 mg/mL) or a PLGA-γ-CDC_{10} mixture (5:1 mg/mL) in acetone and the aqueous phase was polysorbate 80 0.015% (m/v), insulin was added to the aqueous phase.

With the oral route of administration in mind, studies were performed to investigate the release profile of insulin in acidic medium as an indication for the possible resistance of the system during the GIT transit. As depicted in Figure 33, the coating with Eudragit® improved association of insulin to the nanoparticles after HCl treatment. This effect was expected since Eudragit® L30D55 is resistant to acid environment, dissolving at a pH value superior to 5.5.

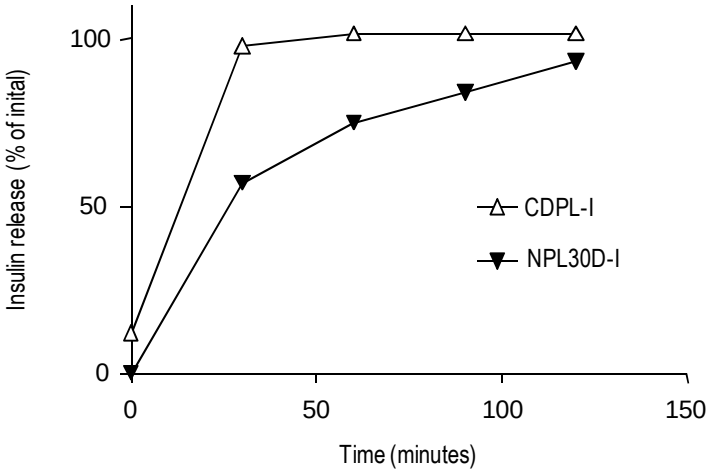

Figure 33 Release studies in HCl 0.1 M, pH 1.2 performed at 37 ºC. Coated (NPL30D-I) and uncoated (CDPL-I) insulin-loaded nanoparticles from the PLGA-γ-CDC_{10} blend were diluted 1/4 in HCl and insulin released to the medium quantified by HPLC.

6.3.4 Biological activity of the nanoparticle formulations

Insulin not associated to the particles remains in the aqueous phase of the suspensions. Thus, when determining the dosage for administration it was taken into consideration the total (free plus nanoparticle-associated) amount of insulin present in the suspensions. Since only a residual amount of insulin was found in the supernatant fraction of the suspensions, most of it being associated to the particles, the *in vivo* effect of the formulations is assumed to be mostly due to the nanoparticle-associated insulin.

6.3.4.1 Subcutaneous administration to non-diabetic rats

After the overnight fasting period, the glycemia observed for the animals was 88 ± 2 mg/dL. Figure 34 shows the glycemia profiles (expressed as percent from the initial value) for all experimental groups following the injection of insulin or placebo formulations.

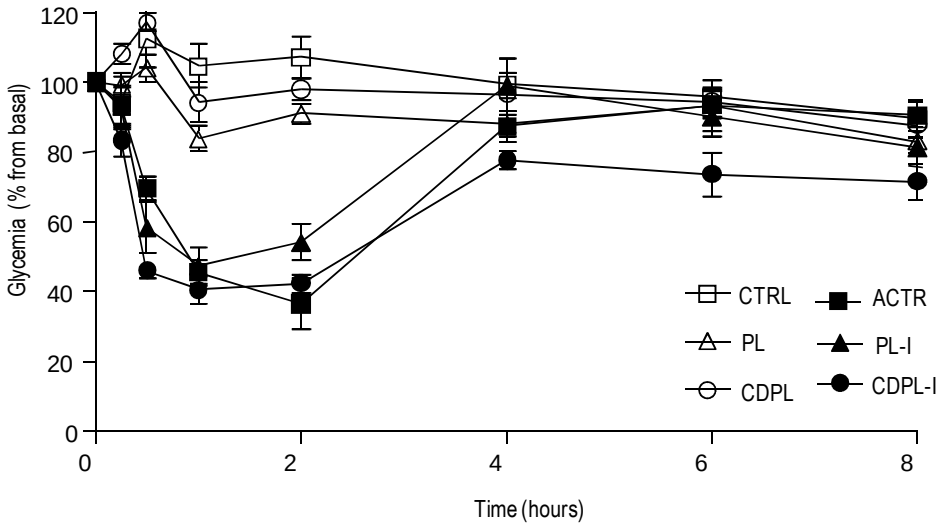

Figure 34 Glycemia profiles for non-diabetic rats after an overnight fasting. Insulin and placebo formulations were administered by the subcutaneous route at time t = 0 hours at a dose of 5 U/kg or equivalent volume. CTRL, control rats not administered with any formulation; PL, rats administered sham nanoparticles from PLGA; CDPL, rats administered sham nanoparticles from the PLGA-γ-CDC_{10} blend; ACTR, rats administered the commercial insulin formulation Actrapid®; PL-I, rats administered insulin-loaded nanoparticles form PLGA; CDPL-I, rats administered insulin-loaded nanoparticles from the PLGA-γ-CDC_{10} blend. See text for statistical differences.

Animals that were injected with placebo formulations (PL and CDPL groups) presented glycemia profiles similar to controls, maintaining the initial blood glucose levels throughout the experimental period with a slight initial increment attributed to manipulation-induced stress. This observation demonstrates that the formulations *per se* don't elicit hypoglycemic response. Also the AAC, which is a measure of the overall hypoglycemic effect, was similar for controls and placebo (35 ± 21, CTRL; 86

± 17, PL; and 51 ± 16, CDPL), further supporting the lack of pharmacological effect of the sham nanoparticles. On the other hand, when insulin formulations were administered to the animals, the hypoglycemic effect was immediate, overcoming the initial stress-induced raise in glycemia, although statistically significant differences were only attained from 0.5 hours onward. The AAC for all the insulin formulations were significantly higher than controls and placebo formulations, as expected.

When animals were injected with the standard insulin formulation (Actrapid®), glycemia decreased progressively until a minimum value (29 ± 6 mg/dL) observed at time t = 2 hours, and 2 hours later animals had regain normoglycemia. Furthermore, the glycemia curve for ACTR group was characterized by a peak-like shape with a minimum at t = 2 hours. In contrast, for both nanoparticle formulations, the negative peak was smoothen and the curves assumed a rounder shape, enlarging the interval for the minimum, which in these cases was sustained from t = 0.5 hours (corresponding to 45 ± 6 mg/dL, PL-I and 39 ± 3 mg/dL, CDPL-I) to t = 2 hours (corresponding to 43 ± 5 mg/dL, PL-I and 36 ± 2 mg/dL, CDPL-I). These observations suggest both formulations from PLGA and PLGA-γ-CDC_{10} blend were able to modulate insulin's hypoglycemic effect that was sustained during that interval. These results are in good agreement with Barichello *et al.* experiments, in which the authors observe a similar sustentation for the minimum glycemia following the s.c. injection of insulin-loaded nanoparticles from PLGA (Barichello *et al.* 1999b). Moreover, it was observed an earlier onset on the hypoglycemic effect for animals administered the formulation containing γ-CDC_{10} along with PLGA ($p < 0.01$ *vs* ACTR at t = 0.5 hours) as well as a prolonged effect, still detected 6 hours past the injection ($p < 0.05$ *vs* all other groups). Additionally, the AAC for CDPL-I was 282 ± 24, significantly higher than that observed for PL-I (172 ± 29) and ACTR (199 ± 22) groups. On the other hand, the AAC for PL-I was not statistically different from that of ACTR.

6.3.4.2 Oral administration to non-diabetic rats

Data from the s.c. administration assay support the inclusion of the γ-CDC_{10} in the nanoparticle core as a means to enhance insulin's biological effect. The next step was to investigate whether that formulation would prove beneficial in the oral administration of insulin. As depicted in Figure 35, following the oral administration of the CDPL-I formulation to overnight fasted rats, no hypoglycemic effect was observed. In fact, all the test groups showed similar glycemic profiles throughout the experimental period maintaining a constant glycemia. Hence, the nanoparticle formulation was unable to protect insulin through the GIT.

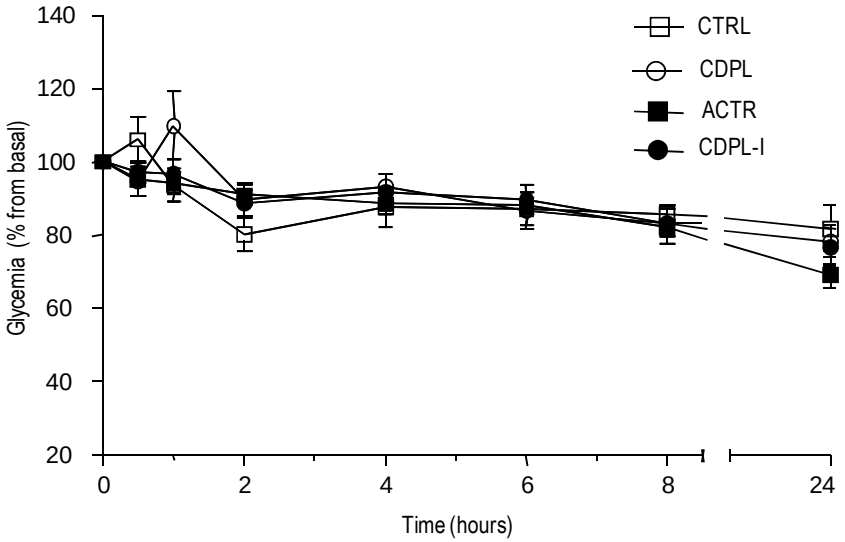

Figure 35 Glycemia profiles for non-diabetic rats after an overnight fasting. Insulin and placebo formulations were administered by oral gavage at time t = 0 hours at a dose of 100 U/kg. CTRL, CDPL, ACTR, CDPL-I as describe in the legend of Figure 34.

Reformulation studies led to the coating of nanoparticles from the PLGA-γ-CDC_{10} blend with a copolymer from ethyl acrilate and methacrilic acid, which is specific for enteric delivery. Upon oral administration of the coated nanoparticles still no hypoglycemic effect was detected against the

sham nanoparticles (Figure 36) suggesting that this strategy failed to protect insulin from degradation in the GIT.

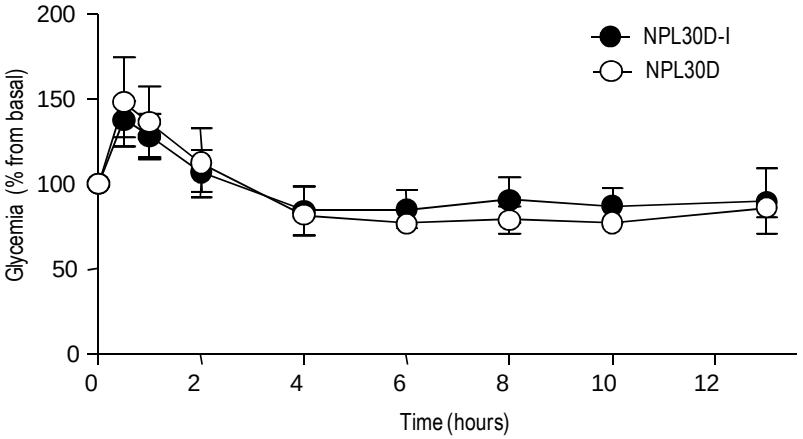

Figure 36 Glycemia profiles for non-diabetic rats after an overnight fasting. Insulin-loaded (NPL30D-I) and sham (NPL30D) nanoparticles from the PLGA-γ-CDC_{10} blend coated with Eudragit® were administered by oral gavage at time t = 0 hours at a dose of 100 U/kg.

6.3.4.3 Subcutaneous administration to STZ-diabetic rats

Since the CDPL-I formulation improved insulin's hypoglycemic effect when delivered to the s.c. route in non-diabetic control rats, it was then evaluated the effect on an animal model of type 1 DM, the STZ-diabetic rat. After an overnight fast the glycemia for STZ-diabetic rats was 224 ± 27 mg/dL, significantly higher than that observed for the non-diabetic rats in study I. Upon the injection of the commercial insulin formulation, glycemia decreased progressively but, unlike the observations for the non-diabetic controls that could rapidly recover from the insulin-induce hypoglycemia, this lowering effect was sustained up until t = 4 hours. As discussed in chapter 3, this is probably due to the lack of appropriate glucagon response in the diabetic rats (Zhou *et al.* 2004). When the animals received the nanoparticle formulation instead of Actrapid®, there were no significant

changes in the glycemic response. In fact, the AAC were similar for both ACTR (399 ± 48) and CDPL-I (283 ± 41) groups.

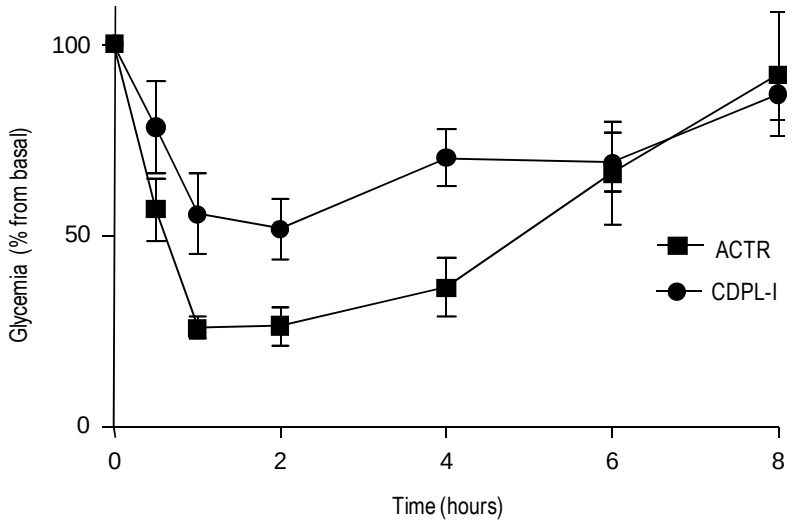

Figure 37 Glycemia profiles for STZ diabetic rats after an overnight fasting. Insulin formulations were administered by subcutaneous injection at time t = 0 hours at a dose of 2.3 U/kg. ACTR and CDPL-I as in legend of Figure 34.

6.3.4.4 Oral glucose tolerance test in STZ-diabetic rats

The performance during the OGTT is an indicator of the glucose disposal capacity. This test was performed in STZ-diabetic rats to establish the effect of insulin formulations under those circumstances. Insulin injection prior to the OGTT successfully prevented the raise in glycemia observed for the STZ-diabetic rats not injected with the hormone (Figure 38). This effect was independent of the formulation. In fact, the AUC determined for ACTR (116 ± 10) was similar to that of CDPL-I (98 ± 12) and both were significantly lower than that of STZ-diabetic animals (339 ± 51).

At the beginning of the study, glycemia values after 24 hours of fasting were 252 ± 29 mg/dL for the STZ-diabetic rats, significantly higher than those observed for non-diabetic controls (65 ± 4 mg/dL, see chapter 2). Three hours after the oral glucose load, glycemia in the STZ group remained elevated (336 ± 41 mg/dL) when comparing with ACTR and CDPL-I

groups. For the animals in the latter groups, glycemia descended to 53 ± 10 mg/dL and 94 ± 27 mg/dL, respectively (p = n.s.). The range observed for the animals injected with the commercial insulin formulation was under that observed for non-diabetic controls in chapter 2 (86 ± 3 mg/dL, $p < 0.01$). This difficulty of STZ-diabetic rats to recover from insulin-induced hypoglycemia had already been observed in the studies described in chapter 3. Interestingly, the STZ-diabetic rats administered the nanoparticle formulation displayed a glycemia value within the physiological range at the end of the test. This effect may be related with the sustained release of insulin to the blood and is in good agreement with the observations from study I.

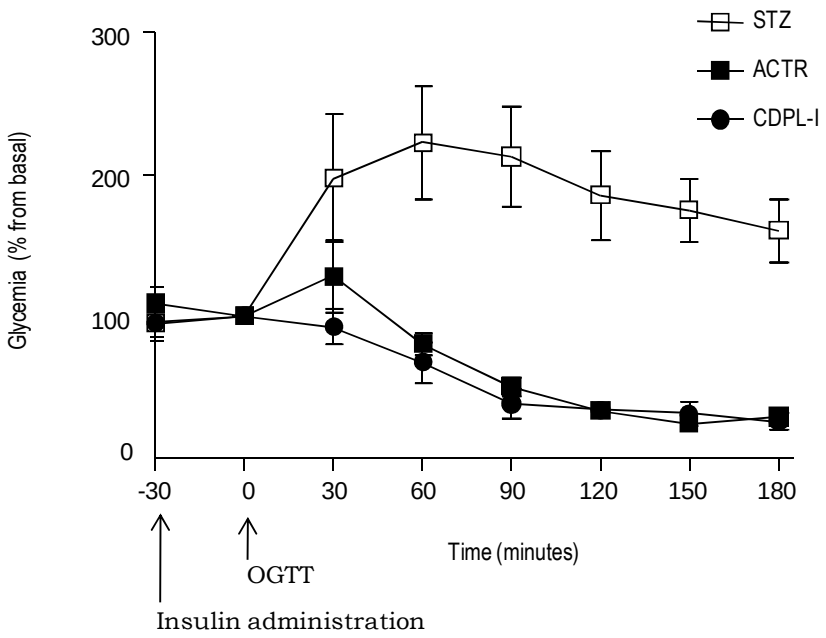

Figure 38 Glycemia curves recorded during the OGTT performed in 24-hour fasted STZ-dibetic rats. Insulin formulations were administered by subcutaneous injection 30 minutes prior to the test at a dose of 5 U/kg. STZ, STZ-diabetic rats not injected with any formulation, ACTR and CDPL-I as in legend of Figure 34.

6.4 Discussion

6.4.1 Formulation considerations

This chapter presented the formulation development study for improving insulin delivery by the use of alternative delivery systems. A novel formulation for insulin delivery was obtained by combining two strategies in the pharmaceutical technology field: the use of polymeric nanoparticles and modified cyclodextrins. An important achievement of this work was the preparation of nanoparticles from two different materials with the ability to self-assemble individually. The nanoprecipitation technique allowed for both the PLGA polymer and the amphiphilic CD derivative γ-CDC_{10} to co-nanoprecipitate and form mixed nanoparticles. This system presented excellent association of insulin, which was due to the presence of the polymer in the matrix of the nanoparticle.

6.4.2 Biological relevance for the inclusion of γ-CDC_{10} in the insulin nanoparticles

The biological relevance of polymeric (from PLGA only) and mixed (from the PLGA-γ-CDC_{10} blend) formulations was first investigated in non-diabetic controls. Those assays showed that both the nanoparticle formulations were able to modulate insulin action towards a more sustained hypoglycemic response in contrast with the peak observed when insulin was administered as a simple solution. This effect may result from a progressive release of insulin associated to the particles and/or a progressive absorption of the particles from the subcutaneous region to the blood stream. Following s.c. administration, nanoparticles and drugs are subjected to an absorption barrier eventually reaching systemic circulation via the blood capillaries or lymph vessels. Polymeric (Owens III *et al.* 2006) and CD esters-based (Gèze *et al.* 2007) nanoparticles accumulate mainly in liver and spleen upon intravenous injection. On the other hand, studies with solid lipid nanoparticles (Reddy *et al.* 2005) indicate that, in the case of s.c.

injection, deposition of nanoparticles in the administration site is responsible for delaying and lowering tissue accumulation. In this experiment it could be observed a rapid hypoglycemic effect following the subcutaneous administration of the insulin-loaded nanoparticles, which is consistent with progressive release of the drug from the carrier to the blood, with the latter remaining at the administration site, similarly to the reports from studies with solid lipid nanoparticles. On the other hand, the late effect detected at 6 hours could be attributed to insulin released from nanoparticles that reach the blood after a delayed absorption. It is possible that the presence of γ-CDC_{10} in the formulation promoted the passage of the nanoparticles to the blood allowing for the 6^{th} hour-effect to be noted for this system and not for the one prepared from PLGA alone. Since many CD derivatives are used in drug delivery as means to promote drug absorption (Sharma *et al.* 2005) it can be hypothesized that the CD esters in the nanoparticles may act as absorption enhancers.

6.4.3 Insulin-carrier interactions and the oral delivery

The excellent association of insulin to the nanoparticles was not compromised when the formulations were diluted in water, under those circumstances ~90% of the amount added to the system remain associated to the carrier. However, upon the s.c. injection of the nanoparticle formulations to non-diabetic rats, most of the biological effect was observed in the first 2 hours, suggesting the interactions between insulin and the nanoparticle carrier are easily broken *in vivo* resulting in the fast (although sustained) release of the drug from the carrier. When insulin was added to a pre-formulated suspension of sham nanoparticles the resulting association efficacy was similar to that observed when the nanoparticles were prepared in the presence of insulin. Taken together these observations support adsorption interactions between insulin and hydrophilic PLGA to be the major forces accounting for the drug's association to the nanoparticle system. This behavior most probably is a consequence of the

nanoprecipitation method, which employs very mild conditions. In other words, nanoparticles fail to afford a sufficient protection of the drug because the adsorption interactions accounting for insulin's association to the carrier can be easily disrupted *in vivo*. Moreover, the weak nature of the insulin-carrier interaction is in perfect agreement with the lack of efficacy upon oral administration of the nanoparticles.

On the other hand, there are some reports on the efficient delivery of insulin by the oral route by means of PLGA-based particles. For example, Cui *et al.* prepared insulin-loaded PLGA nanoparticles by nanoprecipitation and afforded to avoid the initial burst effect (*i.e.* the rapid release of insulin) by including a cellulose derivative for enteric coating in the formulation (Cui *et al.* 2007). Alternatively, Naha *et al.* report that microparticles prepared by the double emulsion method coated with Eudragit® effectively deliver insulin to the oral route (Naha *et al.* 2008). The coating strategy was also pursued in the studies described in this chapter. Eudragit® L30D55 was used as enteric coating but, despite the reduction on insulin release in acidic medium *in vitro*, the coated formulations did not translate into any hypoglycemic effect upon oral administration. Manufacture aspects such as the method of nanoparticle preparation or the amount of polymers in the system may be preventing the oral efficacy of the formulation, relative to the experiments from Cui *et al.* and Naha *et al.* above mentioned. However, increasing the PLGA concentration or the amount of coating material compromised the formation of nanoparticles by the method described in this chapter.

6.4.4 Effect of insulin nanoparticles in the STZ-diabetic rat

When the mixed nanoparticles from PLGA and γ-CDC_{10} were tested in STZ-diabetic rats, no differences could be observed when comparing its effect with that of the commercial insulin formulation. In the STZ-diabetic rat, the hypoglycemic period following insulin injection was longer than that observed in non-diabetic controls. These animals take more time to

recover from insulin-induced hypoglycemia because of the lack of appropriate glucagon response to hypoglycemia (Zhou *et al.* 2004; Cui *et al.* 2007). In their studies, Zhou *et al.* demonstrate that for normal glucagon secretion to occur both hypoglycemia and a discontinuation of the insulin signal to the *a* cell (switch off hypothesis) are required (Zhou *et al.* 2004). Hence, because the physiology of the STZ-diabetic rats is quite distinct from that of non-diabetics a single insulin injection translates into different kinetics in the hypoglycemic response. Thus, the nanoparticle-induced sustained and prolonged hypoglycemic response that was observed in the case of the non-diabetic controls was probably masked in the STZ-diabetic rats due to the already prolonged insulin-induced hypoglycemia.

The efficacy of the nanoparticles was yet investigated in the context of a glucose challenge and again no clear benefits could be attributed to the nanoparticle formulation for insulin delivery in STZ-diabetic rats.

6.5 Conclusions

A novel nanoparticle system for s.c. insulin delivery with high insulin association efficacy was successfully prepared form a mixture of PLGA and an amphiphilic cyclodextrin derivative (γ-CDC_{10}). The biological action of insulin could be enhanced by the use of the formulation, especially when the cyclodextrin derivative was present. This effect was observed in non-diabetic control rats but not in STZ-diabetic animals. The findings from these experiments were strongly dependent on the animal model used. Because of the altered physiology of the STZ-diabetic rat, modest improvements in insulin delivery such as the ones observed in these studies may not be detected.

In drug development, animal studies usually follow an exhaustive set of assays that have established an optimized formulation. In these studies, animal experiments were moved slightly upstream and re-formulation was done in accordance with inputs from animal studies. This

allowed for re-addressing the oral route with the coating approach that unfortunately didn't prove to be effective. Nonetheless, the nanoparticles from PLGA and γ-CDC_{10} promise to be a good carrier for insulin delivery and further formulation development should be undertaken aiming to strengthen the interaction between insulin and the nanoparticle matrix. For example, other preparation method or coating material may be envisaged.

7
CONCLUDING REMARKS

Insulin is an absorptive state hormone acting in many target organs to promote energy storage. In the liver, insulin stimulates glycogen and lipid synthesis and inhibits glucose output after meals. These studies addressed postprandial hepatic metabolism in control and diabetic rats. In all the experiments, hyperglycemia in diabetic rats was accompanied by weight loss, consistent with impairments in glucose disposal and energy storage. Tracer-based experiments and NMR spectroscopy methods provided insight into the mechanisms underlying the metabolic disruptions resulting from the lack of insulin action.

The transition from fasted to fed state is a rapid event and efficient short-term mechanisms must operate to readjust the hepatic metabolic fluxes from a positive glucose output to net storage under those circumstances. This setting was investigated in the carbohydrate challenge experiments described in chapters 2 and 3. In non-diabetic control rats, the gluconeogenic flux accounting to maintain EGP during the fasting period

was diverted to glycogen synthesis and this actually constituted the major source of glycogen in the context of the glucose challenge. Direct conversion of load glucose contributed to ~30% of the glycogen synthesis but this fraction was reduced when other preferential substrate such as galactose was present. Hence, hepatic glycogen is a highly dynamic pool that constitutes a "first line" response in the recuperation of glucose homeostasis after nutritional challenges. Efficient glycogen deposition was parallel to a rapid clearence of glucose from the blood, and at the end of the test, EGP accounted for the majority (~75%) of plasma glucose in non-diabetic rats. This mechanism is necessary to avoid hypoglycemia resulting from a continuous glucose uptake from the blood. Under natural feeding conditions, with constant glucose provision from food intake, EGP contributed to only 40% of plasma glucose.

Diabetic rats have high rates of EGP essentially due to unrestrained gluconeogenesis. Their hepatic glycogen levels do not fall during fasting demonstrating an inability to mobilize hepatic glycogen stores for glucose production. Nonetheless, under normal feeding conditions there was a significant turnover of hepatic glycogen in the diabetic rats, indicating that a futile cycle of glycogen breakdown and synthesis is taking place. In non-diabetic controls the depletion/replenishment are harmonized with the fasting/(re)feeding cycles but that dynamic is no longer observed in the diabetics. Without insulin, the hepatic glycogen pool was unresponsive to fasting, at least in the 24-hour period. Moreover, it also lost the capacity to receive the gluconeogenic flux in response to a glucose load.

In diabetic rats, inefficient glycogen deposition after a glucose load was parallel to elevated EGP and reduced clearance form the blood, resulting in persistent hyperglycemia at the end of the 3-hour glucose tolerance test. A single insulin dose had no effect on improving glycogen synthesis in that context but efficiently controlled the contribution of EGP to plasma glucose levels. However, the most striking action of insulin was to stimulate peripheral glucose uptake. As a consequence, plasma glucose

levels decreased drastically and the animals were in fact hypoglycemic for at least 3-hours after the load.

After a period of insulin replacement for 10 days, pathways for energy storage were enhanced but diabetic animals still experienced abnormal catabolic events like high gluconeogenic and lipolytic fluxes during feeding. This could be a consequence of insufficient or inappropriate insulinization and other therapeutic protocols should be studied to determine whether an efficient glycemic control by insulin replacement is able to normalize all the metabolic disruptions in diabetic rats. With the insulin treatments applied, the pathways for hepatic glycogen synthesis in the diabetic rats were restored to control levels but the hepatic glycogen content was only completely recovered when insulin was delivered to the i.p. route. Thus, targeting insulin to the liver translated into differential benefits on the hepatic glycogen storage. TG metabolism was also sensitive to insulin replacement, which translated into a reduction of plasma TGs and an increase in *de novo* hepatic TGs.

In the context of insulin formulation development, animal studies are simple and straightforward assays that measure a specific pharmacological response, which in the case of insulin typically is the hypoglycemic effect. These assays are important in establishing the biological interest of a particular formulation and should be integrated with formulation re-assessments for optimizing drug delivery. In the experimental work of this thesis, a novel nanoparticle formulation for insulin delivery was developed and its biological relevance demonstrated in a simple animal experimental setting, but those findings were not reproduced when a more complex diabetic rat model was studied and further formulation development is required. After formulation/reformulation studies, animal experiments should include the assays for addressing the hepatic metabolic effects of insulin in the postabsorptive state to determine whether liver-targeted insulin action can be afforded.

REFERENCES

Acheson, KJ, Y Schutz, T Bessard, K Anantharaman, J-P Flatt and E Jéquier (1988) Glycogen storage capacity and de novo lipogenesis during massive carbohydrate overfeeding in man. Am J Clin Nutr 48, 240-247.

Agius, L (2008) Glucokinase and molecular aspects of liver glycogen metabolism. Biochem J 414, 1-18.

Agius, L and M Peak (1993) Intracellular binding of glucokinase in hepatocytes and translocation by glucose, fructose and insulin. Biochem J 296, 785–796.

Agius, L, M Peak, CB Newgard, AM Gomez-Foix and JJ Guinovart (1996) Evidence for a Role of Glucose-induced Translocation of Glucokinase in the Control of Hepatic Glycogen Synthesis. J Biol Chem 271, 30479-30486.

Aguayo-Mazzucato, C and S Bonner-Weir (2010) Stem cell therapy for type 1 diabetes mellitus. Nat Rev Endocrinol 6, 139-148.

Aguiar, MMG, JM Rodrigues and A Silva Cunha (2004) Encapsulation of insulin-cyclodextrin complex in PLGA microspheres: a new approach for prolonged pulmonary insulin delivery. J Microencapsul 21, 553-564.

Akhani, SP, SL Vishwakarma and RK Goyal (2004) Anti-diabetic activity of Zingiber officinale in streptozotocin-induced type I diabetic rats. J Pharm Pharmacol 56, 101-105.

Akirav, EM, O Chan, K Inouye, MC Riddell, SG Matthews and M Vranic (2004) Partial leptin restoration increases hypothalamic-pituitary-adrenal activity while diminishing weight loss and hyperphagia in streptozotocin diabetic rats. Metabolism 53, 1558-1564.

Akkaoui, M, I Cohen, C Esnous, V Lenoir, M Sournac, J Girard and C Prip‐Buus (2009) Modulation of the hepatic malonyl-CoA–carnitine palmitoyltransferase 1A partnership creates a metabolic switch allowing oxidation of de novo fatty acids. Biochem J 420, 429-438.

Allémann, E, R Gurny and E Doelker (1993) Drug-Loaded Nanoparticles - Preparation Methods and Drug Targeting Issues. Eur J Pharm Biopharm 39, 173-191.

Allémann, E, J-C Leroux and R Gurny (1998) Polymeric nano- and microparticles for the oral delivery of peptides and peptidomimetics. Adv Drug Deliv Rev 34, 171-189.

Almon, RR, E Yang, W Lai, IP Androulakis, DC DuBois and WJ Jusko (2008) Circadian Variations in Rat Liver Gene Expression: Relationships to Drug Actions. J Pharmacol Exp Ther 326, 700-716.

Alves, TC, DE Befroy, RG Kibbey, M Kahn, R Codella, RA Carvalho, KF Petersen and GI Shulman (2011) Regulation of hepatic fat and glucose oxidation in rats with lipid-induced hepatic insulin resistance. Hepatology, In press.

Armstrong, S, G Coleman and G Singer (1980) Food and Water Deprivation: Changes in Rat Feeding, Drinking, Activity and Body Weight. Neurosci Biobehav R 4, 377-402.

Atkinson, MA and GS Eisenbarth (2001) Type 1 diabetes: new perspectives on disease pathogenesis and treatment. Lancet 358, 221-229.

Bain, JR, RD Stevens, BR Wenner, O Ilkayeva, DM Muoio and CB Newgard (2009) Metabolomics Applied to Diabetes Research. Diabetes 58, 2429-2443.

Barichello, JM, M Morishita, K Takayama and T Nagai (1999a) Encapsulation of Hydrophilic and Lipophilic Drugs in PLGA Nanoparticles by the Nanoprecipitation Method. Drug Dev Ind Pharm 25, 471–476.

Barichello, JM, M Morishita, K Takayama and T Nagai (1999b) Absorption of insulin from Pluronic F-127 gels following subcutaneous administration in rats. Int J Pharm 184, 189-198.

Baron, AD, G Brechtel, P Wallace and SV Edelman (1988) Rates and tissue sites of non-insulin- and insulin-mediated glucose uptake in humans. Am J Physiol-Endoc M 255, E769-E774.

Barthel, A and D Schmoll (2003) Novel concepts in insulin regulation of hepatic gluconeogenesis. Am J Physiol-Endoc M 285, E685-692.

Bassilian, S, S Ahmed, SK Lim, LG Boros, CS Mao and W-NP Lee (2002) Loss of regulation of lipogenesis in the Zucker diabetic rat. II. Changes in stearate and oleate synthesis. Am J Physiol-Endoc M 282, E507-E513.

Benavides, A, M Siches and M Llobera (1998) Circadian rhythms of lipoprotein lipase and hepatic lipase activities in intermediate metabolism of adult rat. Am J Physiol-Reg I 275, R811-R817.

Bilati, U, E Allemann and E Doelker (2005a) Strategic approaches for overcoming peptide and protein instability within biodegradable nano- and microparticles. Eur J Pharm Biopharm 59, 375-388.

Bilati, U, E Allémann and E Doelker (2005b) Nanoprecipitation Versus Emulsion-based Techniques for the Encapsulation of Proteins Into Biodegradable Nanoparticles and Process-related Stability Issues. AAPS PharmSciTech 6, E594-E604.

Bischof, MG, E Bernroider, M Krssak, M Krebs, H Stingl, P Nowotny, C Yu, GI Shulman, W Waldhausl and M Roden (2002) Hepatic Glycogen Metabolism in Type 1 Diabetes After Long-Term Near Normoglycemia. Diabetes 51, 49-54.

Blondel, O, D Bailbe and B Portha (1989) In vivo insulin resistance in streptozotocin-diabetic rats - evidence for reversal following oral vanadate treatment. Diabetologia 32, 185-190.

Bois-Joyeux, B, M Chanez, B Azzout and J Peret (1986) Studies on the Early Changes in Rat Hepatic Fructose 2,6-Bisphosphate and Enzymes in Response to a High Protein Diet. J Nutr 116, 446-454.

Bolzán, AD and MS Bianchi (2002) Genotoxicity of Streptozotocin. Mutat Res-Rev Mutat 512, 121-134.

Burcelin, R, M Eddouks, J Maury, J Kande, R Assan and J Girard (1995) Excessive glucose production, rather than insulin resistance, accounts for hyperglycaemia in recent-onset streptozotocin-diabetic rats. Diabetologia 38, 283-290.

Caseras, A, I Metón, F Fernández and IV Baanante (2000) Glucokinase gene expression is nutritionally regulated in liver of gilthead sea bream (Sparus aurata). BBA-Gene Struct Expr 1493, 135-141.

Catargi, B (2004) Current status and future of implantable insulin pumps for the treatment of diabetes. Expert Rev Med Devices 1, 181-185.

Chalasani, KB, GJ Russell-Jones, AK Jain, PV Diwan and SK Jain (2007) Effective oral delivery of insulin in animal models using vitamin B12-coated dextran nanoparticles. J Control Release 122, 141-150.

Chandramouli, V, K Ekberg, WC Schumann, SC Kalhan, J Wahren and BR Landau (1997) Quantifying gluconeogenesis during fasting. Am J Physiol-Endoc M 273, E1209-E1215.

Cherrington, AD (1999) Banting Lecture 1997. Control of glucose uptake and release by the liver in vivo. Diabetes 48, 1198-1214.

Chikayama, E, M Suto, T Nishihara, K Shinozaki, T Hirayama and J Kikuchi (2008) Systematic NMR Analysis of Stable Isotope Labeled Metabolite Mixtures in Plant and Animal Systems: Coarse Grained Views of Metabolic Pathways. PLoS ONE 3, e3805.

Choisnard, L, A Gèze, J-L Putaux, Y-S Wong and D Wouessidjewe (2006) Nanoparticles of β-Cyclodextrin Esters Obtained by Self-Assembling of Biotransesterified β-Cyclodextrins. Biomacromolecules 7, 515-520.

Cohen, SM (1987) Carbon-13 NMR study of the effects of fasting and diabetes on the metabolism of pyruvate in the tricarboxylic acid cycle and of the utilization of pyruvate and ethanol in lipogenesis in perfused rat liver. Biochemistry-US 26, 581-589.

Cui, F-d, A-j Tao, D-m Cun, L-q Zhang and K Shi (2007) Preparation of insulin loaded PLGA-Hp55 nanoparticles for oral delivery. J Pharm Sci 96, 421-427.

Damgé, C, P Maincent and N Ubrich (2007) Oral delivery of insulin associated to polymeric nanoparticles in diabetic rats. J Control Release 117, 163-170.

de la Iglesia, N, M Veiga-da-Cunha, E Van Schaftingen, JJ Guinovart and JC Ferrer (1999) Glucokinase regulatory protein is essential for the proper subcellular localisation of liver glucokinase. FEBS Lett 456, 332-338.

Delgado, TC, D Pinheiro, M Caldeira, MMCA Castro, CFGC Geraldes, P López-Larrubia, S Cerdán and JG Jones (2009a) Sources of hepatic triglyceride accumulation during high-fat feeding in the healthy rat. NMR Biomed 22, 310-317.

Delgado, TC, C Silva, I Fernandes, M Caldeira, M Bastos, C Baptista, M Carvalheiro, CFGC Geraldes and JG Jones (2009b) Sources of hepatic glycogen synthesis during an oral glucose tolerance test: Effect of transaldolase exchange on flux estimates. Magn Reson Med 62, 1120-1128.

Dentin, R, J Girard and C Postic (2005) Carbohydrate responsive element binding protein (ChREBP) and sterol regulatory element binding protein-1c (SREBP-1c): two key regulators of glucose metabolism and lipid synthesis in liver. Biochimie 87, 81-86.

Dib, B (1999) Food and water intake suppression by intracerebroventricular administration of substance P in food- and water-deprived rats. Brain Res 830, 38-42.

DiGirolamo, M, JB Fine, K Tagra and R Rossmanith (1998) Qualitative regional differences in adipose tissue growth and cellularity in male Wistar rats fed ad libitum. Am J Physiol-Reg I 274, R1460-R1467.

Dong, H, J Altomonte, N Morral, M Meseck, SN Thung and SLC Woo (2002) Basal Insulin Gene Expression Significantly Improves Conventional Insulin Therapy in Type 1 Diabetic Rats. Diabetes 51, 130-138.

Duchêne, D, D Wouessidjewe and G Ponchel (1999) Cyclodextrins and carrier systems. J Control Release 62, 263-268.

Dunn, A, J Katz, S Golden and M Chenoweth (1976) Estimation of glucose turnover and recycling in rabbits using various [^{3}H, ^{14}C]glucose labels. Am J Physiol 230, 1159-1162.

Fell, D (1997). Understanding the Control of Metabolism. London, Portland Press Ltd.

Fernandes, AAH, ELB Novelli, K Okoshi, MP Okoshi, BPD Muzio, JFC Guimarães and AF Junior (2010) Influence of rutin treatment on biochemical alterations in experimental diabetes. Biomed Pharmacother 64, 214-219.

Ferrannini, E, A Lanfranchi, F Rohner-Jeanrenaud, G Manfredini and G Van de Werve (1990) Influence of long-term diabetes on liver glycogen metabolism in the rat. Metabolism 39, 1082-1088.

Ferrer, JC, C Favre, RR Gomis, JM Fernandez-Novell, M Garcia-Rocha, N de la Iglesia, E Cid and JJ Guinovart (2003) Control of glycogen deposition. FEBS Lett 546, 127-132.

Fessi, H, J-P Devissaguet, F Puisieux and C Thies (1992) Process for the preparation of dispersible colloidal systems of a substance in the form of nanoparticles. US Patent 5118528.

Folch, J, M Lees and GHS Stanley (1957) A Simple Method for the Isolation of Total Lipides from Animal Tissues. J Biol Chem 226, 497-509.

Foufelle, F and P Ferré (2002) New perspectives in the regulation of hepatic glycolytic and lipogenic genes by insulin and glucose: a role for the transcription factor sterol regulatory element binding protein-1c. Biochem J 366, 377-391.

Frayn, KN (2002) Adipose tissue as a buffer for daily lipid flux. Diabetologia 45, 1201-1210.

Friedman, M (1995) Control of energy intake by energy metabolism. Am J Clin Nutr 62, 1096S-1100S.

Friedmann, B, EH Goodman and S Weinhouse (1963) Liver Glycogen Synthesis in Intact Alloxan Diabetic Rats. J Biol Chem 238, 2899-2905.

Gaíva, MH, RC Couto, LM Oyama, GEC Couto, VLF Silveira, EB Ribeiro and CMO Nascimento (2003) Diets rich in polyunsaturated fatty acids: Effect on hepatic metabolism in rats. Nutrition 19, 144-149.

Garvey, WT (2004). Mechanisms of Insulin Signal Transducing. International Textbook of Diabetes Mellitus. RA DeFronzo, E Ferrannini, H Keen and P Zimmet. Chinchester, Jonh Wiley & Sons Ltd. 1: 227-252.

Gèze, A, LT Chau, L Choisnard, J-P Mathieu, D Marti-Batlle, L Riou, J-L Putaux and D Wouessidjewe (2007) Biodistribution of intravenously administered amphiphilic b-cyclodextrin nanospheres. Int J Pharm 344, 135–142.

Goforth, HW, D Laurent, WK Prusaczyk, KE Schneider, KF Petersen and GI Shulman (2003) Effects of depletion exercise and light training on muscle glycogen supercompensation in men. Am J Physiol-Endoc M 285, E1304-E1311.

Grantham, BD and VA Zammit (1988) Role of carnitine palmitoyltransferase I in the regulation of hepatic ketogenesis during the onset and reversal of chronic diabetes. Biochem J 249, 409–414.

Gruetter, R, G Adriany, I-Y Choi, P-G Henry, H Lei and G Öz (2003) Localized in vivo^{13}C NMR spectroscopy of the brain. NMR Biomed 16, 313-338.

Gurney, AL, EA Park, J Liu, M Giralt, MM McGrane, YM Patel, DR Crawford, SE Nizielski, S Savon and RW Hanson (1994) Metabolic Regulation of Gene Transcription. J Nutr 124, 1533S-1539S.

Halban, PA, MS German, SE Kahn and GC Weir (2010) Current Status of Islet Cell Replacement and Regeneration Therapy. J Clin Endocrinol Metab 95, 1034-1043.

Havel, PJ, JY Uriu-Hare, T Liu, KL Stanhope, JS Stern, CL Keen and B Ahrén (1998) Marked and rapid decreases of circulating leptin in streptozotocin diabetic rats: reversal by insulin. Am J Physiol-Endoc M 274, R1482-R1491.

He, Y, C Martinez-Fleites, A Bubb, TM Gloster and GJ Davies (2009) Structural insight into the mechanism of streptozotocin inhibition of O-GlcNAcase. Carbohyd Res 344, 627-631.

Hellerstein, MK, Christiansen, M., Kaempfer, S., Kletke, C., Wu, K., Reid, J. S., Mulligan, K., Hellerstein, N. S., Schackleton, H. L. (1991) Measurement of de novo hepatic lipogenesis in humans using stable isotopes. J. Clin. Invest. 87, 1841-1852.

Hellerstein, MK, DJ Greenblatt and HN Munro (1986) Glycoconjugates as Noninvasive Probes of Intrahepatic Metabolism: Pathways of Glucose Entry into Compartmentalized Hepatic UDP-glucose Pools during Glycogen Accumulation. P Natl Acad Sci USA 83, 7044-7048.

Hellerstein, MK, S Kaempfer, JS Reid, K Wu and CHL Shackleton (1995) Rate of glucose entry into hepatic uridine diphosphoglucose by the direct pathway in fasted and fed states in normal humans. Metabolism 44, 172-182.

Hellerstein, MK and HN Munro (1988) Glycoconjugates as noninvasive probes of intrahepatic metabolism: III. Application to galactose assimilation by the intact rat. Metabolism 37, 312-317.

Hellerstein, MK, JM Schwarz and RA Neese (1996) Regulation of Heatic De Novo Lipogenesis in Humans. Annu Rev Nutr 16, 523-557.

Hellerstein, MK, K Wu, S Kaempfer, C Kletke and CH Shackleton (1991) Sampling the lipogenic hepatic acetyl-CoA pool in vivo in the rat. Comparison of xenobiotic probe to values predicted from isotopomeric distribution in circulating lipids and measurement of lipogenesis and acetyl-CoA dilution. J Biol Chem 266, 10912-10919.

Hidaka, S, H Yoshimatsu, S Kondou, Y Tsuruta, K Oka, H Noguchi, K Okamoto, H Sakino, Y Teshima, T Okeda and T Sakata (2002) Chronic central leptin infusion restores hyperglycemia independent of food intake and insulin level in streptozotocin-induced diabetic rats. FASEB J 16, 509-518.

Holness, MJ, EB Cook and MC Sugden (1988) Regulation of hepatic fructose 2,6-bisphosphate concentrations and lipogenesis after re-feeding in euthyroid and hyperthyroid rats. A regulatory role for glycogenesis. Biochem J 252, 357-350.

Holness, MJ and MC Sugden (1990) Pyruvate dehydrogenase activities and rates of lipogenesis during the fed-to-starved transition in liver and brown adipose tissue of the rat. Biochem J 268, 77–81.

Holness, MJ and MC Sugden (2003) Regulation of pyruvate dehydrogenase complex activity by reversible phosphorylation. Biochem Soc T 31, 1143-1151.

Hosokawa, M, W Dolci and B Thorens (2001) Differential Sensitivity of GLUT1- and GLUT2-Expressing β Cells to Streptozotocin. Biochem Bioph Res Co 289, 1114-1117.

Huang, W, A Metlakunta, N Dedousis, HK Ortmeyer, M Stefanovic-Racic and RM O'Doherty (2009) Leptin Augments the Acute Suppressive Effects of Insulin on Hepatic Very Low-Density Lipoprotein Production in Rats. Endocrinology 150, 2169-2174.

Hwang, J-H, G Perseghin, DL Rothman, GW Cline, I Magnusson, KF Petersen and GI Shulman (1995) Impaired Net Hepatic Glycogen Synthesis in Insulin-dependent Diabetic Subjects during Mixed Meal Ingestion. A ^{13}C Nuclear Magnetic Resonance Spectroscopy Study. J Clin Invest 95, 783-787.

Iwasaki, T, S Takahashi, M Takahashi, Y Zenimaru, T Kujiraoka, M Ishihara, M Nagano, J Suzuki, I Miyamori, H Naiki, J Sakai, T Fujino, NE Miller, TT Yamamoto and H Hattori (2005) Deficiency of the Very Low-Density Lipoprotein (VLDL) Receptors in Streptozotocin-Induced Diabetic Rats: Insulin Dependency of the VLDL Receptor. Endocrinology 146, 3286-3294.

Iynedjian, P (2009) Molecular Physiology of Mammalian Glucokinase. Cell Mol Life Sci 66, 27-42.

Jetton, TL, M Shiota, SM Knobel, DW Piston, AD Cherrington and MA Magnuson (2001) Substrate-induced Nuclear Export and Peripheral Compartmentalization of Hepatic Glucokinase Correlates with Glycogen Deposition. Int J Exp Diabetes Res 2, 173–186.

Jin, ES, K Uyeda, T Kawaguchi, SC Burgess, CR Malloy and AD Sherry (2003) Increased Hepatic Fructose 2,6-Bisphosphate after an Oral Glucose Load Does Not Affect Gluconeogenesis. J Biol Chem 278, 28427-28433.

Johansson, F, E Hjertberg, S Eirefelt, A Tronde and UH Bengtsson (2002) Mechanisms for absorption enhancement of inhaled insulin by sodium taurocholate. Eur J Pharm Sci 17, 63–71.

Johnson, RF and AK Johnson (1990) Light/Dark Cycle Modulates Food to Water Intake Ratios in Rats. Physiol Behav 48, 707-711.

Jones, J, C Barosa, F Gomes, A Carina Mendes, T Delgado, L Diogo, P Garcia, M Bastos, L Barros, A Fagulha, C Baptista, M Carvalheiro and M Madalena Caldeira (2006b) NMR Derivatives for Quantification of ^{2}H and ^{13}C Enrichment of Human Glucuronide from Metabolic Tracers. J Carbohyd Chem 25, 203-217.

Jones, JG, A Fagulha, C Barosa, M Bastos, L Barros, C Baptista, MM Caldeira and M Carvalheiro (2006a) Noninvasive Analysis of Hepatic Glycogen Kinetics Before and After Breakfast with Deuterated Water and Acetaminophen. Diabetes 55, 2294–2300.

Jones, JG, M Merritt and C Malloy (2001) Quantifying tracer levels of $^{2}H_2O$ enrichment from microliter amounts of plasma and urine by ^{2}H NMR. Magn Reson Med 45, 156-158.

Jope, RS and GVW Johnson (2004) The glamour and gloom of glycogen synthase kinase-3. Trends Biochem Sci 29, 95-102.

Junod, A, AE Lambert, W Stauffacher and AE Renold (1969) Diabetogenic action of streptozotocin: relationship of dose to metabolic response. J Clin Invest 48, 2129–2139.

Kamagate, A and HH Dong (2008) FoxO1 integrates insulin signaling to VLDL production. Cell Cycle 7, 3162–3170.

Katz, J, WN Lee, PA Wals and EA Bergner (1989) Studies of glycogen synthesis and the Krebs cycle by mass isotopomer analysis with [U-^{13}C]glucose in rats. J Biol Chem 264, 12994-13004.

Katz, J and JD McGarry (1984) The Glucose Paradox - Is Glucose a Substrate for Liver Metabolism? J Clin Invest 74, 1901-1909.

Khandelwal, RL, SM Zinman and EJ Zebrowski (1977) The effect of streptozotocin-induced diabetes and of insulin supplementation on glycogen metabolism in rat liver. Biochem J 168, 541–548.

Konrad, RJ, I Mikolaenko, JF Tolar, K Liu and JE Kudlow (2001) The potential mechanism of the diabetogenic action of streptozotocin: inhibition of pancreatic beta-cell O-GlcNAc-selective N-acetyl-beta-D-glucosaminidase. Biochem J 356, 31-41.

Kuwajima, M, S Golden, J Katz, RH Unger, DW Foster and JD McGarry (1986) Active hepatic glycogen synthesis from gluconeogenic precursors despite high tissue levels of fructose 2,6-bisphosphate. J Biol Chem 261, 2632-2637.

Kuwajima, M, CB Newgard, DW Foster and JD McGarry (1984) Time Course and Significance of Changes in Hepatic Fructose-2,6-Bisphosphate Levels During Refeeding of Fasted Rats. J Clin Invest 74, 1108-1111.

Landau, BR, J Wahren, V Chandramouli, WC Schumann, K Ekberg and SC Kalhan (1995) Use of $^{2}H_2O$ for Estimating Rates of Gluconeogenesis Application to the Fasted State. J Clin Invest 95, 172-178.

Landau, BR, J Wahren, V Chandramouli, WC Schumann, K Ekberg and SC Kalhan (1996) Contributions of Gluconeogenesis to Glucose Production in the Fasted State. J Clin Invest 98, 378–385.

Landau, BR, J Wahren, V Chandramouli, WC Schumann, K Ekberg and SC Kalhan (1997) Use of $^{2}H_2O$ for Estimating Rates of Gluconeogenesis Application to the Fasted State. J Clin Invest 95, 172-178.

Lanza-Jacoby, S, NR Stevenson and ML Kaplan (1986) Circadian Changes in Serum and Liver Metabolites and Liver Lipogenic Enzymes in Ad Libitum- and Meal-Fed, Lean and Obese Zucker Rats. J Nutr 116, 1798-1809.

Lanza, IR, DM Wigmore, DE Befroy and JA Kent-Braun (2006) In vivo ATP production during free-flow and ischaemic muscle contractions in humans. J Physiol 577, 353-367.

Lee, W-NP, S Bassilian, S Lim and LG Boros (2000) Loss of regulation of lipogenesis in the Zucker diabetic (ZDF) rat. Am J Physiol-Endoc M 279, E425-E432.

Lefèvre, PJ (2004). Biosynthesis, Secretion, and Action of Glucagon. International Textbook of Diabetes Mellitus. RA DeFronzo, E Ferrannini, H Keen and P Zimmet. Chinchester, Jonh Wiley & Sons Ltd. 1: 183-190.

Lenzen, S (2008) The mechanisms of alloxan- and streptozotocin-induced diabetes. Diabetologia 51, 216-226.

Lindon, JC, JK Nicholson and E Holmes (2007). Handbook of Metabonomics and Metabolomics. Amsterdam, Elsevier BV.

Lo, H-C, F-A Tsai, SP Wasser, J-G Yang and B-M Huang (2006) Effects of ingested fruiting bodies, submerged culture biomass, and acidic polysaccharide glucuronoxylomannan of Tremella mesenterica Retz.:Fr. on glycemic responses in normal and diabetic rats. Life Sci 78, 1957-1966.

Loftsson, T and ME Brewster (1996) Pharmaceutical applications of cyclodextrins 1. Drug solubilization and stabilization. J Pharm Sci 85, 1017-1025.

Loftsson, T and D Duchêne (2007) Cyclodextrins and their pharmaceutical applications. Int J Pharm 329, 1-11.

MacQueen, HA, DA Sadler, SA Moore, S Daya, JY Brown, DEG Shuker, M Seaman and WS Wassif (2007) Deleterious effects of a cafeteria diet on the livers of nonobese rats. Nutr Res 27, 38-47.

Magnusson, I, V Chandramouli, WC Schumann, K Kumaran, J Wahren and BR Landau (1987) Quantitation of the Pathways of Hepatic Glycogen Formation on Ingesting a Glucose Load. J Clin Invest 80, 1748-1754.

Marti, L, A Abella, C Carpene, M Palacin, X Testar and A Zorzano (2001) Combined Treatment With Benzylamine and Low Dosages of Vanadate Enhances Glucose Tolerance and Reduces Hyperglycemia in Streptozotocin-Induced Diabetic Rats. Diabetes 50, 2061-2068.

Mason, TM, B Chan, B El-Bahrani, T Goh, N Gupta, J Gamble, Z Qing Shi, M Prentki, G Steiner and A Giacca (2002) The effect of chronic insulin delivery via the intraperitoneal versus the subcutaneous route on hepatic triglyceride secretion rate in streptozotocin diabetic rats. Atherosclerosis 161, 345-352.

Mason, TM, N Gupta, T Goh, B El-Bahrani, J Zannis, G van de Werve and A Giacca (2000) Chronic intraperitoneal insulin delivery, as compared with subcutaneous delivery, improves hepatic glucose metabolism in streptozotocin diabetic rats. Metabolism 49, 1411-1416.

Mendes, AC, MM Caldeira, C Silva, SC Burgess, ME Merritt, F Gomes, C Barosa, TC Delgado, F Franco, P Monteiro, L Providencia and JG Jones (2006) Hepatic UDP-glucose ^{13}C isotopomers from [U-^{13}C]glucose: A simple analysis by ^{13}C NMR of urinary menthol glucuronide. Magn Reson Med 56, 1121-1125.

Metón, I, D Mediavilla, A Caseras, E Cantó, F Fernández and IV Baanante (1999) Effect of diet composition and ration size on key enzyme activities of glycolysis-gluconeogenesis, the pentose phosphate pathway and amino acid metabolism in liver of gilthead sea bream (Sparus aurata). Brit J Nutr 82, 223-232.

Mithieux, G, A Gautier-Stein, F Rajas and C Zitoun (2006) Contribution of intestine and kidney to glucose fluxes in different nutritional states in rat. Comp Biochem Phys B 143, 195-200.

Mithieux, G, F Rajas and A Gautier-Stein (2004) A Novel Role for Glucose 6-Phosphatase in the Small Intestine in the Control of Glucose Homeostasis. J Biol Chem 279, 44231-44234.

Morral, Nr, R McEvoy, H Dong, M Meseck, J Altomonte, S Thung and SLC Woo (2004) Adenovirus-Mediated Expression of Glucokinase in the Liver as an Adjuvant Treatment for Type 1 Diabetes. Hum Gene Ther 13, 1561-1570.

Murphy, EJ (2006) Stable isotope methods for the in vivo measurement of lipogenesis and triglyceride metabolism. J Anim Sci 84, E94-E104.

Naha, PC, V Kanchan, PK Manna and AK Panda (2008) Improved bioavailability of orally delivered insulin using Eudragit-L30D coated PLGA microparticles. J Microencapsul 25, 248-256.

Nevalainen, P, J Lahtela, J Mustonen and A Pasternack (1997) The influence of peritoneal dialysis and the use of subcutaneous and intraperitoneal insulin on glucose metabolism and serum lipids in type 1 diabetic patients. Nephrol Dial Transpl 12, 145-150.

Newgard, CB (2004). Regulation of Glucose Metabolism in the Liver. International Textbook of Diabetes Mellitus. RA DeFronzo, E Ferrannini, H Keen and P Zimmet. Chinchester, Jonh Wiley & Sons Ltd. 1: 253-275.

Newgard, CB, MJ Brady, RM O'Doherty and AR Saltiel (2000) Organizing glucose disposal: emerging roles of the glycogen targeting subunits of protein phosphatase-1. Diabetes 49, 1967-1977.

Newgard, CB, LJ Hirsch, DW Foster and JD McGarry (1983) Studies on the mechanism by which exogenous glucose is converted into liver glycogen in the rat. A direct or an indirect pathway? J Biol Chem 258, 8046-8052.

Newgard, CB, SV Moore, DW Foster and JD McGarry (1984) Efficient hepatic glycogen synthesis in refeeding rats requires continued carbon flow through the gluconeogenic pathway. J Biol Chem 259, 6958-6963.

Niewoehner, CB and B Neil (1992) Mechanism of delayed hepatic glycogen synthesis after an oral galactose load vs. an oral glucose load in adult rats. Am J Physiol-Endoc M 263, E42-49.

Niewoehner, CB, B Neil and T Martin (1990) Hepatic uptake and metabolism of oral galactose in adult fasted rats. Am J Physiol-Endoc M 259, E804-813.

Nobelprize.org. (2010, 4 Nov 2010). The Discovery of Insulin. from http://nobelprize.org/educational/medicine/insulin/discovery-insulin.html.

Nordlie, RC, JD Foster and AJ Lange (1999) Regulation of Glucose Production by the Liver. Annu Rev Nutr 19, 379-406.

Noula, C, P Bonzom, A Brown, WA Gibbons, J Martin and A Nicolaou (2000) ^{1}H-NMR lipid profiles of human blood platelets; links with coronary artery disease. BBA-Mol Cell Biol L 1487, 15-23.

Nunes, PM and JG Jones (2009) Quantifying endogenous glucose production and contributing source fluxes from a single ^{2}H NMR spectrum. Magn Reson Med 62, 802-807.

O'Doherty, RM, PB Jensen, P Anderson, JG Jones, HK Berman, D Kearney and CB Newgard (2000) Activation of direct and indirect pathways of glycogen synthesis by hepatic overexpression of protein targeting to glycogen. J Clin Invest 105, 479-488.

O'Doherty, RM, DL Lehman, J Seoane, AM Gómez-Foix, JJ Guinovart and CB Newgard (1996) Differential Metabolic Effects of Adenovirus-mediated Glucokinase and Hexokinase I Overexpression in Rat Primary Hepatocytes. J Biol Chem 271, 20524-20530.

Okamoto, T, N Kanemoto, Y Ohbuchi, M Okano, H Fukui and T Sudo (2008) Characterization of STZ-Induced Type 2 Diabetes in Zucker Fatty Rats. Exp Anim Tokyo 57, 335-345.

Owens III, DE and NA Peppas (2006) Opsonization, biodistribution, and pharmacokinetics of polymeric nanoparticles. Int J Pharm 307, 93-102.

Palou, M, T Priego, J Sánchez, E Villegas, A Rodríguez, A Palou and C Picó (2008) Sequential changes in the expression of genes involved in lipid metabolism in adipose tissue and liver in response to fasting. Pflug Arch Europ J Phy 456, 825-836.

Pauletti, GM, S Gangwar, GT Knipp, MM Nerurkar, FW Okumu, K Tamura, TJ Siahaan and RT Borchardt (1996) Structural requirements for intestinal absorption of peptide drugs. J Control Release 41, 3-17.

Peak, M, JJ Rochford, AC Borthwick, SJ Yeaman and L Agius (1998) Signalling pathways involved in the stimulation of glycogen synthesis by insulin in rat hepatocytes. Diabetologia 41, 16-25.

Pedersen, NR, JB Kristensen, G Bauw, BJ Ravoo, R Darcy, KL Larsen and LH Pedersen (2005) Thermolysin catalyses the synthesis of cyclodextrin esters in DMSO. Tetrahedron-Asymmetr 16, 615-622.

Perdigoto, R, TB Rodrigues, AL Furtado, A Porto, CFGC Geraldes and JG Jones (2003) Integration of [U-^{13}C]glucose and $^{2}H_2O$ for quantification of hepatic glucose production and gluconeogenesis. NMR Biomed 16, 189-198.

Peroni, O, V Large, F Diraison and M Beylot (1997) Glucose production and gluconeogenesis in postabsorptive and starved normal and streptozotocin-diabetic rats. Metabolism 46, 1358-1363.

Petersen, KF, T Price, GW Cline, DL Rothman and GI Shulman (1996) Contribution of net hepatic glycogenolysis to glucose production during the early postprandial period. Am J Physiol-Endoc M 270, E186-191.

Petersen, KF, TB Price and R Bergeron (2004) Regulation of Net Hepatic Glycogenolysis and Gluconeogenesis during Exercise: Impact of Type 1 Diabetes. J Clin Endocr Metab 89, 4656-4664.

Pighin, D, L Karabatas, C Pastorale, E Dascal, C Carbone, A Chicco, YB Lombardo and JC Basabe (2005) Role of lipids in the early developmental stages of experimental immune diabetes induced by multiple low-dose streptozotocin. J Appl Physiol 98, 1064-1069.

Pillai, O and R Panchagnula (2001) Insulin therapies - past, present and future. Drug Discov Today 6, 1056-1061.

Pinto Reis, C, RJ Neufeld, AJ Ribeiro and F Veiga (2006) Nanoencapsulation II. Biomedical applications and current status of peptide and protein nanoparticulate delivery systems. Nanomedicine-UK 2, 53-65.

Postic, C, R Dentin and J Girard (2004) Role of the liver in the control of carbohydrate and lipid homeostasis. Diabetes Metab 30, 398-408.

Radziuk, J, S Pye, DE Seigler, JS Skyler, R Offord and G Davies (1994) Splanchnic and systemic absorption of intraperitoneal insulin using a new double-tracer method. Am J Physiol-Endoc M 266, E750-759.

Randle, PJ (1998) Regulatory interactions between lipids and carbohydrates: the glucose fatty acid cycle after 35 years. Diabetes Metab Rev 14, 263-283.

Reddy, LH, RK Sharma, K Chuttani, AK Mishra and RSR Murthy (2005) Influence of administration route on tumor uptake and biodistribution of etoposide loaded solid lipid nanoparticles in Dalton's lymphoma tumor bearing mice. J Control Release 105 185–198.

Reis, CP, FJ Veiga, AJ Ribeiro, RJ Neufeld and C Damgé (2008) Nanoparticulate biopolymers deliver insulin orally eliciting pharmacological response. J Pharm Sci 97, 5290-5305.

Ren, J, I Dimitrov, AD Sherry and CR Malloy (2008) Composition of adipose tissue and marrow fat in humans by ^{1}H NMR at 7 Tesla. J Lipid Res 49, 2055-2062.

Roden, M, G Perseghin, KF Petersen, J-H Hwang, GW Cline, K Gerow, DL Rothman and GI Shulman (1996) The Roles of Insulin and Glucagon in the Regulation of Hepatic Glycogen Synthesis and Turnover in Humans. J Clin Invest 97, 642-648.

Roden, M, KF Petersen and G Shulman (2001) Nuclear Magnetic Resonance Studies of Hepatic Glucose Metabolism in Humans. Recent Prog Horm Res 56, 219-238.

Ruderman, NB, AK Saha, D Vavvas and LA Witters (1999) Malonyl-CoA, fuel sensing, and insulin resistance. Am J Physiol-Endoc M 276, E1-18.

Saadatian, M, O Peroni and M Beylot (2000) In vivo measurement of gluconeogenesis in animals and humans with deuterated water: a simplified method. Diabetes Metab 26, 202-209.

Saltiel, AR and CR Kahn (2001) Insulin signalling and the regulation of glucose and lipid metabolism. Nature 414, 799-806.

Sarmento, B, A Ribeiro, F Veiga and D Ferreira (2006) Development and validation of a rapid reversed-phase HPLC method for the determination of insulin from nanoparticulate systems. Biomed Chromatogr 20, 898–903.

Scott, DK, JJ Collier, TTT Doan, AS Bunnell, MC Daniels, DT Eckert and RM O'Doherty (2003) A modest glucokinase overexpression in the liver promotes fed expression levels of glycolytic and lipogenic enzyme genes in the fasted state without altering SREBP-1c expression. Mol Cell Biochem 254, 327-337.

Sena, CM, C Barosa, E Nunes, R Seiça and JG Jones (2007) Sources of endogenous glucose production in the Goto-Kakizaki diabetic rat. Diabetes Metab 33, 296-302.

Seoane, J, A Barbera, S Telemaque-Potts, CB Newgard and JJ Guinovart (1999) Glucokinase Overexpression Restores Glucose Utilization and Storage in Cultured Hepatocytes from Male Zucker Diabetic Fatty Rats. J Biol Chem 274, 31833-31838.

Shapiro, AMJ, JRT Lakey, EA Ryan, GS Korbutt, E Toth, GL Warnock, NM Kneteman and RV Rajotte (2000) Islet Transplantation in Seven Patients with Type 1 Diabetes Mellitus Using a Glucocorticoid-Free Immunosuppressive Regimen. N Engl J Med 343, 230-238.

Sharma, P, MVS Varma, HPS Chawla and R Panchagnula (2005) Absorption enhancement, mechanistic and toxicity studies of medium chain fatty acids, cyclodextrins and bile salts as peroral absorption enhancers. Farmaco 60, 884-893.

Shimomura, I, Y Bashmakov, S Ikemoto, JD Horton, MS Brown and JL Goldstein (1999) Insulin selectively increases SREBP-1c mRNA in the livers of rats with streptozotocin-induced diabetes. P Natl Acad Sci USA 96, 13656-13661.

Shulman, GI, G Cline, WC Schumann, V Chandramouli, K Kumaran and BR Landau (1990) Quantitative comparison of pathways of hepatic glycogen repletion in fed and fasted humans. Am J Physiol-Endoc M 259, E335-341.

Shulman, GI, DL Rothman, D Smith, CM Johnson, JB Blair, RG Shulman and RA DeFronzo (1985) Mechanism of liver glycogen repletion in vivo by nuclear magnetic resonance spectroscopy. J Clin Invest 76, 1229–1236.

Silva, AM, F Martins, JG Jones and R Carvalho (2011) $^{2}H_2O$ Incorpration Into Hepatic Acetyl-CoA and De novo Lipogenesis as Measured by Krebs Cycle-Mediated ^{2}H-Enrichment of Glutamate and Glutamine. Magn Res Med, In press.

Sindelar, DK, PJ Havel, RJ Seeley, CW Wilkinson, SC Woods and MW Schwartz (1999) Low plasma leptin levels contribute to diabetic hyperphagia in rats. Diabetes 48, 1275-1280.

Sinha, R, S Dufour, KF Petersen, V LeBon, S Enoksson, Y-Z Ma, M Savoye, DL Rothman, GI Shulman and S Caprio (2002) Assessment of Skeletal Muscle Triglyceride Content by 1H Nuclear Magnetic Resonance Spectroscopy in Lean and Obese Adolescents. Diabetes 51, 1022-1027.

Sparks, JD and HH Dong (2009) FoxO1 and hepatic lipid metabolism. Curr Opin Lipidol 20, 217–226.

Stingl, H, V Chandramouli, WC Schumann, A Brehm, P Nowotny, W Waldhäusl, BR Landau and M Roden (2006) Changes in hepatic glycogen cycling during a glucose load in healthy humans. Diabetologia 49, 360-368.

Strumiło, S (2005) Short-term regulation of the mammalian pyruvate dehydrogenase complex. Acta Biochim Pol 52, 759-764.

Suthagar, E, S Soudamani, S Yuvaraj, A Ismail Khan, MM Aruldhas and K Balasubramanian (2009) Effects of streptozotocin (STZ)-induced diabetes and insulin replacement on rat ventral prostate. Biomed Pharmacother 63, 43-50.

Sutherland, DER, AC Gruessner and RWG Gruessner (1998) Pancreas transplantation: a review. Transplant Proc 30, 1940-1943.

Szkudelski, T (2001) The mechanism of alloxan and streptozotocin action in B cells of the rat pancreas. Physiol Res 50, 537-546.

Takada, J, MH Fonseca-Alaniz, TBF de Campos, S Andreotti, AB Campana, M Okamoto, CN Borges-Silva, UF Machado and FB Lima (2008) Metabolic recovery of adipose tissue is associated with improvement in insulin resistance in a model of experimental diabetes. J Endocrinol 198, 51-60.

Taylor, R, I Magnusson, DL Rothman, GW Cline, A Caumo, C Cobelli and GI Shulman (1996) Direct Assessment of Liver Glycogen Storage by ^{13}C Nuclear Magnetic Resonance Spectroscopy and Regulation of Glucose Homeostasis after a Mixed Meal in Normal Subjects. J Clin Invest 97, 126-132.

Towle, HC (2005) Glucose as a regulator of eukaryotic gene transcription. Trends Endocrin Met 16, 489-494.

Turner, SM, EJ Murphy, RA Neese, F Antelo, T Thomas, A Agarwal, C Go and MK Hellerstein (2003) Measurement of TG synthesis and turnover in vivo by $^{2}H_2O$ incorporation into the glycerol moiety and application of MIDA. Am J Physiol-Endoc M 285, E790-E803.

Uekama, K, F Hirayama and T Irie (1998) Cyclodextrin Drug Carrier Systems. Chem Rev 98, 2045-2076.

Utzschneider, KM, DP Jr and SE Kahn (2004). Normal Insulin Secretion in Humans. International Textbook of Diabetes Mellitus. RA DeFronzo, E Ferrannini, H Keen and P ZImmet. Chichester, John Wiley Sons, Ltd. 1: 139-151.

van Zijl, PCM, CK Jones, J Ren, CR Malloy and AD Sherry (2007) MRI detection of glycogen in vivo by using chemical exchange saturation transfer imaging (glycoCEST). P Natl Acad Sci USA 104, 4359-4364.

Velho, G, KF Petersen, G Perseghin, J-H Hwang, DL Rothman, ME Pueyo, GW Cline, P Froguel and GI Shulman (1996) Impaired Hepatic Glycogen Synthesis in Glucokinase-deficient (MODY-2) Subjects. J Clin Invest 98, 1755–1761.

Vergès, B (2009) Lipid disorders in type 1 diabetes. Diabetes Metab 35, 353-360.

Villar-Palasi, C and JJ Guinovart (1997) The role of glucose 6-phosphate in the control of glycogen synthase. FASEB J 11, 544-558.

Wagner, RT, J Lewis, A Cooney and L Chan (2010) Stem cell approaches for the treatment of type 1 diabetes mellitus. Transl Res 156, 169-179.

Wan, CKN, A Giacca, M Matsuhisa, B El-Bahrani, L Lam, C Rodgers and ZQ Shi (2000) Increased responses of glucagon and glucose production to hypoglycemia with intraperitoneal versus subcutaneous insulin treatment. Metabolism 49, 984-989.

Wehrli, S, R Reynolds and S Segal (2007) Metabolic fate of administered [^{13}C]galactose in tissues of galactose-1-phosphate uridyl transferase deficient mice determined by nuclear magnetic resonance. Mol Genet Metab 90, 42-48.

Wei, M, L Ong, MT Smith, FB Ross, K Schmid, AJ Hoey, D Burstow and L Brown (2003) The streptozotocin-diabetic rat as a model of the chronic complications of human diabetes. Heart Lung Circ 12, 44-50.

WHO (1999). Definition, Diagnosis and Classification of Diabetes Mellitus and its Complications: Report of a WHO Consultation. Part 1: Diagnosis and Classification of Diabetes Mellitus. Geneva, World Health Organization.

WHO (2006). Definition and Diagnosis of Diabetes Mellitus and Intermediate Hyperglycemia: Report of a WHO/IDF Consultation. Geneva, World Health Organization.

Wi, JK, JK Kim and JH Youn (1998) Reduced glucose clearance as the major determinant of postabsorptive hyperglycemia in diabetic rats. Am J Physiol-Endoc M 274, E257-264.

Williams, TD, JB Chambers, OL May, RP Henderson, ME Rashotte and JM Overton (2000) Concurrent reductions in blood pressure and metabolic rate during fasting in the unrestrained SHR. Am J Physiol-Reg I 278, R255-262.

Wollheim, CB and P Maechler (2004). β-Cell Biology of Insulin Secretion. International Textbook of Diabetes Mellitus. RA DeFronzo, E Ferrannini, H Keen and P Zimmet. Chinchester, Jonh Wiley & Sons Ltd. 1: 125-138.

Wren, AM, CJ Small, CR Abbott, WS Dhillo, LJ Seal, MA Cohen, RL Batterham, S Taheri, SA Stanley, MA Ghatei and SR Bloom (2001) Ghrelin Causes Hyperphagia and Obesity in Rats. Diabetes 50, 2540-2547.

Yabaluri, N and M Bashyam (2010) Hormonal regulation of gluconeogenic gene transcription in the liver. J Biosci 35, 473-484.

Yamaoka, I, M Nakayama, T Miki, T Yokoyama and Y Takeuchi (2008) Dietary Protein Modulates Circadian Changes in Core Body Temperature and Metabolic Rate in Rats. J Physiol Sci 58, 75-81.

Zhang, P, C-C Ling, AW Coleman, H Parrot-Lopez and H Galons (1991) Formation of amphiphilic cyclodextrins via hydrophobic esterification at the secondary hydroxyl face. Tetrahedron Lett 32, 2769-2770.

Zhou, H, POT Tran, S Yang, T Zhang, E LeRoy, E Oseid and RP Robertson (2004) Regulation of α-Cell Function by the β-Cell During Hypoglycemia in Wistar Rats: the "Switch-off" Hypothesis. Diabetes 53, 1482-1487.